# Mutual repression between JNK/AP-1 and JAK/STAT stratifies cell behaviors during tissue regeneration

Janhvi Jaiswal [1,2], Raphael Engesser [3], Andrea Armengol Peyroton [1], Vanessa Weichselberger [1,2], Carlo Crucianelli [1], Isabelle Grass [1,4], Jens Timmer [3,4,5] and Anne-Kathrin Classen* [1,4,5]

* corresponding author

*1 Hilde-Mangold-Haus, University of Freiburg, Germany*
*2 Spemann Graduate School of Biology and Medicine (SGBM), University of Freiburg, Germany*
*3 Institute of Physics and Freiburg Centre for Data Analysis and Modeling, University of Freiburg, Germany*
*4 CIBSS Centre for Integrative Biological Signalling Studies, University of Freiburg, Germany*
*5 BIOSS Centre for Biological Signalling Studies, University of Freiburg, Germany*

**Abstract**

Epithelial repair relies on the activation of stress signaling pathways to coordinate cellular repair behaviors. Their deregulation is implicated in chronic wound and cancer pathologies. Despite such translational importance, an understanding of how spatial patterns of signaling pathways and repair behaviors arise in damaged tissues remains elusive. Using TNF-α/Eiger-mediated inflammatory damage to *Drosophila* imaginal discs, we uncover that JNK/AP-1 signaling cells act as paracrine organizers and initiate a mutual repression network that spatially segregates JNK/AP-1 and JAK/STAT signaling cells into distinct populations. While JNK/AP-1 signaling cells produce JAK/STAT-activating Upd ligands, these signal-sending cells suppress activation of JAK/STAT via Ptp61F. Conversely, responding cells with activated JAK/STAT suppress JNK activation via Zfh2. The resulting bistable segregation of signaling domains is associated with distinct cellular tasks and regenerative potential. While JNK/AP-1 signaling cells at the wound center act as paracrine organizers, their cell cycle is senescently arrested. Thus, compensatory proliferation occurs exclusively in JAK/STAT signaling cells at the wound periphery. This spatial stratification is essential for proper tissue repair, as co-activation of JNK/AP-1 and JAK/STAT in the same cells creates conflicting inputs on cell cycle progression, leading to excess apoptosis of senescently arrested organizer cells. Finally, we demonstrate that bistable spatial segregation of JNK/AP-1 and JAK/STAT drives senescent and proliferative behaviors in transient as well as chronic tissue damage models, and importantly, in *Ras*$^{V12}$*, scrib* tumors under the influence of JNK/AP-1 activity. Revealing this previously uncharacterized regulatory network between JNK/AP-1, JAK/STAT and associated cell behaviors have important implications for our conceptual understanding of tissue repair, chronic wound pathologies and tumor microenvironments, where both pathways are strongly implicated.

## Introduction

Wound repair programs rely on the coordination of distinct responses to damage [1, 2]. Upon damage, wound-derived factors initiate inflammation and stress-signaling pathways which drive cellular responses like apoptosis, proliferation, survival and tissue remodeling [3-6]. While these responses are essential, it is critical that they remain spatio-temporally restricted to avoid the establishment of chronic wounds [7-9]. Chronic wounds are characterized by sustained inflammation, and deregulated proliferation and apoptosis [10]. The finding that these are also hallmarks of tumor microenvironments supported the idea that tumors resemble chronic, non-healing wounds [11-13]. Yet, the tissue-level coordination of signaling pathways and repair behaviors upon wounding, and the conditions under which they turn pathological remain elusive.

A myriad of wound models identified specific signaling pathways required for regeneration, of which several have also been shown to drive tumor growth. In particular, the JNK/AP-1 and the JAK/STAT pathways are consistently implicated in regeneration [14-17] as well as in tumors [18-23]. In the context of wound-healing, JNK/AP-1 activation is indispensable for regeneration [24-26]. JNK/AP-1 is one of the earliest signaling responses to damage, proposedly activated by wound-derived ROS signals [27, 28]. In this role, JNK/AP-1 regulates a variety of conflicting cell behaviors including apoptosis [29, 30], survival [31] and compensatory proliferation [32, 33]. These paradoxical behaviors have been extensively characterized individually [34-36], yet how they are organized on a tissue scale to ensure regeneration is not known.

We recently reported that high JNK/AP-1 signaling facilitates survival in wounds and tumors by mediating a cell cycle stall in G2 which is characterized by anti-apoptotic and senescent features [31]. Forced exit of these cells from G2 into mitosis and G1 caused a substantial increase in apoptosis, suggestive of the JNK-mediated G2 stall being a protective state during regeneration (Fig. S1A) [31]. This model is supported by recent evidence that the universal integrator of molecular damage, p53, is activated by the G2/M kinase Cdk1 to induce apoptosis competence upon exit from G2 [37]. The G2 protective state is critical as high JNK/AP-1 signaling cells are shown to produce mitogens necessary to induce compensatory proliferation and regeneration [28, 38-40]. Paradoxically, this reveals a cell population at the center of wounds which produces pro-proliferative signals but itself is prohibited from proliferation. These findings highlight the necessity of a mechanism, which ensures that high JNK/AP-1 signaling cells maintain a G2 stall in the presence of mitogenic signals, thereby outsourcing proliferation to other cells. Alternatively, it requires the existence of a mechanism that promotes cycling as well as survival of JNK-signaling cells. This illustrates that the underlying

84 mechanisms and molecular effectors that resolve these conflicting cell behaviors downstream
85 of JNK/AP-1 signaling in the same tissues remains elusive.
86
87 Prominent cytokines produced by JNK/AP-1 signaling cells belong to the Unpaired (Upd) family
88 [41-45] and activate the JAK/STAT pathway which, in turn, plays a significant role in mediating
89 proliferation [18, 20, 28, 39, 46-50] and cell survival during tissue stress [51, 52]. Interestingly,
90 we have previously also shown that JAK/STAT is required in the disc to restrict the expansion
91 of JNK/AP-1 signaling [51]. This is essential as JNK/AP-1 signaling within the tissue can self-
92 propagate by promoting an increase in the expression of its own paracrine activators - the
93 TNF-α/Eiger (Egr) cytokine [53, 54], as well as ROS [28, 55, 56].
94
95 These observations indicate an interdependence between the JNK/AP-1 and JAK/STAT
96 signaling pathways, whose coexistence has been consistently reported in wounds [14-17] and
97 tumor tissues [18-23]. Yet the regulatory network of the two pathways, beyond the regulation
98 of *upd's* by JNK, remains so far unexplored. As JNK/AP-1 and JAK/STAT drive contradicting
99 yet critical cell behaviors - namely G2 stalling and proliferation, linked by their regulation of
100 survival - characterizing their regulatory interactions is essential to understand how these
101 pathways cooperatively organize tissue stress responses.

102 **Results**
103

104 **Figure 1**
105 **JNK/AP-1 and JAK/STAT segregate into distinct spatial domains upon tissue damage**
106
107 To characterize the JNK/AP-1 and JAK/STAT signaling pathways at wound sites in detail, we
108 analyzed signaling dynamics and repair behaviors induced by targeted expression of the TNF-
109 α homologue *eiger* (*egr*) in the wing disc pouch (Fig. S1.1B,C). Ectopic *egr*-expression has
110 been extensively used as a model to genetically induce wounds and study regeneration [57].
111 *egr*-expression activates the stress-signaling pathway JNK/AP-1, assessed by the sensitive
112 JNK/AP-1 reporter - *TRE>RFP* (Fig. 1A,B) [58], which leads to loss of polarity, epithelial barrier
113 dysfunction (Fig. S1.1D-E') and inflammation [24, 25, 59]. Specifically, expression of *egr* also
114 induces *upd1-3* cytokine expression [51], MMP-1 production [60-62], ROS production [8, 63]
115 and protective responses including UPR [64] and, ultimately, NF-κB signaling upregulation [65]
116 (Fig.S1.1F-O, see also Fig.1E,F) in high JNK/AP-1 signaling cells – which are all known
117 hallmarks of inflammatory, and by extension, chronic wounds [6, 10]. In addition, high JNK/AP-
118 1 activity at the center of the *egr*-expressing domain (Fig. 1A,B) induces a senescent-like G2
119 cell cycle stall (Fig. 1C,D) which is essential for cell survival (Fig. S1.1A), as assessed using
120 the Fly-FUCCI toolkit [31, 66]. Indeed, we found that proliferation was excluded from the

121 inflammatory JNK-signaling domain at the center of the disc and was restricted to the wound
122 periphery (Fig. 1C,D,N). These observations highlight a pronounced spatial segregation of
123 regenerative cell behaviors linked to JNK-induced tissue damage responses.
124
125 Upon tissue damage, *upd's* - the pro-mitogenic cytokines for the JAK/STAT pathway - are
126 generally upregulated at wound sites where JNK/AP-1 activity is high (Fig. 1E,F,M, see also
127 S1.1F,G) [20, 28, 49, 51]. Consistent with their paracrine function [67, 68], JAK/STAT signaling
128 was broadly induced in the pouch periphery and hinge of *egr*-expressing discs (Fig. 1G,H),
129 coinciding with regions of proliferation (Fig. 1K,L,N). Yet, high JNK-signaling cells in *egr*-
130 expressing discs that upregulated the transcriptional reporters for *upd1* and *upd3* (Fig.
131 S1.1F,G; Fig. 1E,F,M) [69] did not undergo proliferation and, importantly, did not exhibit
132 JAK/STAT activity, as assessed by the *10xStat92E>dGFP reporter* (Fig. 1I,J) [70]. This was in
133 stark contrast to wing disc development where ligand expression and pathway activation
134 patterns largely coincide [70-73]. Our unexpected finding that JAK/STAT signaling is low in
135 *upd*-producing cells, strongly suggests that a distinct regulatory network controls JAK/STAT
136 activation during JNK-driven responses to tissue damage.
137
138 To further support this conclusion, we first wanted to rule out that the observed JAK/STAT
139 activation pattern in the periphery of *egr*-expressing discs perpetuated from early hinge
140 patterns of developing discs due to a Dilp8-induced developmental delay (Fig. S1.2 A) [74].
141 Hence, we monitored temporal changes in JAK/STAT activity via a time course of 0h, 7h and
142 14h of *egr*-expression. We consistently observed ectopic induction of the JAK/STAT reporter
143 in the hinge, above developmental levels and with an altered pattern (Fig. S1.2 B-M). This data
144 confirmed that *upd1-3*-driven JAK/STAT activity is induced *de novo* in the hinge and pouch
145 periphery upon tissue damage.
146
147 In summary, we find that JNK/AP-1 activation in the *egr*-expressing pouch coincides with the
148 expression of *upd* cytokines. We show that *upd* cytokines activate JAK/STAT only non-
149 autonomously in a cell population spatially segregated from high JNK-signaling and *upd*-
150 producing cells. In addition to the well-described non-autonomous activation of JAK/STAT by
151 JNK/AP-1 activation, this strongly indicates that cell-autonomous repression of JAK/STAT
152 signaling may be an important consequence of JNK/AP-1 activation (Fig. 1O). This is
153 consistent with recent observations of JNK/AP-1 and JAK/STAT activity segregation during
154 tissue stress in other tissue types, such as epidermal wounds [14]. We therefore demonstrate
155 a recurring theme of spatial segregation of JNK/AP-1 and JAK/STAT signaling upon tissue
156 damage. Importantly, we also show that such spatial patterns of segregating JNK/AP-1 and

157 JAK/STAT signals strongly correlate with spatial segregation of regenerative cell behaviors,
158 specifically G2 stalling and proliferation, into spatially distinct signaling domains.
159

160 **Figure 2**
161 **JNK/AP-1 signaling represses JAK/STAT activity**
162

163 We wanted to first understand whether JNK/AP-1 directly represses JAK/STAT activity and
164 thereby restricts it to the wound periphery. We therefore tested if clonal expression of JNK/AP-
165 1 directly represses JAK/STAT activity, by co-expressing a constitutively activated form of the
166 JNKK Hep along with p35 to prevent cell death [75, 76]. Indeed, *hep*$^{act}$ clones cell-
167 autonomously repressed JAK/STAT activity (Fig. 2A-D, S2A), both when non-autonomously
168 activating it in surrounding cells in the peripheral pouch, hinge or peripodium (Fig. 2A-C, S2A),
169 as well as when within developmentally patterned activity in the hinge (Fig. 2D) [72]. These
170 experiments demonstrate that JNK/AP-1 represses JAK/STAT signaling cell-autonomously,
171 even when JNK/AP-1 has the ability to activate JAK/STAT non-autonomously.
172

173 In these mosaic experiments, hinge cells activated JAK/STAT signaling more robustly than
174 cells of the central pouch (Fig. 2A-B), likely as a result of developmental pre-patterns conferring
175 distinct competence [72]. Namely, the transcription factors Nubbin (Nub) and Rotund (Rn)
176 reduce developmental Stat92E activity in the pouch [77]. To first exclude the possibility that
177 JNK/AP-1 represses JAK/STAT by inducing pouch-specific transcription factors [77], we
178 assessed Nub and Rn levels within *hep*$^{act}$ clones. *hep*$^{act}$ clones did not ectopically induce Nub
179 or Rn, in fact, Nub was distinctly downregulated (Fig. S2B-D). Furthermore, we expressed *egr*
180 in the posterior compartment of the wing disc and examined whether JAK/STAT could be
181 activated in the adjacent anterior pouch (Fig. S1.1B). The cells highly positive for the JNK/AP-
182 1 target gene - MMP-1 [78] did not activate JAK/STAT signaling. However, JAK/STAT signaling
183 could be distinctly activated in the surrounding tissue, including the anterior pouch (Fig. 2E,F).
184 These experiments confirm that JAK/STAT signaling can *in principle* be activated *de novo* in
185 the pouch by cell non-autonomous activity of JNK/AP-1 signaling cells. Altogether, these
186 experiments demonstrate that tissue damage associated with high levels of JNK/AP-1
187 signaling repress JAK/STAT activity in a cell autonomous manner, independent of
188 developmental competence.
189

190 Accordingly, we wanted to better understand if JAK/STAT repression by JNK/AP-1 may
191 depend on JNK/AP-1 signaling strength or time. We therefore analyzed the temporal evolution
192 of JNK/AP-1 and JAK/STAT activity in the JNK-signaling domain of *egr*-expressing discs. A
193 time course analysis revealed that JAK/STAT was mildly elevated during short-term JNK-

194 signaling in the pouch by 7 h of *egr*-expression, and increased even further with 14 h of *egr*-
195 expression (Fig. 2K,L,N,O, Fig. S2E,F,H,I,K,). Interestingly, cells displayed co-existence of
196 both pathways at moderate levels, but also often displayed exclusive activation of either
197 reporter (Fig. S2L,M). After 24 h of sustained *egr*-expression, high JNK/AP-1 signaling was
198 observed in the pouch, but notably, JAK/STAT activity had now largely disappeared from this
199 domain (Fig. 2M,P, Fig. S2G,J,K). These observations reveal that short-term or moderate
200 activity of JNK/AP-1 facilitates local, intermixed activation of JAK/STAT. However, sustained
201 and high activation of JNK/AP-1 efficiently excludes JAK/STAT activity cell autonomously. As
202 a consequence, JNK/AP-1 and JAK/STAT signaling are increasingly segregated into distinct
203 cell populations within the tissue.
204
205 Notably, these signaling dynamics are synchronously followed by cell behavior dynamics. We
206 observed that prolonged JNK/AP-1 signaling correlated with an increased exclusion of
207 proliferation from the pouch (Fig. 2G-J; Fig. 1K,L,N). Altogether, these data suggest that
208 chronic and high levels of JNK/AP-1 activation drive spatial wound site signaling and cell
209 behavior patterns from a local intermixed state to a larger, segregated and bistable field.
210

211 **Figure 3**
212 **JNK/AP-1 acts as a wound organizer by employing a mutual-repression network**
213
214 We wanted to understand the type of regulatory interactions between JNK/AP-1 and
215 JAK/STAT pathways that establish spatially segregated signaling domains on a tissue scale
216 [79-82]. Regulatory networks describe how components of different signaling pathways
217 interact [83-85] or are integrated to define a cell's signaling state and establish distinct cellular
218 outcomes [86, 87]. How regulatory networks can also organize cellular behaviors to influence
219 tissue-level outcomes has been extensively described using mathematical modeling [88-90].
220
221 To characterize the rules of the regulatory network between JNK/AP-1 and JAK/STAT that
222 ultimately drives emergence of spatial segregation to organize tissue stress responses, we
223 developed a mathematical model using partial differential equations. These described the
224 spatio-temporal evolution of JNK/AP-1 and JAK/STAT activation depending on relative
225 concentrations of components in the system (Fig. 3A-C) [86, 91]. We defined a set of
226 experimentally determined rules, namely: (1) JNK/AP-1 effectors propagate JNK/AP-1 via
227 production of paracrine factors, such as *egr* or diffusible ROS [28, 54, 92]; (2) JNK/AP-1
228 effectors activate JAK/STAT via production of paracrine factors, such as *upd*'s [20, 28, 49, 51];
229 (3) Both pathways use positive feedback loops to enhance and stabilize their own activation
230 [42, 55, 56, 93] and (4) JAK/STAT represses JNK/AP-1 cell-autonomously, via the ZEB-1

homologue Zfh2 (Fig. S3A-C) [51]. To simplify the model (Fig. 3B), we excluded negative feedback loops on JNK/AP-1 and JAK/STAT [94-96], as they often have a more modulatory function in noise buffering, temporal processing or saturation dynamics [97].

As we found experimentally that JNK/AP-1 repressed JAK/STAT cell-autonomously, we also designed a mutual repression model that, together with the aforementioned rules, included a rule that JNK/AP-1 represses JAK/STAT signaling (Fig. 3A,B') [98]. Using an unbiased sampling approach of a large parameter space, we compared the ability of the two models to produce simple bistable patterns (Fig. 3D). We found that the mutual repression model produced 140-fold more positive outcomes than a uni-directional model (10588 vs. 72 solutions) (Fig. 3E). When we switched from scoring simple bistable patterns (Fig. 3D) to observed bistable patterns (Fig. 3D') of JNK/AP-1 and JAK/STAT signaling in *egr*-expressing wing discs, the difference in competencies between the two models became even more prominent (Fig. 3E'). The uni-directional model was not sufficient to recapitulate observed bistable patterns, which suggests that the rule of JNK/AP-1 cell-autonomously repressing JAK/STAT is necessary for generating the segregated JNK/AP-1 and JAK/STAT signaling patterns seen during tissue stress. Accordingly, we show that a mutual-repression network lies at the core of JNK/AP-1 and JAK/STAT signaling interactions in response to tissue damage. Supporting this result, mutual repression networks have been extensively described to guide the formation of bistable states [99-105]. Furthermore, these networks can be further enhanced by self-activation loops, such as those integrated in our model [98, 102, 106]. Indeed, if JNK/AP-1 and JAK/STAT cross-talk were to completely lack mutual repression, JNK/AP-1 and JAK/STAT signaling would be expected to expand from the wound site in an unrestrained manner. Thus, the mutual repression regulatory network also ensures that these signaling pathways remain restricted during regeneration.

The length scale-independent space utilized by the model raises the possibility that this mutual repression network could act at length scales ranging from neighboring cells to multicellular tissues. *In vivo*, length scales may depend on the level of network activation and thus the concentration of non-autonomously acting cytokines (Egr, Upd's), as suggested by experiments shown in (Fig. 2K-P and Fig. S1.2). Indeed, we observed that the number of segregating solutions produced by the model increased with increasing rates of JNK/AP-1 activity (Fig. S3D). This observation parallels the progressive segregation of signaling domains found experimentally upon chronic activation of JNK/AP-1 signaling (Fig. 2K-P).

Taken together we propose that JNK/AP-1 initiates a mutual repression network between JNK/AP-1 and JAK/STAT signaling that, via the production of Upd's, facilitates the spatial

268 segregation of these two pathways. The spatial segregation of JNK/AP-1 and JAK/STAT via
269 mutual repression allows the tissue to maintain a JNK-dependent G2 stall in the presence of
270 pro-mitogenic signals, and restricts proliferation to a separate cell population. Thus, induction
271 of JNK/AP-1 signaling upon tissue damage and mutual repression with JAK/STAT is sufficient
272 to set up temporal and spatial signaling patterns, and functionally distinct cell populations.
273

274 **Figure 4**
275 **Ptp61F represses JAK/STAT activity in JNK/AP-1 signaling cells**
276

277 To understand how JNK/AP-1 may cell-autonomously repress JAK/STAT activation, we first
278 asked if JNK/AP-1 downregulates core components of the JAK/STAT pathway. Our previous
279 study demonstrated that the core components *dome*, *hop* and *stat92E* [107] were not
280 transcriptionally altered in *egr*-expressing discs [51]. Supporting this observation, we found
281 that the expression of GFP-tagged Hop [108] and Stat92E proteins from functionally validated
282 lines were unaltered in *egr*-expressing cells (Fig. S4.1A-I). This suggested that repression of
283 JAK/STAT signaling was likely due to altered function of regulators of JAK/STAT signaling. We
284 thus analyzed known negative regulators in *egr*-expressing discs. Levels of dPIAS/Su(var)2-
285 10 [109] and Apontic [110] were unchanged, but *ken* expression [111] was elevated in *egr*-
286 expressing discs (Fig. S4.2A-F). However, neither knock-down of *ken* nor *dPIAS/Su(var)2-10*
287 increased JAK/STAT activity in *egr*-expressing cells (Fig. S4.2G-L). Similarly, we could not
288 reproduce findings that knockdown of *apontic* reinstated JAK/STAT signaling in *egr*-expressing
289 discs (Fig. S4.2M-O) [112].
290

291 We then turned to the tyrosine phosphatase *Ptp61F,* a known repressor of Stat92E activation
292 [113, 114] which is transcriptionally induced in JNK-dependent tumors and other stress
293 conditions [23, 115]. Repression of JAK/STAT signaling by Ptp61F may occur at the level of
294 receptor complex signaling or Stat92E activity [113, 114, 116]. We found that knock-down of
295 *ptp61F* caused upregulation of the Stat92E reporter activity in high JNK-signaling cells of *egr*-
296 expressing discs (Fig. 4A-E, Fig. S4.3A-C). This suggests that Ptp61F is specifically required
297 in JNK-signaling cells to suppress Stat92E activity. Hence, to test if dephosphorylation of
298 Stat92E in JNK-signaling cells is rate-limiting for JAK/STAT signaling, we overexpressed an
299 HA-tagged Stat92E [117] in *egr*-expressing cells to saturate the dephosphorylation capacity of
300 Ptp61F. Indeed, *egr,stat92E-HA*-coexpressing cells in the central pouch domain activated the
301 JAK/STAT reporter at higher levels when compared to *egr*-expressing discs (Fig. 4F-J, Fig.
302 S4.3D,E). In contrast, co-expression of the JAK *hop* failed to induce JAK/STAT reporter activity
303 in *egr*-expressing discs (Fig. S4.3F-I). Importantly, this demonstrates that while signal
304 transduction from Upd ligands down to the effector Stat92E is in principle active in JNK-

305 signaling cells, it is the Ptp61F-mediated dephosphorylation of Stat92E that becomes rate-
306 limiting for JAK/STAT signaling.
307

308 **Figure 5**
309 **JAK/STAT repression is required for the G2 stall and protects central wound cells from**
310 **apoptosis**
311

312 As spatial segregation of JNK/AP-1 and JAK/STAT signaling domains was a robust feature of
313 *egr*-expressing discs, we wondered if the mutual repression network was necessary for
314 regeneration. We therefore forced expression of Stat92E in high JNK/AP-1 signaling cells, and
315 closely monitored cell and tissue level responses, such as cell survival and proliferation. The
316 loss of JNK/AP-1 and JAK/STAT segregation led to a pronounced increase in apoptosis (Fig.
317 5A-D). Co-expression of UAS-GFP confirmed that these apoptotic cells originated from cells
318 where JNK/AP-1 and JAK/STAT were forcibly co-activated (Fig. S5A-D).
319

320 We thus hypothesized that JAK/STAT interfered with the protective G2-stall of high JNK-
321 signaling cells, and thereby increased apoptosis [31, 37], While Stat92E expression altered
322 the proportion of S-phase cells in undamaged control discs, we observed no changes in the
323 proportion of cells in G1 or G2 (Fig. S5E-H). In contrast, a cell cycle analysis of *egr,Stat92E-*
324 *HA* co-expressing domains revealed a substantial increase in G1 and S-phase cells, indicating
325 that JNK-signaling cells failed to stall in G2 (Fig. 5E-J). Thus, forced Stat92E activation in high
326 JNK-signaling cells overrides the protective JNK-induced G2 stall and consequently increases
327 apoptosis. Supporting these results, we found that knock-down of Ptp61F in *egr*-expressing
328 discs also led to an increase in cycling cells in the tissue (Fig. 5O,P) correlating with increased
329 levels of apoptosis (Fig. 5K-N). This highlights the necessity of JNK/AP-1 and JAK/STAT
330 signaling segregation within the tissue, as it maintains the G2 stalled cell population. Thus, the
331 JNK-induced mutual repression network ensures the establishment of two distinct and
332 indispensable cell populations - one that stalls in G2 to prevent apoptosis and secrete
333 necessary pro-mitogenic factors like Upd and other paracrine effectors like Dilp8 and ImpL2
334 [20, 74], and a second that is able to respond to mitogenic signals and undergoes proliferation
335 necessary for regeneration. The strong similarities with paracrine signaling centers regulating
336 spatial patterning networks linked to specific cell behaviors and fate during development
337 encourages us to propose that the JNK-induced mutual repression network with JAK/STAT
338 functions as a central wound organizer network [118, 119].
339

340 **Figure 6**
341 **The wound organizer network segregates JNK/AP-1 and JAK/STAT signaling to drive**
342 **oncogenic growth**
343
344 Our observation that tissue repair processes after chronic damage support the establishment
345 of a signaling-sending and a responding cell population, which are respectively G2-stalled or
346 proliferative, led us to speculate that such a wound organizer network could well-support a
347 tumor microenvironment. Interestingly, the coexistence of JNK/AP-1 and JAK/STAT pathways
348 in tumors has been extensively described [18-23] and the existence of signal-sending G2-
349 stalled cells controlling non-autonomous proliferation has been demonstrated [31]. However,
350 their spatial patterns have not been well defined.
351
352 To understand if JNK/AP-1 and JAK/STAT also engage in a mutual repression network under
353 tumor conditions, we analyzed discs with a reduction in the well-characterized *scrib* tumor-
354 suppressor gene [120] or ectopic expression of oncogenic $Ras^{V12}$ [121, 122]. To generate a
355 large genetically homogenous tissue, we used the pouch specific *rn-GAL4* driver to express
356 $Ras^{V12}$ or *scrib-RNAi* in the entire wing pouch. A wing pouch expressing oncogenic $Ras^{V12}$ for
357 44 h did not activate JNK/AP-1 or JAK/STAT reporters, demonstrating that $Ras^{V12}$ alone does
358 not co-opt either pathway (Fig. 6A,B, Fig. S6A,B). RNAi-driven knock-down of *scrib* induced
359 barrier dysfunction (Fig. S6C,D) and, consistent with previous reports [123, 124], moderately
360 activated both JNK/AP-1 and JAK/STAT in the pouch (Fig. S6E-H). A closer examination,
361 however, revealed that the *scrib-RNAi* expressing pouch predominantly segregated JNK/AP-
362 1 and JAK/STAT signaling at the level of small cell clusters, while only few cell clusters
363 displayed co-activation of both pathways (Fig. 6C). This pattern mirrored our observations of
364 short-term *egr*-expression (Fig. S2L,M), thus suggesting that different contexts of mild JNK-
365 activation cause segregation at short distances. These observations indicate that JNK/AP-1
366 activation upon barrier dysfunction via disruption of cell polarity also induces the wound
367 organizer network, which subsequently sets up a bistable segregation of both pathways even
368 at a short range between neighboring cells.
369
370 Curiously, if $Ras^{V12}$ and *scrib* mutations occur in the same cell, they cooperate to cause
371 dramatic overproliferation of imaginal discs, which is not observed in single $Ras^{V12}$ or *scrib*
372 mutant tissues. This cooperativity is thought to be driven by activation of JNK/AP-1, as a
373 consequence of *scrib* disrupting cell polarity. JNK/AP-1 signaling then induces *upd's* and
374 JAK/STAT activation, which can be utilized by a $Ras^{V12}$ controlled network to drive overgrowth
375 [18, 122]. We thus wondered if $Ras^{V12}$ may disable the mutual repression motif between
376 JNK/AP-1 and JAK/STAT. This would allow autocrine activation of JAK/STAT by JNK signaling
377 in the same cell, as generally described in the literature [18, 122]. Cells driven to cycle despite

activation of JNK/AP-1 may then be protected by anti-apoptotic functions of $Ras^{V12}$. We wanted to test this hypothesis and closely monitored JNK/AP-1 and JAK/STAT signaling as well as cell proliferation in $Ras^{V12}$ and *scrib RNAi*-coexpressing discs. Surprisingly, we found that JNK/AP-1 and JAK/STAT activation were still clearly segregated into exclusive signaling domains (Fig. 6D-F, Fig. S6I) with proliferation still predominantly associated with JAK/STAT (Fig. 6G-I). This suggests that even in a $Ras^{V12}$ and *scrib* cooperativity model, where all cells are genetically identical, bistability driven by the mutual repression network organizes the pouch into distinct JNK/AP-1 or JAK/STAT-signaling domains. This observation aligns with previous observations that cooperativity between Ras and *scrib* can rely, in principle, on non-autonomous interactions [18, 125]. Crucially however, our observations demonstrate that non-autonomous cooperation between JNK/AP-1-activating and $Ras^{V12}$ mutation arises as a self-organizing principle from a wound organizer network creating segregating signaling domains in a genetically homogenous tumorigenic tissue. Moreover, it suggests that activation of this wound organizer network and segregation of signaling and proliferative tasks may provide an advantage to tumors over autocrine integration of JNK/AP-1 and JAK/STAT signaling in the same cell.

## Discussion

Previous studies established a role for JNK/AP-1 in promoting regeneration upon injury [35, 59]. This role is, in part, mediated by the expression of *upd's* which are essential to promote proliferation and survival via JAK/STAT signaling in a non-autonomous manner [28, 35, 48, 51, 126-129]. By identifying a mutual repression network between JNK/AP-1 and JAK/STAT, we conceptually establish JNK as a core organizer of tissue repair with parallels to organizers of cell fate patterning in developing tissues. The rules of the wound regulatory network we describe have important implications. Previous reports suggest that JNK/AP-1 activates itself non-autonomously, for example via activation of paracrine *egr* or ROS [28, 54, 92]. This implies that JNK/AP-1 activation could result in unchecked spatial expansion of JNK/AP-1-signaling, and accordingly of JAK/STAT signaling. Their unrestrained co-expansion would likely result in chronic inflammation. However, the mutual repression motif restrains the expansion of both JNK/AP-1 and JAK/STAT signaling domains, thus defining stable regions of inflammatory (mitogenic signals) and regenerative (pro-proliferative) responses at the start of the tissue repair process. We demonstrate that molecular mediators of mutual repression are Zfh2 downstream of JAK/STAT [51], and Ptp61F downstream of JNK.

At the level of cell behaviors, JNK/AP-1 and JAK/STAT generate mutually exclusive responses (Fig. 7B). JNK/AP-1 signaling supports wound center behaviors like tissue sealing [24, 25, 78],

415 cell fusion [14], establishment of paracrine signaling and importantly, an apoptosis-resistant
416 state that depends on a G2 cell cycle stall [31]. In contrast, JAK/STAT signaling supports
417 wound-distal behaviors, such as compensatory proliferation, potentially via upregulation of G1-
418 S cyclins such as CycD or CycE [130, 131].
419
420 By reducing Stat92E activation upon damage, JNK/AP-1 creates a permissive state for the G2
421 stall by preventing cycling, thereby protecting cells from apoptosis in a cytotoxic, inflammatory
422 environment (Fig. 7C; Fig. S1A). When high levels of both pathways are co-activated in the
423 same cell, the anti-apoptotic state of the G2 stall is in conflict with proliferative outcomes and
424 therefore active cycling which causes an increase in apoptosis. Consequently, apoptosis of
425 these wound center signaling cells could jeopardize wound organizer function and ultimately
426 tissue repair behaviors (Fig.7D). Therefore, the JNK-activated G2-stall and JAK/STAT-
427 activated cell cycling need to be spatially segregated. Importantly, our observations indicate
428 that, with exceptions [132], even successful tumors avoid coexistence of JNK and JAK/STAT
429 signaling in the same cell as they do not profit from the conflicting cell-autonomous inputs on
430 proliferation and survival decisions. Instead, tumors may highjack a wound organizer network
431 to chronically activate paracrine mitogenic signals but outsource proliferation to other cells as
432 a consequence of the senescent properties of JNK-signaling, G2-stalled cells [31].
433
434 We find that spatial patterns generated by the JNK/AP-1 and JAK/STAT regulatory network
435 act at different length scales, depending on the duration and strength of JNK/AP-1 activation
436 (Fig. 7A). Transient or low JNK/AP-1 activity generates short range spatial segregation of
437 JNK/AP-1 and JAK/STAT. Specifically, we observed their segregation between neighboring
438 cells upon transient expression of *egr* or mild disruption of barrier function in *scrib*-RNAi
439 expressing tissue. Cell-by-cell segregation may allow tissue repair processes to respond
440 dynamically. Switching between (1) a stalled, apoptosis-resistant state supporting survival and
441 paracrine signaling in an inflammatory environment or (2) a regenerative, proliferative
442 phenotype could facilitate continuous integration of the repair state. As wound healing
443 progresses and the JNK/AP-1 signaling field shrinks, shifting spatial probabilities of stalled and
444 cycling cells would ultimately resolve the damage.
445
446 In contrast, prolonged or high JNK/AP-1 activity segregates JAK/STAT signaling more robustly
447 and consequently into larger bistable fields, prolonging wound resolution and increasing the
448 risk for chronic wound pathologies. Indeed, prolonged JNK/AP-1 activity in $Ras^{v12}$,*scrib*-RNAi
449 tumors or by chronic expression of *egr* drives robust bistable segregation of JNK/AP-1 and
450 JAK/STAT signaling into larger domains. Similarly, chronic wounds in human patients display
451 striking segregation of cellular responses. In a central inflammatory domain, cells acquire

452 senescent phenotypes, arrest and fail to proliferate. In the periphery, a hyperproliferative edge
453 is evidence of chronic mitogenic signals emanating from the wound [3, 9, 10, 133]. These
454 clinical patterns resemble patterning in *egr*-expressing discs, thereby suggesting that
455 *Drosophila* imaginal discs may represent a suitable model to study wound pathologies driven
456 by prolonged activation of inflammatory signaling.

457 **Materials and Methods**

458

459 **Fly stocks**

460 All fly stocks and experimental crosses were maintained on standard media and raised at 18 °C
461 or room temperature (22 °C) unless otherwise specified. For detailed genotypes, please refer
462 to Table S1 and S2.

463

464 Table S1 Key Resources Table

| **Designation - Genetic reagent** (*D. melanogaster*) | **Source or Reference** | **Identifiers** | **Additional information** |
|---|---|---|---|
| *'RFP': Act5C>FRT.CD2>GAL4, UAS-RFP* | PMID: 29494583 | BDSC: 30558 | |
| *'apt-RNAi': UAS-apt RNAi (TRiP.JF02134)* | PMID: 26320097 | BDSC: 26236 | |
| *'Dif-GFP': Pbac(Dif-GFP.FPTB)VK00033* | | BDSC: 42673 | |
| *dome$^{G0441}$* | PMID: 11751581 | BDSC: 12030 | |
| *'dome-GFP': FlyFos (dome::TGVBF)* | PMID: 26896675 | VDRC: 318098 | |
| *'E2F1-FUCCI, CycB-FUCCI'; Ubi-GFP.E2f1$^{1-230}$, Ubi-mRFP1.NLS.CycB$^{1-266}$* | PMID: 24726363 | BDSC: 55123 | |
| *'egr$^{ts}$': tub-GAL80ts, UAS-egr* | | | I.Hariharan, University of California, Berkeley |
| *'en>RFP': enGAL4, UAS-mRFP.NLS* | | BDSC: 30557 | |
| *GFP-HP-1* | PMID: 18316477 | BDSC: 30561 | |
| *gstD-GFP* | PMID: 18194654 | | D. Bohmann, University of Rochester Medical Center |
| *'hep$^{act}$': UAS-hep$^{act}$* | PMID: 10903185 | BDSC: 9306 | |
| *'hop': UAS-hop.H* | PMID: 7796812 | BDSC: 79033 | |
| *hop$^{34}$* | PMID: 3095163 | | N. Perrimon |
| *'hop-GFP': FlyFos (hop::TGVBF)* | PMID: 26896675 | VDRC: 318158 | |
| *hsflp$^{122}$* | | | D. Bilder, University of California, Berkeley |
| *'GFP': UAS-GFP S56T* | | BDSC: 1521 | |
| *'ken-LacZ': P{PZ}ken$^{02970}$* | PMID: 10471706 | BDSC: 11244 | |
| *'ken-RNAi': UAS-ken-RNAi (TRiP.HMS01219)* | PMID: 26320097 | | |
| *'ptp61f-RNAi': UAS-ptp61f-RNAi $^{i2-5}$* | PMID: 19398577 | BDSC: 56510 | |
| *'p35': UAS-p35.H* | PMID: 9144202 | BDSC: 5072 | |
| *'rn(ts)>': rn$^{GAL4\text{-}DeltaS}$, tubGAL80$^{ts}$* | | BDSC: 8142 | recombinant |
| *'rn(ts)>egr': rn$^{GAL4\text{-}5}$, UAS-egr, tubP-GAL80$^{ts}$* | | BDSC: 8142; BDSC: 7018 | recombinant; I.Hariharan, University of California, Berkeley |
| *'Ras$^{v12}$, scrib-RNAi': UAS-Ras$^{v12}$,scrib-RNAi* | | | M. Uhlirova, University of Cologne |
| *'Ras$^{v12}$': UAS-Ras$^{v12}$* | | | H. Richardson, University of Melbourne |
| *'rnE/F-EGFP': rn(E/F)-EGFP (ds Red+)* | PMID: 26497147 | | P. Volkan, Duke University School of Medicine |
| *'scrib-RNAi': UAS-scrib RNAi* | | | M. Uhlirova, University of Cologne |
| *'Stat92E': UAS-Stat92E.ORF.3xHA* | PMID: 23583758 | Fly-ORF F000750 | |
| *'Stat92E$^{85c9}$ ': FRT82B stat92E$^{85c9}$* | | | E. Bach, New York University School of Medicine |
| *'Stat92E>dGFP': 10xStat92E>dGFP* | PMID: 17008134 | | |

| | | | |
|---|---|---|---|
| *'Stat92E>GFP': 10xStat92E>GFP* | PMID: 17008134 | | |
| *'Stat92E-GFP': PBac{Stat92E-GFP.FLAG}$^{VK00037}$* | | BDSC: 38670 | |
| *'su(var)2-10-GFP': PBac{Su(var)2-10-GFP.FPTB}$^{VK00037}$* | PMID: 29284660 | BDSC: 64795 | |
| *'su(var)2-10-RNAi': UAS- Su(var)2-10-RNAi $^{TRiP.HMS00750}$* | PMID: 26320097 | BDSC: 32956 | |
| *'TRE>RFP': TRE-DsRed.T4* | PMID: 22509270 | | |
| *'Xbp1-GFP': UAS-Xbp1-GFP.HG* | PMID: 23160805 | BDSC: 60731 | |
| *upd3.1-3-LacZ* | | | I.Hariharan, University of California, Berkeley |
| *upd-LacZ: upd>LacZ (PD1)* | PMID: 8582614 | | Y. H. Sun, Academia Sinica, Taipei |
| *$w^{118}$* | | | |
| *'zfh2': UAS-Zfh2[EAB]* | PMID: 24172131 | | F. Diaz-Benjumea, Universidad Autónoma de Madrid |

| **Antibodies / Commercial Kits** | **Source or Reference** | **Identifiers** | **Dilution** |
|---|---|---|---|
| Chicken anti-GFP | Abcam | Cat. #: ab13970 | (1:1000) |
| Mouse anti-H3-pS10 | Abcam | Cat. #: ab14955 | (1:2000) |
| Mouse anti-β-Galactosidase | Promega | Cat. #: Z3782 | (1:1000) |
| Mouse monoclonal anti-MMP-1 | DSHB | Cat. #: 3A6B4 | (1:30) |
| Mouse monoclonal anti-MMP-1 | DSHB | Cat. #: 3B8D12 | (1:30) |
| Mouse monoclonal anti-MMP-1 | DSHB | Cat. #: 5H7B11 | (1:30) |
| Mouse monoclonal anti-Nubbin | DSHB | Cat. #: 2D4 | (1:100) |
| Mouse monoclonal anti-α-Tubulin | Sigma-Aldrich | Cat. #: T9026 | (1:5000) |
| Rabbit anti-cleaved Dcp-1 | Cell Signaling | Cat. #: 9578 | (1:200) |
| Rabbit monoclonal anti-GFP | Invitrogen | Cat. #: G10362 | (1:200) |
| Rabbit polyclonal anti-apt | R. Schuh, MPI-MS, Göttingen | NA | (1:200) |
| Rat monoclonal anti-GFP | Chromotek | Cat. #: 3H9-100 | (1:1000) |
| Rat monoclonal anti-HA | Monoclonal Antibody Core Facillity at the Helmholtz Zentrum München | Clone #: 3F10 | (1:20) |
| Rat monoclonal anti-RFP | | Clone #: 5F8 | (1:20) |
| Click-iT Plus EdU Alexa Fluor 647 Imaging Kit | Invitrogen | Cat. #: C10640 | |

PMID – PubMed Identifier; BDSC – Bloomington Drosophila Stock Center; DSHB – Developmental Studies Hybridoma Bank, VDRC – Vienna Drosophila Stock Collection, FlyORF – University of Zurich ORFeome Project

465

466 Table S2. Detailed Genotypes

| **Figure** | **Panel** | **Genotype** | **Temperature shift** | **Recovery** |
|---|---|---|---|---|
| Figure 1 | A | *TRE-RFP; 10xStat92E>dGFP* | 24h 30°C, D7 AED | - |
| Figure 1 | B | *TRE-RFP; 10xStat92E>dGFP/rn-GAL4, tub-GAL80$^{ts}$, UAS-egr* | 24h 30°C, D7 AED | - |
| Figure 1 | C | *Ubi-GFP.E2f1$^{1-230}$, Ubi-mRFP1.NLS.CycB$^{1-266}$; rn-GAL4, tub-GAL80$^{ts}$* | 24h 30°C, D7 AED | - |
| Figure 1 | D | *Ubi-GFP.E2f1$^{1-230}$, Ubi-mRFP1.NLS.CycB$^{1-266}$; rn-GAL4, tub-GAL80$^{ts}$, UAS-egr* | 24h 30°C, D7 AED | - |
| Figure 1 | E | *TRE-RFP; Upd3.1-3-LacZ/rn-GAL4, tub-GAL80$^{ts}$* | 24h 30°C, D7 AED | - |
| Figure 1 | F,M | *TRE-RFP; Upd3.1-3-LacZ/rn-GAL4, tub-GAL80$^{ts}$, UAS-egr* | 24h 30°C, D7 AED | - |
| Figure 1 | G,I,K | *TRE-RFP; 10xStat92E>dGFP/rn-GAL4, tub-GAL80$^{ts}$* | 24h 30°C, D7 AED | - |
| Figure 1 | H,J,L,N | *TRE-RFP; 10xStat92E>dGFP/rn-GAL4, tub-GAL80$^{ts}$, UAS-egr* | 24h 30°C, D7 AED | - |
| Figure S1.1 | D | *rn-GAL4, tub-GAL80$^{ts}$* | 24h 30°C, D7 AED | - |

| | | | | |
|---|---|---|---|---|
| Figure S1.1 | E | *rn-GAL4, tub-GAL80$^{ts}$, UAS-egr* | 24h 30°C, D7 AED | - |
| Figure S1.1 | F | *Upd-LacZ/X; TRE-RFP; TM6B, tub-GAL80* | 24h 30°C, D7 AED | - |
| Figure S1.1 | G | *Upd-LacZ/X; TRE-RFP; rn-GAL4, tub-GAL80$^{ts}$, UAS-egr* | 24h 30°C, D7 AED | - |
| Figure S1.1 | H | *SuVar2-10 GFP/rn-GAL4, tub-GAL80$^{ts}$* | 24h 30°C, D7 AED | - |
| Figure S1.1 | I | *SuVar2-10 GFP/rn-GAL4, tub-GAL80$^{ts}$, UAS-egr* | 24h 30°C, D7 AED | - |
| Figure S1.1 | J | *gstD-GFP; rn-GAL4, tub-GAL80$^{ts}$* | 24h 30°C, D7 AED | - |
| Figure S1.1 | K | *gstD-GFP; rn-GAL4, tub-GAL80$^{ts}$, UAS-egr* | 24h 30°C, D7 AED | - |
| Figure S1.1 | L | *UAS-Xbp1-GFP.HG/ rn-GAL4, tub-GAL80$^{ts}$* | 24h 30°C, D7 AED | - |
| Figure S1.1 | M | *UAS-Xbp1-GFP.HG/ rn-GAL4, tub-GAL80$^{ts}$, UAS-egr* | 24h 30°C, D7 AED | - |
| Figure S1.1 | N | *TRE-RFP; Dif-GFP/rn-GAL4, tub-GAL80$^{ts}$* | 24h 30°C, D7 AED | - |
| Figure S1.1 | O | *TRE-RFP; Dif-GFP/rn-GAL4, tub-GAL80$^{ts}$, UAS-egr* | 24h 30°C, D7 AED | - |
| Figure S1.2 | B,E | *TRE-RFP; 10xStat92E>dGFP/rn-GAL4, tub-GAL80$^{ts}$* | 0h 30°C, D7 AED | - |
| Figure S1.2 | C,F | *TRE-RFP; 10xStat92E>dGFP/rn-GAL4, tub-GAL80$^{ts}$* | 7h 30°C, D7 AED | - |
| Figure S1.2 | D,G | *TRE-RFP; 10xStat92E>dGFP/TM6B, tub-GAL80$^{ts}$* | 14h 30°C, D7 AED | - |
| Figure S1.2 | H,K | *TRE-RFP; 10xStat92E>dGFP/rn-GAL4, tub-GAL80$^{ts}$, UAS-egr* | 0h 30°C, D7 AED | - |
| Figure S1.2 | I,L | *TRE-RFP; 10xStat92E>dGFP/rn-GAL4, tub-GAL80$^{ts}$, UAS-egr* | 7h 30°C, D7 AED | - |
| Figure S1.2 | J,M | *TRE-RFP; 10xStat92E>dGFP/rn-GAL4, tub-GAL80$^{ts}$, UAS-egr* | 14h 30°C, D7 AED | - |
| Figure 2 | A | *hsflp$^{122}$; UAS-p35; 10xStat92E>dGFP/Act5C.GAL4 (FRT.CD2), UAS-RFP* | 10' HS 37°C, D7 AED | 28h 22°C |
| Figure 2 | B,C | *hsflp$^{122}$; UAS-p35/UAS-hep$^{act}$; 10xStat92E>dGFP/Act5C.GAL4 (FRT.CD2), UAS-RFP* | 10' HS 37°C, D7 AED | 28h 22°C |
| Figure 2 | D | *hsflp$^{122}$; UAS-p35/UAS-hep$^{act}$; 10xStat92E>dGFP/Act5C.GAL4 (FRT.CD2), UAS-RFP* | 7' HS 37°C, D5 AED | 48h 22°C |
| Figure 2 | E | *TRE-RFP; 10xStat92E>dGFP* | 24h 30°C, D7 AED | - |
| Figure 2 | F | *enGAL4-mRFP.NLS/TRE-RFP; 10xStat92E>dGFP/tub-GAL80$^{ts}$, UAS-egr* | 24h 30°C, D7 AED | - |
| Figure 2 | G | *TRE-RFP; 10xStat92E>dGFP/rn-GAL4, tub-GAL80$^{ts}$* | 7h 30°C, D7 AED | - |
| Figure 2 | H,K,N | *TRE-RFP; 10xStat92E>dGFP/rn-GAL4, tub-GAL80$^{ts}$, UAS-egr* | 7h 30°C, D7 AED | - |
| Figure 2 | I | *TRE-RFP; 10xStat92E>dGFP/rn-GAL4, tub-GAL80$^{ts}$* | 14h 30°C, D7 AED | - |
| Figure 2 | J,L,O | *TRE-RFP; 10xStat92E>dGFP/rn-GAL4, tub-GAL80$^{ts}$, UAS-egr* | 14h 30°C, D7 AED | - |
| Figure 2 | M,P | *TRE-RFP; 10xStat92E>dGFP/rn-GAL4, tub-GAL80$^{ts}$, UAS-egr* | 24h 30°C, D7 AED | - |
| Figure S2 | A | *hsflp$^{122}$; UAS-p35; 10xStat92E>dGFP/Act5C.GAL4 (FRT.CD2), UAS-RFP* | 10' HS 37°C, D7 AED | 28h 22°C |
| Figure S2 | B | *hsflp$^{122}$; UAS-p35; 10xStat92E>dGFP/Act5C.GAL4 (FRT.CD2), UAS-RFP* | 7' HS 37°C, D7 AED | 28h 22°C |
| Figure S2 | C | *hsflp$^{122}$; UAS-p35/UAS-hep$^{act}$; 10xStat92E>dGFP/Act5C.GAL4 (FRT.CD2), UAS-RFP* | 7' HS 37°C, D7 AED | 28h 22°C |
| Figure S2 | D | *hsflp$^{122}$; UAS-p35; rn(E/F)-EGFP/Act5C.GAL4 (FRT.CD2), UAS-RFP* | 7' HS 37°C, D7 AED | 28h 22°C |
| Figure S2 | E,F,G | *TRE-RFP; 10xStat92E>dGFP/rn-GAL4, tub-GAL80$^{ts}$* | 0h,7h,14h 30°C, D7 AED | - |
| Figure S2 | H,I,J,K | *TRE-RFP; 10xStat92E>dGFP/rn-GAL4, tub-GAL80$^{ts}$, UAS-egr* | 0h,7h,14h 30°C, D7 AED | - |
| Figure S2 | L | *TRE-RFP; 10xStat92E>dGFP/rn-GAL4, tub-GAL80$^{ts}$* | 7h 30°C, D7 AED | - |
| Figure S2 | M | *TRE-RFP; 10xStat92E>dGFP/rn-GAL4, tub-GAL80$^{ts}$, UAS-egr* | 7h 30°C, D7 AED | - |
| Figure S3 | A, C | *rn-GAL4, tub-GAL80$^{ts}$, UAS-egr* | 24h 30°C, D7 AED | - |
| Figure S3 | B, C | *rn-GAL4, tub-GAL80$^{ts}$, UAS-egr; UAS-zfh2$^{EAB}$-mCherry* | 24h 30°C, D7 AED | - |

| | | | | |
|---|---|---|---|---|
| Figure 4 | A | *10xStat92E>dGFP/UAS-ptp61F RNAi$^{i2-5}$; rn-GAL4, tub-GAL80$^{ts}$* | 24h 30°C, D7 AED | - |
| Figure 4 | B,D,E | *10xStat92E>dGFP; rn-GAL4, tub-GAL80$^{ts}$, UAS-egr* | 24h 30°C, D7 AED | - |
| Figure 4 | C,D,E | *10xStat92E>dGFP/UAS-ptp61F RNAi$^{i2-5}$; rn-GAL4, tub-GAL80$^{ts}$, UAS-egr* | 24h 30°C, D7 AED | - |
| Figure 4 | F,J | *CycE-lacZ/10xStat92E>dGFP; rn-GAL4, tub-GAL80$^{ts}$* | 24h 30°C, D7 AED | - |
| Figure 4 | G,J | *CycE-lacZ/10xStat92E>dGFP; UAS-Stat92E-3xHA/rn-GAL4, tub-GAL80$^{ts}$* | 24h 30°C, D7 AED | - |
| Figure 4 | H,J | *CycE-lacZ/10xStat92E>dGFP; rn-GAL4, tub-GAL80$^{ts}$, UAS-egr* | 24h 30°C, D7 AED | - |
| Figure 4 | I,J | *CycE-lacZ/10xStat92E>dGFP; UAS-Stat92E-3xHA/rn-GAL4, tub-GAL80$^{ts}$, UAS-egr* | 24h 30°C, D7 AED | - |
| Figure S4.1 | A | *dome$^{G0441}$;; \| dome$^{G0441}$;;dome-GFP* | 24h 30°C, D7 AED | - |
| Figure S4.1 | B | *hop$^{34}$;; \| hop$^{34}$;;hop-GFP* | 24h 30°C, D7 AED | - |
| Figure S4.1 | C | *stat$^{85c9}$/TM6c \| stat$^{85c9}$/stat$^{85c9}$ \| Stat92E-GFP; stat$^{85c9}$/TM6c \| Stat92E-GFP; stat$^{85c9}$/stat$^{85c9}$* | 24h 30°C, D7 AED | - |
| Figure S4.1 | D | *Stat92E-GFP \| GFP-HP1 \| w$^{[118]}$* | D7 AED | - |
| Figure S4.1 | E | *w$^{[118]}$* | 24h 30°C, D7 AED | - |
| Figure S4.1 | F | *hop-GFP/TM6B, tub-GAL80* | 24h 30°C, D7 AED | - |
| Figure S4.1 | G | *hop-GFP/rn-GAL4, tub-GAL80$^{ts}$, UAS-egr* | 24h 30°C, D7 AED | - |
| Figure S4.1 | H,J,M | *Stat92E-GFP;* | 24h 30°C, D7 AED | - |
| Figure S4.1 | I | *Stat92E-GFP; rn-GAL4, tub-GAL80$^{ts}$, UAS-egr* | 24h 30°C, D7 AED | - |
| Figure S4.1 | K,M | *UAS-p35/Stat92E-GFP; rn-GAL4, tub-GAL80$^{ts}$, UAS-egr* | 24h 30°C, D7 AED | - |
| Figure S4.2 | A | *Su(var)2-10-GFP; rn-GAL4, tub-GAL80$^{ts}$* | 24h 30°C, D7 AED | - |
| Figure S4.2 | B | *Su(var)2-10-GFP; rn-GAL4, tub-GAL80$^{ts}$, UAS-egr* | 24h 30°C, D7 AED | - |
| Figure S4.2 | C | *TRE-RFP; 10xStat92E>dGFP/rn-GAL4, tub-GAL80$^{ts}$* | 24h 30°C, D7 AED | - |
| Figure S4.2 | D | *TRE-RFP; 10xStat92E>dGFP/rn-GAL4, tub-GAL80$^{ts}$, UAS-egr* | 24h 30°C, D7 AED | - |
| Figure S4.2 | E | *ken-LacZ$^{02970}$;* | 24h 30°C, D7 AED | - |
| Figure S4.2 | F | *ken-LacZ$^{02970}$; rn-GAL4, tub-GAL80$^{ts}$, UAS-egr* | 24h 30°C, D7 AED | - |
| Figure S4.2 | G | *10xStat92E>dGFP/UAS-ken-RNAi; rn-GAL4, tub-GAL80$^{ts}$* | 24h 30°C, D7 AED | - |
| Figure S4.2 | H,K | *10xStat92E>dGFP; rn-GAL4, tub-GAL80$^{ts}$, UAS-egr* | 24h 30°C, D7 AED | - |
| Figure S4.2 | I | *10xStat92E>dGFP/UAS-ken-RNAi; rn-GAL4, tub-GAL80$^{ts}$, UAS-egr* | 24h 30°C, D7 AED | - |
| Figure S4.2 | J | *10xStat92E>dGFP; UAS-Su(var)2-10-RNAi/rn-GAL4, tub-GAL80$^{ts}$* | 24h 30°C, D7 AED | - |
| Figure S4.2 | L | *10xStat92E>dGFP; UAS-Su(var)2-10-RNAi/rn-GAL4, tub-GAL80$^{ts}$, UAS-egr* | 24h 30°C, D7 AED | - |
| Figure S4.2 | M | *10xStat92E>dGFP; UAS-apt-RNAi/rn-GAL4, tub-GAL80$^{ts}$* | 48h 30°C, D5 AED | - |
| Figure S4.2 | N | *10xStat92E>dGFP; rn-GAL4, tub-GAL80$^{ts}$, UAS-egr* | 48h 30°C, D5 AED | - |
| Figure S4.2 | O | *10xStat92E>dGFP; UAS-apt-RNAi/rn-GAL4, tub-GAL80$^{ts}$, UAS-egr* | 48h 30°C, D5 AED | - |
| Figure S4.3 | A,C | *CyO; 10xStat92E>dGFP* | D7 AED | - |
| Figure S4.3 | B,C | *enGAL4, UAS-mRFP.NLS/UAS-ptp61F RNAi; 10xStat92E>dGFP* | D7 AED | - |
| Figure S4.3 | D | *UAS-GFP; rn-GAL4, tub-GAL80$^{ts}$* | 12h 30°C, D7 AED | - |
| Figure S4.3 | E | *UAS-GFP; UAS-Stat92E-3xHA/rn-GAL4, tub-GAL80$^{ts}$* | 12h 30°C, D7 AED | - |
| Figure S4.3 | F | *10xStat92E>dGFP; rn-GAL4, tub-GAL80$^{ts}$* | 24h 30°C, D7 AED | - |
| Figure S4.3 | G | *10xStat92E>dGFP/UAS-hop.H; rn-GAL4, tub-GAL80$^{ts}$* | 24h 30°C, D7 AED | - |

| | | | | |
|---|---|---|---|---|
| Figure S4.3 | H | *10xStat92E>dGFP; rn-GAL4, tub-GAL80$^{ts}$, UAS-egr* | 24h 30°C, D7 AED | - |
| Figure S4.3 | I | *10xStat92E>dGFP/UAS-hop.H; rn-GAL4, tub-GAL80$^{ts}$, UAS-egr* | 24h 30°C, D7 AED | - |
| Figure 5 | A,C,D | *TRE-RFP; rn-GAL4, tub-GAL80$^{ts}$, UAS-egr* | 24h 30°C, D7 AED | - |
| Figure 5 | B,C ,D | *TRE-RFP; UAS-Stat92E-3xHA/rn-GAL4, tub-GAL80$^{ts}$, UAS-egr* | 24h 30°C, D7 AED | - |
| Figure 5 | E,G,H | *Ubi-GFP.E2f1$^{1-230}$, Ubi-mRFP1.NLS.CycB$^{1-266}$; rn-GAL4, tub-GAL80$^{ts}$* | 24h 30°C, D7 AED | - |
| Figure 5 | F,G,H | *Ubi-GFP.E2f1$^{1-230}$, Ubi-mRFP1.NLS.CycB$^{1-266}$; UAS-Stat92E-3xHA/rn-GAL4, tub-GAL80$^{ts}$, UAS-egr* | 24h 30°C, D7 AED | - |
| Figure 5 | I | *UAS-GFP; rn-GAL4, tub-GAL80$^{ts}$, UAS-egr* | 24h 30°C, D7 AED | - |
| Figure 5 | J | *UAS-Stat92E-3xHA/rn-GAL4, tub-GAL80$^{ts}$, UAS-egr* | 24h 30°C, D7 AED | - |
| Figure 5 | K,O,M,N | *UAS-GFP; rn-GAL4, tub-GAL80$^{ts}$, UAS-egr* | 24h 30°C, D7 AED | - |
| Figure 5 | L,P,M ,N | *UAS-GFP/UAS-ptp61F RNAi$^{i2-5}$; rn-GAL4, tub-GAL80$^{ts}$, UAS-egr* | 24h 30°C, D7 AED | - |
| Figure S5 | A | *UAS-GFP; rn-GAL4, tub-GAL80$^{ts}$* | 24h 30°C, D7 AED | - |
| Figure S5 | B | *UAS-GFP; UAS-Stat92E-3xHA/rn-GAL4, tub-GAL80$^{ts}$* | 24h 30°C, D7 AED | - |
| Figure S5 | C | *UAS-GFP; rn-GAL4, tub-GAL80$^{ts}$, UAS-egr* | 24h 30°C, D7 AED | - |
| Figure S5 | D | *UAS-GFP; UAS-Stat92E-3xHA/rn-GAL4, tub-GAL80$^{ts}$, UAS-egr* | 24h 30°C, D7 AED | - |
| Figure S5 | E | *Ubi-GFP.E2f1$^{1-230}$, Ubi-mRFP1.NLS.CycB$^{1-266}$; rn-GAL4, tub-GAL80$^{ts}$* | 24h 30°C, D7 AED | - |
| Figure S5 | F | *Ubi-GFP.E2f1$^{1-230}$, Ubi-mRFP1.NLS.CycB$^{1-266}$; rn-GAL4, tub-GAL80$^{ts}$, UAS-egr* | 24h 30°C, D7 AED | - |
| Figure S5 | G | *UAS-GFP; rn-GAL4, tub-GAL80$^{ts}$* | 24h 30°C, D7 AED | - |
| Figure S5 | H | *UAS-Stat92E-3xHA/rn-GAL4, tub-GAL80$^{ts}$* | 24h 30°C, D7 AED | - |
| Figure 6 | A | *TRE-RFP; 10xStat92E>dGFP/rn-GAL4, tub-GAL80$^{ts}$* | 44h 30°C, D6 AED | - |
| Figure 6 | B | *UAS-Ras$^{v12}$/TRE-RFP; 10xStat92E>dGFP/rn-GAL4, tub-GAL80$^{ts}$* | 44h 30°C, D6 AED | - |
| Figure 6 | C,C',G | *UAS-scrib-RNAi/TRE-RFP; 10xStat92E>dGFP/rn-GAL4, tub-GAL80$^{ts}$* | 44h 30°C, D6 AED | - |
| Figure 6 | D,D',E,F,H,I | *UAS-Ras$^{v12}$,scrib-RNAi/TRE-RFP; 10xStat92E>dGFP/rn-GAL4, tub-GAL80$^{ts}$* | 44h 30°C, D6 AED | - |
| Figure S6.1 | A,E | *TRE-RFP; 10xStat92E>dGFP/rn-GAL4, tub-GAL80$^{ts}$* | 44h 30°C, D6 AED | - |
| Figure S6.1 | B | *UAS-Ras$^{v12}$/TRE-RFP; 10xStat92E>dGFP/rn-GAL4, tub-GAL80$^{ts}$* | 44h 30°C, D6 AED | - |
| Figure S6.1 | C | *10xStat92E>dGFP/rn-GAL4, tub-GAL80$^{ts}$* | 48h 30°C, D6 AED | - |
| Figure S6.1 | D | *UAS-scrib-RNAi; 10xStat92E>dGFP/rn-GAL4, tub-GAL80$^{ts}$* | 48h 30°C, D6 AED | - |
| Figure S6.1 | F | *UAS-scrib-RNAi/TRE-RFP; 10xStat92E>dGFP/rn-GAL4, tub-GAL80$^{ts}$* | 44h 30°C, D6 AED | - |
| Figure S6.1 | G,I | *UAS-Ras$^{v12}$,scrib-RNAi/TRE-RFP; 10xStat92E>dGFP/rn-GAL4, tub-GAL80$^{ts}$* | 44h 30°C, D6 AED | - |
| Figure S6.1 | H | *TRE-RFP; 10xStat92E>dGFP/rn-GAL4, tub-GAL80$^{ts}$, UAS-egr* | 44h 30°C, D6 AED | - |

467

468

469

470

471 **Fly genetics**

472 Fosmids carrying GFP-tagged *hop* (VDRC 318158) and *Stat92E* (BDSC 38670) alleles,
473 expressed proteins at expected molecular weights and, at least partially complemented
474 respective null alleles, suggesting that both GFP-fusion proteins are functional. A potential
475 Dome-GFP fosmid (VDRC 318098) failed to give rise to a GFP protein by immunofluorescence
476 and Western blot analysis and failed to complement a *dome* allele, thus Dome levels could not
477 directly be analyzed. Genetic complementation assays were carried out by crossing the GFP-
478 tagged fosmids into the background of LOF mutants (*dome*$^{G0441}$, *hop*$^{9p5}$ and *stat*$^{85C9}$). For X-
479 linked *dome*$^{G0441}$ and *hop*$^{9p5}$ alleles, we calculated the percentage of hemizygous viable adult
480 males emerging from control and experimental crosses (Fig. S4.1A,B). For the autosomal
481 *stat*$^{85C9}$ allele, we determined pupariation success of homozygous mutant larvae by counting
482 the number of pupariated larvae in control and experimental crosses (Fig. S4.1C).

483

484 We validated RNAi lines by demonstrating that they caused changes to the developmental
485 pattern of JAK/STAT activity in the hinge if expressed throughout normal wing disc
486 development. Crosses were set as previously described, using the *en-GAL4* driver to express
487 the RNAi in the posterior compartment. Larvae were kept at 18°C till D7 AEL. On D7, early L3
488 staged larvae were dissected, showing characteristic JAK/STAT reporter activity pattern in the
489 hinge. Following dissection and staining, sibling controls and RNAi expressing discs were
490 mounted on the same slide. All discs were imaged at the same settings and the JAK/STAT
491 reporter intensities were quantified in selected regions in the anterior and posterior hinge (Fig.
492 S4.3C). Intensity values from the anterior compartment (not expressing the RNAi) was used
493 as the internal control.

494

495 **Flip-out clones**

496 GAL4/UAS-driven 'flip-out' overexpression experiments utilized heat-shock-driven expression
497 of a flippase to clonally express *a UAS* construct of choice. After 6h of egg collections, heat-
498 shock was induced on developmental day 5 or 6 at 37°C for 7-10 min . Larvae were dissected
499 at wandering 3rd instar stage or as indicated (28h or 48h after heat-shock, Fig. 2A-D, S2.A-
500 D).

501

502 **Genetic cell ablation using Gal4/UAS/Gal80ts**

503 To induce expression of *egr*, experiments were carried out as described in [31, 38, 51] with
504 few modifications. Briefly, larvae of genotype *rn-GAL4, tub-GAL80*$^{ts}$ and carrying the desired
505 *UAS*-transgenes were staged with a 6h egg collection and raised at 18°C at a density of 50
506 larvae/vial. Overexpression of transgenes was induced by shifting the temperature to 30°C for
507 24h at D7 after egg deposition (AED), and larvae dissected at recovery time point R0 h (Fig.

508 S1.1C) unless noted otherwise. For time course and tumor experiments, transgenes were
509 induced by shifting the temperature to 30°C for 0h, 7h, 14h or 24h at D7 (Fig. S1.2, 2 and S2),
510 or 44h at D6 (Fig. 6 and S6) respectively. Larvae were subsequently dissected for analysis or
511 allowed to recover at 22°C for the indicated time. All images represent R0 h unless noted
512 otherwise. Control genotypes were either *rn*$^{ts}$>, or sibling animals (*+/TM6B, tubGAL80 or*
513 *+/TM6c*) (Smith-Bolton et al. 2009). All experiments were performed with ≥ 2 biological
514 replicates.
515
516 **Immunohistochemistry**
517 Wing discs from third instar larvae were dissected and fixed for 15 min at room temperature in
518 4% paraformaldehyde in PBS. Washing steps were performed in PBS containing 0.1%
519 TritonX-100 (PBT). Discs were then incubated with primary antibodies (described in **Table S1)**
520 in PBT, gently mixing overnight at 4°C. Tissues were counterstained with DAPI (0.25 ng/µl,
521 Sigma, D9542), Phalloidin-Alexa Fluor 488/647 (1:100, Life Technologies) or Phalloidin-
522 conjugated TRITC (1:400, Sigma) during incubation with cross-absorbed secondary antibodies
523 coupled to Alexa Fluorophores (Invitrogen or Abcam) at room temperature for 2h. Tissues were
524 mounted using SlowFade Gold Antifade (Invitrogen, S36936). Whenever possible,
525 experimental and control discs were processed in the same vial and mounted on the same
526 slides to ensure comparability in staining between different genotypes. Images were acquired
527 using the Leica TCS SP8 Microscope, using the same confocal settings and processed using
528 tools in Fiji. Of note, all wing discs expressing the *10xStat92E>dGFP* reporter were boosted
529 with an anti-GFP antibody.
530
531 **EdU Labelling**
532 EdU incorporation was performed using the Click-iT Plus EdU Alexa Fluor 647 Imaging Kit,
533 (described in **Table S1)** prior to primary antibody incubation. Briefly, larval cuticles were
534 inverted in Schneider's medium and incubated with EdU (10µM final concentration) at RT for
535 15 minutes. Cuticles were then fixed in 4% PFA/PBS for 15 minutes, washed for 30 minutes
536 in PBT 0.5%. EdU-Click-iT labeling was performed according to manufacturer's guidelines.
537 Tissues were washed in PBT 0.1%, after which immunostainings, sample processing and
538 imaging were carried out as described above.
539
540 **Western Blots**
541 Cell lysates from third instar wing imaginal discs and brains were prepared in lysis buffer (50
542 mM Tris-HCl pH 7.5, 300mM NaCl, 0.1mM EDTA, 1% Triton X-100, 0.1% SDS, 5% Glycerol,
543 1mM PMSF, 1/10 tablet of Complete Mini Protease Inhibitor Cocktail) on ice. Protein samples
544 were loaded onto a 10% polyacrylamide gel, along with Chameleon Duo Pre-stained Protein

545 Ladder (LI-COR, P/N 928-60000) as a molecular weight ladder and run at 150V. After SDS-
546 PAGE, proteins were transferred onto a nitrocellulose membrane (Bio-Rad, 162-0115,
547 0.45µm) in transfer buffer (25 mM Tris, 192 mM glycine, 20% (v/v) methanol) using the wet-
548 tank method with a current density of 300mA for 1h. Prior to antibody incubation, membranes
549 were blocked with 5% milk in PBS. Membrane was incubated with primary antibodies in PBS-
550 T (1% Triton-X in 1xPBS) - rat anti-GFP (Chromotek, 3H9-100, 1:1000) and mouse anti-α-
551 tubulin (Sigma, T9026, 1:5000) on a rotative plate at 4°C overnight. Primary antibodies were
552 removed and washed in $dH_20$ twice for 5 mins each. Membrane was then incubated with
553 secondary antibodies diluted in PBS-T - donkey α-mouse secondary (LI-COR, 926-68072,
554 1:20000) labelled with a 700nm IRDye and goat α-rat (LI-COR, 926-32219, 1:20000) labelled
555 with an 800nm IRDye. Membrane was washed in $dH_20$ twice for 5 mins each before detection
556 using the Image Studio Software on the Odyssey SA system (LI-COR) (Fig. S4.1D).
557
558 **Image Analysis and Quantification**
559
560 **General comments**
561 Images were processed, analyzed and quantified using tools in Fiji (ImageJ v2.0.0) [134].
562 Extreme care was taken to apply consistent methods (i.e. number of projected sections,
563 thresholding methods, processing) for image analysis. Figure panels were assembled using
564 Affinity Designer v1.10. Statistical analyses were performed in Graphpad Prism or R v3.3.3
565 (www.R-project.org).
566
567 **Total disc area quantification**
568 Maximum intensity projections of z-stacks for each disc were obtained in Fiji. Masks were
569 generated after applying a fixed threshold (10-255) to the DAPI channel and noise was reduced
570 using the 'Despeckle' function. Area measurement from the resulting masks were obtained
571 using the 'Measure' function.
572
573 ***10xStat92E>dGFP* quantification**
574 Maximum intensity projections of selected confocal sections were taken, excluding the
575 peripodium and carefully chosen to capture signaling activity within the disc proper. In the *egr*-
576 expressing or *egr,transgene*-coexpressing discs, a mask of the pouch domain was generated.
577 Region Of Interest (ROI) outlines were either manually drawn on the DAPI channel to include
578 the pouch and hinge domains till the medial hinge fold or by thresholding Nubbin staining.
579 Centroid co-ordinates were identified using the 'Measure' function and marked with a point
580 tool. To measure the fluorescence intensity of the *Stat92E>dGFP* reporter, a square ROI

581 (25x25μm) was placed centrally over the centroid and mean intensity within the ROI was
582 obtained using the 'Measure' function in Fiji. (Fig. 4)
583
584 **Dcp-1 area quantification**
585 Maximum intensity projections of stacks for each disc were obtained in Fiji. Masks were
586 obtained by thresholding for signal of interest. Signal to noise ratio was enhanced by 'Remove
587 outliers' (bright, radius = 1.5) or 'Despeckle' functions. The '3D object counter' function was
588 used to obtain surface area of the generated mask. To control for differences arising from the
589 total size of the discs, ratios between the Dcp-1 area and total WID area were obtained for
590 each disc and reported as percentage values. (Fig. 5C,D,M,N)
591
592 **Tracing JNK, JAK/STAT, EdU and Upd reporters profiles**
593 Partial max projections from confocal stacks of the disc proper were generated, carefully
594 excluding any peripodial signal. For hinge profiles of the JAK/STAT reporter, size-matched
595 discs were chosen and line traces were manually drawn along the hinge using the polygon
596 selection tool. Reporter intensity values from the 'Plot profile' function were averaged for 0h,
597 7h and 14h control and *egr*-expressing discs and plotted. (Fig. S1.2)
598 For reporter patterns along disc center to disc periphery, JNK/AP-1 masks were made using
599 thresholding tools and ROI outlines were generated. Based on ROIs, the centroid value was
600 determined and $n \geq 15$ tracks were drawn from the centroid outwards towards the hinge for a
601 fixed distance - covering the JNK/AP-1 domain, the JNK/AP-1-JAK/STAT interface, and the
602 JAK/STAT signaling domain respectively. Using the 'Plot profile' function in Fiji, the
603 fluorescence intensity values of each reporter was obtained along these tracks and averaged.
604 Reporter patterns for each disc was graphed by scaling the averaged values from each track,
605 between 0 to 1 and plotted on the Y-axis. This was done independently for n≥3 discs, and a
606 representative image was selected for visualization of the spatial trends of the reporters. (Fig
607 1M,N)
608
609 **Density plots for JNK/AP-1 and JAK/STAT reporters**
610 For combined pouch and hinge regions (Fig. 1I,J), the ROI outlines were manually drawn on
611 the DAPI channel to include the pouch and hinge domains till the medial hinge fold. Partial
612 max projections of z-sections from the disc proper were generated, carefully excluding any
613 peripodial signal.
614
615 For time course experiments with *egr*-expressing discs (S2.H-K), a central z-section was
616 chosen and ROIs generated by thresholding the *TRE-RFP* channel to include only the JNK-
617 signaling pouch domain. After applying a 'Gaussian blur' filter (sigma=2), masks were

618 generated by applying a low fixed threshold (value = 10) based on early, 7h *egr*-expressing
619 discs. Noise removal was done using the 'Despeckle' function, followed by 'Fill Hole' function.
620 ROI outlines were generated using 'Create selection'. All ROIs were placed on the source
621 *TRE>RFP* and *Stat92E>dGFP* reporter channels. 'Save X-Y co-ordinates' function was used
622 to obtain pixel fluorescence intensity values for both reporters within the ROI, and the
623 distribution of fluorescence intensities across the samples were graphed by generating a
624 binned (bins = 16) 2D histogram plot using R. After all NA values were set to 0, data density
625 per bin for each disc was calculated as a percentage. Values were averaged across
626 corresponding bins for all discs within a timepoint to generate the average fluorescence
627 intensity distribution profile. To distinguish regions with low, medium and high signaling for
628 each pathway, the graphs were subdivided into sections s1-s9 by defining a threshold to
629 distinguish low, medium and high JNK/AP-1 and JAK/STAT signal intensities (Fig. S2K).
630 Percentage of datapoints within each section was determined from the averaged fluorescence
631 intensity distribution profile. Ordinary 2-way ANOVA with Dunnett's multiple comparisons test
632 was carried out for statistical analysis. Alpha was set at 0.05
633
634 **Cell cycle profiles**
635 Representative sections were selected per disc and a square ROI area (75x75μm$^2$) was placed
636 over the central pouch cells. Only viable cells stained with characteristic euchromatic and
637 heterochromatic DAPI staining were chosen. Using the 'Multi point' tool, cells showing a G1
638 profile (green), G2 profile (yellow+red) or neither (black) were counted. Percentage values for
639 the gap phases were calculated for n≥3 discs per genotype and visualized. T-tests were
640 performed on the calculated G1:G2 ratios per disc. (Fig 5G,H)
641
642 **JAK/STAT reporter quantifications for testing RNAi lines**
643 Crosses were setup as previously described and wing discs from larvae were dissected on D7
644 AED. Single sections at similar focal planes were carefully chosen during imaging. Using
645 drawing tools in Fiji, ROIs were generated to include JAK/STAT signaling cells in the hinge
646 within A and P compartments. The mean JAK/STAT reporter intensity within the ROI was
647 obtained from control and RNAi expressing discs using the 'Measure' function in Fiji. For each
648 dataset, paired t-tests were performed between A and P fluorescence intensity values for the
649 same genotype. (Fig. S4.3A-C)
650
651 **Nuclear translocation of Stat92E-GFP**
652 Images from the pouch (n=12) and hinge (n=9) domains of control discs and pouch (n=16) and
653 hinge (n=12) domains of *p35+egr* expressing discs were obtained to track the intra-cellular
654 localization of *Stat92E-GFP* within the nucleus and cytoplasm. Images were taken at high

655 magnification (63x). After thresholding ('Huang'), the selection tool was used to generate a
656 nuclear ROI using the DAPI channel. The inverse selection tool was used to generate a
657 corresponding cytoplasmic ROI for each image (Fig S4.1L). These nuclear and cytoplamic
658 ROIs were then placed on the *Stat92E-GFP* channel and mean fluorescence intensity values
659 were obtained for each subcellular fraction and unpaired t-tests were performed. (Fig. S4.1M)
660

661 **MMP-1 intensity quantification**

662 To measure the fluorescence intensity of MMP-1 in *egr*-expressing and *egr,zfh2-co*expressing
663 discs, maximum intensity projections of confocal sections were taken. Sections were carefully
664 chosen to capture JNK/AP-1 signaling activity in the disc proper, avoiding the peripodium and
665 cell debris. Square ROIs of fixed length (30 µm) were placed in 3 non-overlapping regions in
666 the pouch domain, and mean intensity was calculated using the 'Measure' function in Fiji. Mean
667 fluorescence intensities obtained from ROIs were averaged per disc and values from each disc
668 per genotype were used for statistical analysis. (Fig. S3A-C)
669

670 **JNK$^+$ and JNK$^-$ Area and intensity quantifications (*Ras$^{v12}$,scrib-RNAi* tumors)**

671 A representative z-section was selected per disc. As our interest was in quantitating the spatial
672 segregation, only JNK/AP-1 or JAK/STAT signaling regions in the tumor were chosen. After
673 applying a 'Gaussian blur' filter (sigma=2), 'Moments' thresholding and 'Despeckle' function
674 for noise correction was applied to generate masks for regions showing *TRE>RFP* (JNK) and
675 *Stat92E>dGFP* (JAK/STAT) reporter activity. From the 'Image calculator' function, 'AND' and
676 'Subtract' operations on JNK/AP-1 and STAT masks were carried out to obtain the JNK$^+$STAT$^+$
677 mask, and the exclusive JNK$^+$ (JNK-STAT) or exclusive JNK$^-$(STAT-JNK) masks respectively.
678 Area of each mask was obtained using the 'Measure' function. Summed area of these masks
679 were considered as the total area and each area was then represented as a percentage of
680 total. One-way paired ANOVA with Holm-Šídák's multiple comparison test was performed to
681 test for statistical significance. Mean intensity for *TRE>RFP* or *10xStat92E>dGFP* reporters
682 were measured inside the JNK/AP-1 mask (JNK$^+$) and the exclusive JNK$^-$ masks. Paired t-
683 tests were performed to test for statistical significance. (Fig. 6E,F and S6I)
684

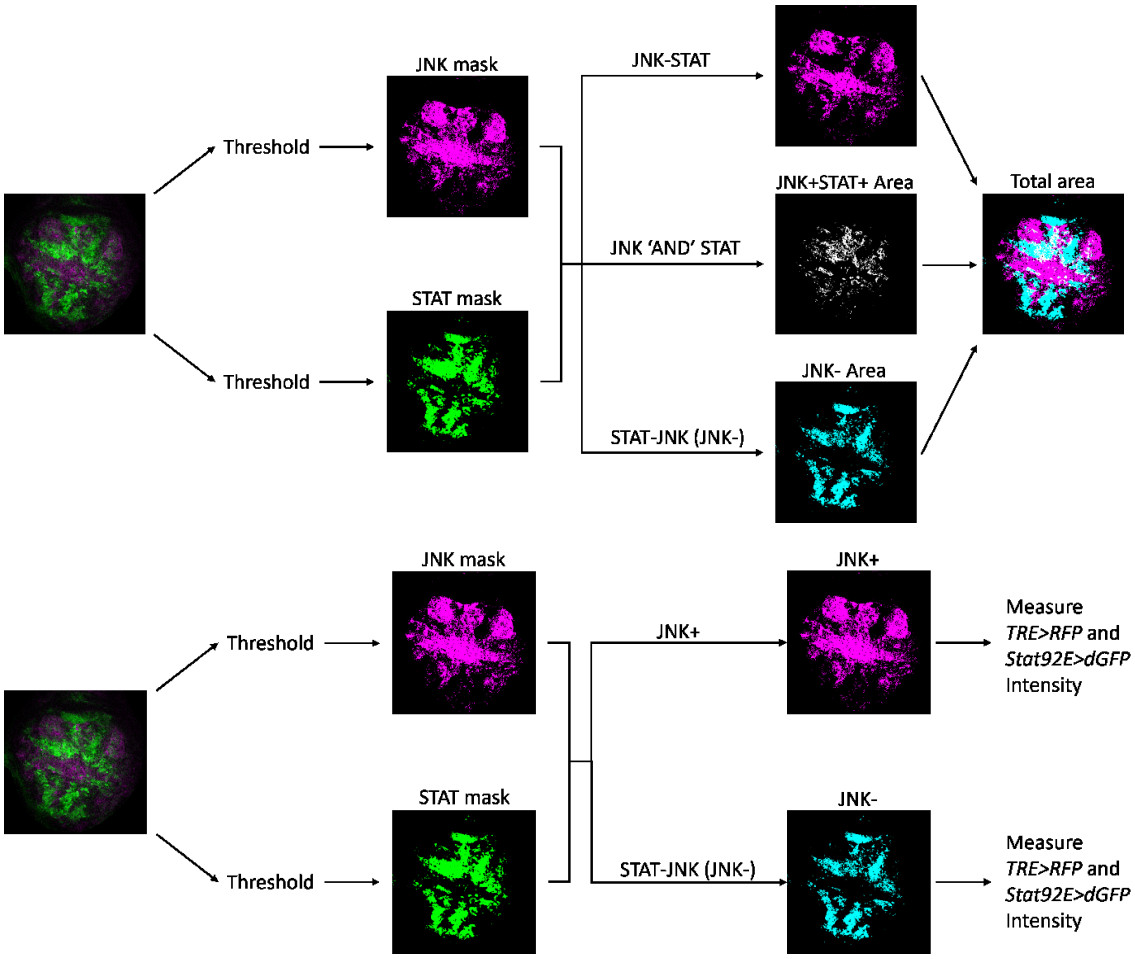


**ph3 counts**

Partial maximum intensity projection of three central z-sections were taken per disc. To generate masks for regions showing *Stat92E>dGFP* reporter activity ($STAT^+$), a 'Gaussian blur' filter (sigma=1), 'Moments' threshold and 'Despeckle' function for noise correction was applied. The DAPI channel was used to manually outline the pouch domain and generate masks. Using the 'Image calculator' function, $STAT^+$ mask was 'Subtract'-ed from the pouch mask to generate the $STAT^-$ mask. Areas of the $STAT^+$ and $STAT^-$ regions in the pouch were obtained using the 'Measure' function. Then, the ph3 channel was duplicated and 'Li' threshold was applied. 'Remove outlier' (radius=5 threshold=50) and 'Despeckle' function for noise correction, followed by 'Watershed' function was applied to generate a ph3 mask. Using the 'AND' operator, the ph3 mask was overlayed with the $STAT^+$ and $STAT^-$ masks. '3D object counter' function was then used to obtain ph3 'Object counts' within the $STAT^+$ and $STAT^-$ regions and divided by area of each ROI to get the ph3 counts per $mm^2$. Paired t-tests were performed to test for statistical significance. (Fig. 6I)

## Mathematical modelling

To test for the existence of a regulatory motif within our signaling network, a mathematical model was derived to describe the temporal dynamics of the concentration of specific molecules over a fixed 2D space. The system was modeled as a set of ordinary differential equations (ODEs) (see also Fig. 3C). Two sets of modeling equations were established, that reflected conditions which include or exclude repression of JAK/STAT by JNK. The term describing repression of JAK/STAT (referred to as 'JAK' in the modeling equations and hereafter) by JNK/AP-1 is highlighted in red.

Uni-directional repression model (see also Fig. 3B):

$$
\begin{aligned}
\frac{d\mathrm{EIG}(t,x)}{dt} &= b_{EIG}(x) - k_{deg,EIG}\mathrm{EIG} + k_{act,EIG}\frac{\mathrm{JNK}^{n_1}}{K^{n_1}_{m,act,EIG} + \mathrm{JNK}^{n_1}} + D_{EIG}\nabla^2 EIG \\
\frac{d\mathrm{JNK}(t,x)}{dt} &= b_{JNK} - k_{deg,JNK}\mathrm{JNK} + k_{act,JNK}\frac{\mathrm{EIG}^{n_2}}{(K^{n_2}_{m,act,JNK} + \mathrm{EIG}^{n_2})(1 + k^{ni1}_{inh,JNK,by,JAK}\mathrm{JAK}^{ni1})} \\
\frac{d\mathrm{JAK}(t,x)}{dt} &= b_{JAK} - k_{deg,JAK}\mathrm{JAK} + k_{act,JAK}\mathrm{UPD}\frac{\mathrm{JAK}^{n_3}}{(K^{n_3}_{m,act,JAK} + \mathrm{JAK}^{n_3})} \\
\frac{d\mathrm{UPD}(t,x)}{dt} &= b_{UPD} - k_{deg,UPD}\mathrm{UPD} + k_{act,UPD}\frac{\mathrm{JNK}^{n_4}}{K^{n_4}_{m,act,UPD} + \mathrm{JNK}^{n_4}} + D_{UPD}\nabla^2 UPD
\end{aligned}
$$

Mutual repression model (see also Fig. 3B'):

$$
\begin{aligned}
\frac{d\mathrm{EIG}(t,x)}{dt} &= b_{EIG}(x) - k_{deg,EIG}\mathrm{EIG} + k_{act,EIG}\frac{\mathrm{JNK}^{n_1}}{K^{n_1}_{m,act,EIG} + \mathrm{JNK}^{n_1}} + D_{EIG}\nabla^2 EIG \\
\frac{d\mathrm{JNK}(t,x)}{dt} &= b_{JNK} - k_{deg,JNK}\mathrm{JNK} + k_{act,JNK}\frac{\mathrm{EIG}^{n_2}}{(K^{n_2}_{m,act,JNK} + \mathrm{EIG}^{n_2})(1 + k^{ni1}_{inh,JNK,by,JAK}\mathrm{JAK}^{ni1})} \\
\frac{d\mathrm{JAK}(t,x)}{dt} &= b_{JAK} - k_{deg,JAK}\mathrm{JAK} + k_{act,JAK}\mathrm{UPD}\frac{\mathrm{JAK}^{n_3}}{(K^{n_3}_{m,act,JAK} + \mathrm{JAK}^{n_3})(1 + k^{ni2}_{inh,JAK,by,JNK}\mathrm{JNK}^{ni2})} \\
\frac{d\mathrm{UPD}(t,x)}{dt} &= b_{UPD} - k_{deg,UPD}\mathrm{UPD} + k_{act,UPD}\frac{\mathrm{JNK}^{n_4}}{K^{n_4}_{m,act,UPD} + \mathrm{JNK}^{n_4}} + D_{UPD}\nabla^2 UPD
\end{aligned}
$$

Characteristic units are represented by state (u), space (x) and time (t). The mathematical terms include, among others, basal rate of production (*b*), activation rate ($k_{act}$), linear degradation rate ($k_{deg}$), Michaelis–Menten constant ($K_m$), inhibition constant ($k_{inh}$), diffusion co-efficients ($D_{EIG}$, $D_{UPD}$), Hill co-efficients to model cooperativity ($n_1, n_2, n_3, n_4$, $ni_1, ni_2$) and Hill kinetics to describe self-amplification and mutual repression.

The first equation describes the dynamics of the concentration of Egr, produced at a basal rate dependent on the spatial co-ordinate x and degraded at a linear rate. Hill kinetics describe the production of Egr induced by JNK/AP-1 and its diffusion away from the source. The second equation describes the dynamics of the concentration of the JNK/AP-1 TF, produced at a basal rate and degraded linearly. Hill kinetics describe production of JNK/AP-1 induced by *egr* as well as inhibition of JNK/AP-1 by JAK [51]. The third equation describes the dynamics of the

concentration of the JAK TF, produced at a basal rate and degraded linearly. Hill kinetics describe positive feedback dependent on Upd. Inhibition of JAK by JNK/AP-1 is described and the model is tested with and without this mathematical term (highlighted in red) to check if this interaction exists within the system. The fourth equation describes the dynamics of the concentration of Upd, produced at a basal rate and degraded linearly. Hill kinetics describe the production of Upd induced by JNK/AP-1 and its diffusion [28, 48, 51].

Technically, the modeling was done based on a non-dimensionalized version of the model, rescaled to reduce the number of free parameters. The system was then defined as follows:

$$
\begin{aligned}
\frac{d\mathrm{EIG}(t,x)}{dt} &= \gamma\left(1(x) - \mathrm{EIG} + k_{act,EIG}\frac{\mathrm{JNK}^{n_1}}{K^{n_1}_{m,act,EIG} + \mathrm{JNK}^{n_1}}\right) + \nabla^2 EIG \\
\frac{d\mathrm{JNK}(t,x)}{dt} &= \gamma\left(1 - k_{deg,JNK}\mathrm{JNK} + k_{act,JNK}\frac{\mathrm{EIG}^{n_2}}{(K^{n_2}_{m,act,JNK} + \mathrm{EIG}^{n_2})(1 + k^{ni1}_{inh,JNK,by,JAK}\mathrm{JAK}^{ni1})}\right) \\
\frac{d\mathrm{JAK}(t,x)}{dt} &= \gamma\left(1 - k_{deg,JAK}\mathrm{JAK} + k_{act,JAK}\mathrm{UPD}\frac{\mathrm{JAK}^{n_3}}{(K^{n_3}_{m,act,JAK} + \mathrm{JAK}^{n_3})(1 + k^{ni2}_{inh,JAK,by,JNK}\mathrm{JNK}^{ni2})}\right) \\
\frac{d\mathrm{UPD}(t,x)}{dt} &= \gamma\left(1 - k_{deg,UPD}\mathrm{UPD} + k_{act,UPD}\frac{\mathrm{JNK}^{n_4}}{K^{n_4}_{m,act,UPD} + \mathrm{JNK}^{n_4}}\right) + d\nabla^2 UPD
\end{aligned}
$$

For each dimensionless parameter, the parameter dependencies and the scanned parameter range are represented in the table below:

| Dimensionless parameter | Functional relation to systems parameter | Scanned parameter range |
|---|---|---|
| $\gamma$ | $k_{deg,EIG}\ L^2\ /\ D_{EIG}$ | 0.01 ... 10000 |
| $\hat{k}_{deg,JNK}$ | $k_{deg,JNK}\ /\ k_{deg,EIG}$ | 0.01 ... 10000 |
| $\hat{k}_{deg,JAK}$ | $k_{deg,JAK}\ /\ k_{deg,EIG}$ | 0.01 ... 10000 |
| $\hat{k}_{deg,Upd}$ | $k_{deg,Upd}\ /\ k_{deg,EIG}$ | 0.01 ... 10000 |
| $\hat{k}_{act,EIG}$ | $k_{act,EIG}\ /\ b_{EIG}$ | 0.00001 ... 10 |
| $\hat{k}_{act,JNK}$ | $k_{act,JNK}\ /\ b_{JNK}$ | 0.01 ... 10000 |
| $\hat{k}_{act,JAK}$ | $k_{act,JAK}\ D_{EIG}\ /\ L^2\ /\ b_{UPD}\ /\ b_{JAK}$ | 0.01 ... 10000 |
| $\hat{k}_{act,UPD}$ | $k_{act,UPD}\ /\ b_{UPD}$ | 0.01 ... 10000 |
| $\hat{K}_{m,act,EIG}$ | $K_{m,act,EIG}\ D_{EIG}\ /\ L^2\ /\ b_{EIG}$ | 0.00001 ... 10 |
| $\hat{K}_{m,act,JNK}$ | $K_{m,act,JNK}\ D_{EIG}\ /\ L^2\ /\ b_{JNK}$ | 0.01 ... 10000 |
| $\hat{K}_{m,act,JAK}$ | $K_{m,act,JAK}\ D_{EIG}\ /\ L^2\ /\ b_{JAK}$ | 0.01 ... 10000 |
| $\hat{K}_{m,act,UPD}$ | $K_{m,act,UPD}\ D_{EIG}\ /\ L^2\ /\ b_{UPD}$ | 0.01 ... 10000 |
| $\hat{k}_{inh,JAK,by,JNK}$ | $k_{inh,JAK,by,JNK}\ b_{JAK}\ L^2\ /\ D_{EIG}$ | 0.01 ... 10000 |
| $\hat{k}_{inh,JNK,by,JAK}$ | $k_{inh,JNK,by,JAK}\ b_{JNK}\ L^2\ /\ D_{EIG}$ | 0.01 ... 10000 |
| $\hat{n}_i$ | $n_i$ | 1 ... 4 |
| $d$ | $D_{UPD}\ /\ D_{EIG}$ | 1.5 ... 4 |

We performed a global analysis by sampling approach introduced in *Rausenberger et. al* [135]. The models were simulated on a 1D spatial domain x = [0 1]. To represent the wound site, a high basal production of Egr was fixed within a finite space at x = [0 0.05], while basal rate of production of Egr for the rest of the region was set to zero. The rate of production of Upd was defined as a function of JNK/AP-1 activity [18, 20, 39, 51]. For all states, initial condition was set as u (t=0,x) = 0.1. Solutions for each model (with and without repression) were simulated using $10^6$ parameter sets, drawn uniformly from an interval from $10^{-3}$ to $10^{+2}$ on a logarithmic scale, and tested under different conditions of diffusion – $D_{Upd} > D_{Egr}$ , $D_{Upd} < D_{Egr}$ and $D_{Upd} = D_{Egr}$. The resulting solutions were automatically scored for countergradient endpoint features extracted from the experimentally observed gradient patterns.

Using this approach [135], positive solutions for a generic bistable pattern from the scanned parameter range were automatically extracted based on the following features:

i. JAK at x = 0 lower than JAK at x = 1
ii. JNK/AP-1 at x = 0 higher than JNK/AP-1 at x = 1
iii. Relative difference of JAK higher than 10%
iv. Relative difference of JNK/AP-1 higher than 10%

Positive solutions for a specific bistable pattern which mimics biologically observed patterns were automatically extracted based on the additional features:
v. JAK has a local maximum which is not at the boundary of the simulated domain
vi. Height of local JAK maximum at least 5%

## Author Contributions

Conceptualization JJ, VW, AKC

Validation JJ, AA, IG, AKC

Investigation JJ, RE, AA, CC, AKC

Writing JJ, VW, RE, JT, AKC

Visualization JJ, RE, VW, AKC

Supervision JT, AKC

Funding Acquisition AKC


## Acknowledgements

We thank the LIC facility (University of Freiburg) for technical help with imaging. We thank Erika Bach, David Bilder, Dirk Bohmann, Stephen Cohen, Fernando Diaz-Benjumea, Iswar Hariharan, Norbert Perrimon, Helena Richardson, Reinhardt Schuh, Y. Henry Sun, Mirka Uhlirova and Pelin Volkan for sharing reagents and the Bloomington Drosophila Stock Center (BDSC), the Vienna Drosophila Stock Collection (VDRC), the University of Zurich ORFeome Project (FlyORF), the Developmental Studies Hybridoma Bank (DSHB) and the Monoclonal Antibody Core Facility at the Helmholtz Zentrum Munich for providing fly stocks and antibodies. Thanks to Florian Steinberg (University of Freiburg) for support with protocol, reagents and imaging equipment for Western blot assays. We also thank the SGBM graduate school for support.

## Funding

Funding for this work was provided by the Deutsche Forschungsgemeinschaft (DFG, German Research Foundation) under Germany´s Excellence Strategy (CIBSS – EXC-2189 – Project ID 390939984), the Emmy Noether Programme (CL490/1-1), the Heisenberg Program (CL490/3-1) and by the Boehringer Ingelheim Foundation (Plus3 Programme).

801 **References**
802


803 1. Shaw TJ, Martin P. Wound repair at a glance. J Cell Sci. 2009;122(Pt 18):3209-13. Epub
804 2009/09/04. doi: 10.1242/jcs.031187. PubMed PMID: 19726630; PubMed Central PMCID:
805 PMCPMC2736861.

806 2. Marchiando AM, Graham WV, Turner JR. Epithelial barriers in homeostasis and disease.
807 Annu Rev Pathol. 2010;5:119-44. doi: 10.1146/annurev.pathol.4.110807.092135. PubMed PMID:
808 20078218.

809 3. Eming SA, Martin P, Tomic-Canic M. Wound repair and regeneration: mechanisms, signaling,
810 and translation. Sci Transl Med. 2014;6(265):265sr6. Epub 2014/12/05. doi:
811 10.1126/scitranslmed.3009337. PubMed PMID: 25473038; PubMed Central PMCID:
812 PMCPMC4973620.

813 4. Neves J, Demaria M, Campisi J, Jasper H. Of flies, mice, and men: evolutionarily conserved
814 tissue damage responses and aging. Dev Cell. 2015;32(1):9-18. Epub 2015/01/15. doi:
815 10.1016/j.devcel.2014.11.028. PubMed PMID: 25584795; PubMed Central PMCID:
816 PMCPMC4450349.

817 5. Niethammer P. The early wound signals. Curr Opin Genet Dev. 2016;40:17-22. Epub
818 20160605. doi: 10.1016/j.gde.2016.05.001. PubMed PMID: 27266971; PubMed Central PMCID:
819 PMCPMC5278878.

820 6. Hotamisligil GS, Davis RJ. Cell Signaling and Stress Responses. Cold Spring Harb Perspect
821 Biol. 2016;8(10). Epub 2016/10/05. doi: 10.1101/cshperspect.a006072. PubMed PMID: 27698029.

822 7. Ayello EA, Dowsett C, Schultz GS, Sibbald RG, Falanga V, Harding K, et al. TIME heals all
823 wounds. Nursing. 2004;34(4):36-41; quiz, -2. Epub 2004/07/13. doi: 10.1097/00152193-200404000-
824 00040. PubMed PMID: 15247672.

825 8. Schafer M, Werner S. Oxidative stress in normal and impaired wound repair. Pharmacol Res.
826 2008;58(2):165-71. Epub 20080619. doi: 10.1016/j.phrs.2008.06.004. PubMed PMID: 18617006.

827 9. Wilkinson HN, Hardman MJ. Wound healing: cellular mechanisms and pathological outcomes.
828 Open Biol. 2020;10(9):200223. Epub 20200930. doi: 10.1098/rsob.200223. PubMed PMID: 32993416;
829 PubMed Central PMCID: PMCPMC7536089.

830 10. Martin P, Nunan R. Cellular and molecular mechanisms of repair in acute and chronic wound
831 healing. Br J Dermatol. 2015;173(2):370-8. Epub 20150714. doi: 10.1111/bjd.13954. PubMed PMID:
832 26175283; PubMed Central PMCID: PMCPMC4671308.

833 11. Dvorak HF. Tumors: wounds that do not heal. Similarities between tumor stroma generation
834 and wound healing. N Engl J Med. 1986;315(26):1650-9. Epub 1986/12/25. doi:
835 10.1056/NEJM198612253152606. PubMed PMID: 3537791.

836 12. Coussens LM, Werb Z. Inflammation and cancer. Nature. 2002;420(6917):860-7. Epub
837 2002/12/20. doi: 10.1038/nature01322. PubMed PMID: 12490959; PubMed Central PMCID:
838 PMCPMC2803035.

839 13. Rybinski B, Franco-Barraza J, Cukierman E. The wound healing, chronic fibrosis, and cancer
840 progression triad. Physiol Genomics. 2014;46(7):223-44. Epub 2014/02/13. doi:
841 10.1152/physiolgenomics.00158.2013. PubMed PMID: 24520152; PubMed Central PMCID:
842 PMCPMC4035661.

843 14. Lee JH, Lee CW, Park SH, Choe KM. Spatiotemporal regulation of cell fusion by JNK and
844 JAK/STAT signaling during Drosophila wound healing. J Cell Sci. 2017;130(11):1917-28. Epub
845 20170419. doi: 10.1242/jcs.187658. PubMed PMID: 28424232.

846 15. Purice MD, Ray A, Munzel EJ, Pope BJ, Park DJ, Speese SD, et al. A novel Drosophila injury
847 model reveals severed axons are cleared through a Draper/MMP-1 signaling cascade. Elife. 2017;6.
848 Epub 2017/08/22. doi: 10.7554/eLife.23611. PubMed PMID: 28825401; PubMed Central PMCID:
849 PMCPMC5565368.

850 16. Ahmed-de-Prado S, Diaz-Garcia S, Baonza A. JNK and JAK/STAT signalling are required for
851 inducing loss of cell fate specification during imaginal wing discs regeneration in Drosophila
852 melanogaster. Dev Biol. 2018. Epub 2018/06/06. doi: 10.1016/j.ydbio.2018.05.021. PubMed PMID:
853 29870691.

854 17. Worley MI, Alexander LA, Hariharan IK. CtBP impedes JNK- and Upd/STAT-driven cell fate
855 misspecifications in regenerating Drosophila imaginal discs. Elife. 2018;7. Epub 2018/01/27. doi:
856 10.7554/eLife.30391. PubMed PMID: 29372681.

857 18. Wu M, Pastor-Pareja JC, Xu T. Interaction between Ras(V12) and scribbled clones induces
858 tumour growth and invasion. Nature. 2010;463(7280):545-8. Epub 2010/01/15. doi:
859 10.1038/nature08702. PubMed PMID: 20072127; PubMed Central PMCID: PMCPMC2835536.

860 19. Woodfield SE, Graves HK, Hernandez JA, Bergmann A. De-regulation of JNK and JAK/STAT
861 signaling in ESCRT-II mutant tissues cooperatively contributes to neoplastic tumorigenesis. PLoS
862 One. 2013;8(2):e56021. doi: 10.1371/journal.pone.0056021. PubMed PMID: 23418496; PubMed
863 Central PMCID: PMCPMC3572140.

864 20. Bunker BD, Nellimoottil TT, Boileau RM, Classen AK, Bilder D. The transcriptional response to
865 tumorigenic polarity loss in Drosophila. Elife. 2015;4. Epub 20150226. doi: 10.7554/eLife.03189.
866 PubMed PMID: 25719210; PubMed Central PMCID: PMCPMC4369581.

867 21. Atkins M, Potier D, Romanelli L, Jacobs J, Mach J, Hamaratoglu F, et al. An Ectopic Network
868 of Transcription Factors Regulated by Hippo Signaling Drives Growth and Invasion of a Malignant
869 Tumor Model. Curr Biol. 2016;26(16):2101-13. Epub 2016/08/02. doi: 10.1016/j.cub.2016.06.035.
870 PubMed PMID: 27476594.

871 22. Yang SA, Portilla JM, Mihailovic S, Huang YC, Deng WM. Oncogenic Notch Triggers
872 Neoplastic Tumorigenesis in a Transition-Zone-like Tissue Microenvironment. Dev Cell.
873 2019;49(3):461-72 e5. Epub 2019/04/16. doi: 10.1016/j.devcel.2019.03.015. PubMed PMID:
874 30982664; PubMed Central PMCID: PMCPMC6504601.

875 23. Hamaratoglu F, Atkins M. Rounding up the Usual Suspects: Assessing Yorkie, AP-1, and Stat
876 Coactivation in Tumorigenesis. Int J Mol Sci. 2020;21(13). Epub 20200627. doi:
877 10.3390/ijms21134580. PubMed PMID: 32605129; PubMed Central PMCID: PMCPMC7370090.

878 24. Ramet M, Lanot R, Zachary D, Manfruelli P. JNK signaling pathway is required for efficient
879 wound healing in Drosophila. Dev Biol. 2002;241(1):145-56. Epub 2002/01/11. doi:
880 10.1006/dbio.2001.0502. PubMed PMID: 11784101.

881 25. Bosch M, Serras F, Martin-Blanco E, Baguna J. JNK signaling pathway required for wound
882 healing in regenerating Drosophila wing imaginal discs. Dev Biol. 2005;280(1):73-86. Epub
883 2005/03/16. doi: 10.1016/j.ydbio.2005.01.002. PubMed PMID: 15766749.

884 26. Mattila J, Omelyanchuk L, Kyttala S, Turunen H, Nokkala S. Role of Jun N-terminal Kinase
885 (JNK) signaling in the wound healing and regeneration of a Drosophila melanogaster wing imaginal
886 disc. Int J Dev Biol. 2005;49(4):391-9. Epub 2005/06/22. doi: 10.1387/ijdb.052006jm. PubMed PMID:
887 15968584.

888 27. Finkel T. Signal transduction by reactive oxygen species. J Cell Biol. 2011;194(1):7-15. Epub
889 2011/07/13. doi: 10.1083/jcb.201102095. PubMed PMID: 21746850; PubMed Central PMCID:
890 PMCPMC3135394.

891 28. Santabarbara-Ruiz P, Lopez-Santillan M, Martinez-Rodriguez I, Binagui-Casas A, Perez L,
892 Milan M, et al. ROS-Induced JNK and p38 Signaling Is Required for Unpaired Cytokine Activation
893 during Drosophila Regeneration. PLoS Genet. 2015;11(10):e1005595. Epub 20151023. doi:
894 10.1371/journal.pgen.1005595. PubMed PMID: 26496642; PubMed Central PMCID:
895 PMCPMC4619769.

896 29. Moreno E, Yan M, Basler K. Evolution of TNF signaling mechanisms: JNK-dependent
897 apoptosis triggered by Eiger, the Drosophila homolog of the TNF superfamily. Curr Biol.
898 2002;12(14):1263-8. Epub 2002/08/15. PubMed PMID: 12176339.

899 30. Kanda H, Miura M. Regulatory roles of JNK in programmed cell death. J Biochem.
900 2004;136(1):1-6. Epub 2004/07/23. doi: 10.1093/jb/mvh098. PubMed PMID: 15269233.

901 31. Cosolo A, Jaiswal J, Csordas G, Grass I, Uhlirova M, Classen AK. JNK-dependent cell cycle
902 stalling in G2 promotes survival and senescence-like phenotypes in tissue stress. Elife. 2019;8. Epub
903 20190208. doi: 10.7554/eLife.41036. PubMed PMID: 30735120; PubMed Central PMCID:
904 PMCPMC6389326.

905 32. Ryoo HD, Gorenc T, Steller H. Apoptotic cells can induce compensatory cell proliferation
906 through the JNK and the Wingless signaling pathways. Dev Cell. 2004;7(4):491-501. Epub
907 2004/10/08. doi: 10.1016/j.devcel.2004.08.019. PubMed PMID: 15469838.

908 33. Morata G, Shlevkov E, Perez-Garijo A. Mitogenic signaling from apoptotic cells in Drosophila.
909 Dev Growth Differ. 2011;53(2):168-76. Epub 2011/02/23. doi: 10.1111/j.1440-169X.2010.01225.x.
910 PubMed PMID: 21338343.

911 34. Tournier C. The 2 Faces of JNK Signaling in Cancer. Genes Cancer. 2013;4(9-10):397-400.
912 Epub 2013/12/19. doi: 10.1177/1947601913486349. PubMed PMID: 24349637; PubMed Central
913 PMCID: PMCPMC3863340.

914 35. Pinal N, Calleja M, Morata G. Pro-apoptotic and pro-proliferation functions of the JNK pathway
915 of Drosophila: roles in cell competition, tumorigenesis and regeneration. Open Biol. 2019;9(3):180256.
916 Epub 2019/03/07. doi: 10.1098/rsob.180256. PubMed PMID: 30836847; PubMed Central PMCID:
917 PMCPMC6451367.

918 36. La Marca JE, Richardson HE. Two-Faced: Roles of JNK Signalling During Tumourigenesis in
919 the Drosophila Model. Front Cell Dev Biol. 2020;8:42. Epub 2020/03/03. doi:
920 10.3389/fcell.2020.00042. PubMed PMID: 32117973; PubMed Central PMCID: PMCPMC7012784.

921 37. Ruiz-Losada M, Gonzalez R, Peropadre A, Gil-Galvez A, Tena JJ, Baonza A, et al.
922 Coordination between cell proliferation and apoptosis after DNA damage in Drosophila. Cell Death
923 Differ. 2021. Epub 20211125. doi: 10.1038/s41418-021-00898-6. PubMed PMID: 34824391.

924 38. Smith-Bolton RK, Worley MI, Kanda H, Hariharan IK. Regenerative growth in Drosophila
925 imaginal discs is regulated by Wingless and Myc. Dev Cell. 2009;16(6):797-809. doi:
926 10.1016/j.devcel.2009.04.015. PubMed PMID: 19531351; PubMed Central PMCID:
927 PMCPMC2705171.

928 39. Jiang H, Patel PH, Kohlmaier A, Grenley MO, McEwen DG, Edgar BA. Cytokine/Jak/Stat
929 signaling mediates regeneration and homeostasis in the Drosophila midgut. Cell. 2009;137(7):1343-
930 55. Epub 2009/07/01. doi: 10.1016/j.cell.2009.05.014. PubMed PMID: 19563763; PubMed Central
931 PMCID: PMCPMC2753793.

932 40. Bergantinos C, Corominas M, Serras F. Cell death-induced regeneration in wing imaginal
933 discs requires JNK signalling. Development. 2010;137(7):1169-79. doi: 10.1242/dev.045559. PubMed
934 PMID: 20215351.

935 41. Harrison DA, McCoon PE, Binari R, Gilman M, Perrimon N. Drosophila unpaired encodes a
936 secreted protein that activates the JAK signaling pathway. Genes Dev. 1998;12(20):3252-63. Epub
937 1998/10/24. doi: 10.1101/gad.12.20.3252. PubMed PMID: 9784499; PubMed Central PMCID:
938 PMCPMC317220.

939 42. Hombria JC, Brown S, Hader S, Zeidler MP. Characterisation of Upd2, a Drosophila
940 JAK/STAT pathway ligand. Dev Biol. 2005;288(2):420-33. Epub 2005/11/10. doi:
941 10.1016/j.ydbio.2005.09.040. PubMed PMID: 16277982.

942 43. Agaisse H, Petersen UM, Boutros M, Mathey-Prevot B, Perrimon N. Signaling role of
943 hemocytes in Drosophila JAK/STAT-dependent response to septic injury. Dev Cell. 2003;5(3):441-50.
944 Epub 2003/09/12. doi: 10.1016/s1534-5807(03)00244-2. PubMed PMID: 12967563.

945 44. Gilbert MM, Weaver BK, Gergen JP, Reich NC. A novel functional activator of the Drosophila
946 JAK/STAT pathway, unpaired2, is revealed by an in vivo reporter of pathway activation. Mech Dev.
947 2005;122(7-8):939-48. Epub 2005/06/01. doi: 10.1016/j.mod.2005.03.004. PubMed PMID: 15925495.

948 45. Toggweiler J, Willecke M, Basler K. The transcription factor Ets21C drives tumor growth by
949 cooperating with AP-1. Sci Rep. 2016;6:34725. Epub 2016/10/08. doi: 10.1038/srep34725. PubMed
950 PMID: 27713480; PubMed Central PMCID: PMCPMC5054425.

951 46. Classen AK, Bunker BD, Harvey KF, Vaccari T, Bilder D. A tumor suppressor activity of
952 Drosophila Polycomb genes mediated by JAK-STAT signaling. Nat Genet. 2009;41(10):1150-5. Epub
953 20090913. doi: 10.1038/ng.445. PubMed PMID: 19749759; PubMed Central PMCID:
954 PMCPMC2782793.

955 47. Davie K, Jacobs J, Atkins M, Potier D, Christiaens V, Halder G, et al. Discovery of
956 transcription factors and regulatory regions driving in vivo tumor development by ATAC-seq and
957 FAIRE-seq open chromatin profiling. PLoS Genet. 2015;11(2):e1004994. doi:
958 10.1371/journal.pgen.1004994. PubMed PMID: 25679813; PubMed Central PMCID:
959 PMCPMC4334524.

960 48. Katsuyama T, Comoglio F, Seimiya M, Cabuy E, Paro R. During Drosophila disc regeneration,
961 JAK/STAT coordinates cell proliferation with Dilp8-mediated developmental delay. Proc Natl Acad Sci
962 U S A. 2015;112(18):E2327-36. Epub 20150420. doi: 10.1073/pnas.1423074112. PubMed PMID:
963 25902518; PubMed Central PMCID: PMCPMC4426433.

964 49. Pastor-Pareja JC, Wu M, Xu T. An innate immune response of blood cells to tumors and
965 tissue damage in Drosophila. Dis Model Mech. 2008;1(2-3):144-54; discussion 53. Epub 20080918.
966 doi: 10.1242/dmm.000950. PubMed PMID: 19048077; PubMed Central PMCID: PMCPMC2562178.

967 50. Lin G, Xu N, Xi R. Paracrine Unpaired Signaling through the JAK/STAT Pathway Controls
968 Self-renewal and Lineage Differentiation of Drosophila Intestinal Stem Cells. J Mol Cell Biol. 2009.
969 Epub 2009/10/03. doi: mjp028 [pii]

970 10.1093/jmcb/mjp028. PubMed PMID: 19797317.

971 51. La Fortezza M, Schenk M, Cosolo A, Kolybaba A, Grass I, Classen AK. JAK/STAT signalling
972 mediates cell survival in response to tissue stress. Development. 2016;143(16):2907-19. Epub
973 20160706. doi: 10.1242/dev.132340. PubMed PMID: 27385008.

974 52. Betz A, Ryoo HD, Steller H, Darnell JE, Jr. STAT92E is a positive regulator of Drosophila
975 inhibitor of apoptosis 1 (DIAP/1) and protects against radiation-induced apoptosis. Proc Natl Acad Sci
976 U S A. 2008;105(37):13805-10. Epub 20080908. doi: 10.1073/pnas.0806291105. PubMed PMID:
977 18779571; PubMed Central PMCID: PMCPMC2544535.

978 53. Kauppila S, Maaty WS, Chen P, Tomar RS, Eby MT, Chapo J, et al. Eiger and its receptor,
979 Wengen, comprise a TNF-like system in Drosophila. Oncogene. 2003;22(31):4860-7. Epub
980 2003/08/02. doi: 10.1038/sj.onc.1206715. PubMed PMID: 12894227.

981 54. Muzzopappa M, Murcia L, Milan M. Feedback amplification loop drives malignant growth in
982 epithelial tissues. Proc Natl Acad Sci U S A. 2017;114(35):E7291-E300. Epub 20170814. doi:
983 10.1073/pnas.1701791114. PubMed PMID: 28808034; PubMed Central PMCID: PMCPMC5584413.

984 55. Khan SJ, Abidi SNF, Skinner A, Tian Y, Smith-Bolton RK. The Drosophila Duox maturation
985 factor is a key component of a positive feedback loop that sustains regeneration signaling. PLoS
986 Genet. 2017;13(7):e1006937. Epub 2017/07/29. doi: 10.1371/journal.pgen.1006937. PubMed PMID:
987 28753614; PubMed Central PMCID: PMCPMC5550008.

988 56. Pinal N, Martin M, Medina I, Morata G. Short-term activation of the Jun N-terminal kinase
989 pathway in apoptosis-deficient cells of Drosophila induces tumorigenesis. Nat Commun.
990 2018;9(1):1541. Epub 2018/04/20. doi: 10.1038/s41467-018-04000-6. PubMed PMID: 29670104;
991 PubMed Central PMCID: PMCPMC5906466.

992 57. Fox DT, Cohen E, Smith-Bolton R. Model systems for regeneration: Drosophila. Development.
993 2020;147(7). Epub 20200406. doi: 10.1242/dev.173781. PubMed PMID: 32253254; PubMed Central
994 PMCID: PMCPMC7157589.

995 58. Chatterjee N, Bohmann D. A versatile PhiC31 based reporter system for measuring AP-1 and
996 Nrf2 signaling in Drosophila and in tissue culture. PLoS One. 2012;7(4):e34063. Epub 2012/04/18.
997 doi: 10.1371/journal.pone.0034063. PubMed PMID: 22509270; PubMed Central PMCID:
998 PMCPMC3324472.

999 59. Hariharan IK, Serras F. Imaginal disc regeneration takes flight. Curr Opin Cell Biol.
1000 2017;48:10-6. Epub 20170401. doi: 10.1016/j.ceb.2017.03.005. PubMed PMID: 28376317; PubMed
1001 Central PMCID: PMCPMC5591769.

1002 60. Trengove NJ, Stacey MC, MacAuley S, Bennett N, Gibson J, Burslem F, et al. Analysis of the
1003 acute and chronic wound environments: the role of proteases and their inhibitors. Wound Repair
1004 Regen. 1999;7(6):442-52. Epub 2000/01/13. doi: 10.1046/j.1524-475x.1999.00442.x. PubMed PMID:
1005 10633003.

1006 61. Yager DR, Nwomeh BC. The proteolytic environment of chronic wounds. Wound Repair
1007 Regen. 1999;7(6):433-41. Epub 2000/01/13. doi: 10.1046/j.1524-475x.1999.00433.x. PubMed PMID:
1008 10633002.

1009 62. Caley MP, Martins VL, O'Toole EA. Metalloproteinases and Wound Healing. Adv Wound Care
1010 (New Rochelle). 2015;4(4):225-34. Epub 2015/05/07. doi: 10.1089/wound.2014.0581. PubMed PMID:
1011 25945285; PubMed Central PMCID: PMCPMC4397992.

1012 63. Moseley R, Hilton JR, Waddington RJ, Harding KG, Stephens P, Thomas DW. Comparison of
1013 oxidative stress biomarker profiles between acute and chronic wound environments. Wound Repair
1014 Regen. 2004;12(4):419-29. Epub 2004/07/21. doi: 10.1111/j.1067-1927.2004.12406.x. PubMed PMID:
1015 15260807.

1016 64. Chipurupalli S, Samavedam U, Robinson N. Crosstalk Between ER Stress, Autophagy and
1017 Inflammation. Front Med (Lausanne). 2021;8:758311. Epub 20211105. doi:
1018 10.3389/fmed.2021.758311. PubMed PMID: 34805224; PubMed Central PMCID: PMCPMC8602556.

1019 65. Wu C, Chen C, Dai J, Zhang F, Chen Y, Li W, et al. Toll pathway modulates TNF-induced
1020 JNK-dependent cell death in Drosophila. Open Biol. 2015;5(7):140171. Epub 2015/07/24. doi:
1021 10.1098/rsob.140171. PubMed PMID: 26202785; PubMed Central PMCID: PMCPMC4632500.

1022 66. Zielke N, Korzelius J, van Straaten M, Bender K, Schuhknecht GFP, Dutta D, et al. Fly-FUCCI:
1023 A versatile tool for studying cell proliferation in complex tissues. Cell Rep. 2014;7(2):588-98. Epub
1024 2014/04/15. doi: 10.1016/j.celrep.2014.03.020. PubMed PMID: 24726363.

1025 67. Wright VM, Vogt KL, Smythe E, Zeidler MP. Differential activities of the Drosophila JAK/STAT
1026 pathway ligands Upd, Upd2 and Upd3. Cell Signal. 2011;23(5):920-7. Epub 20110122. doi:
1027 10.1016/j.cellsig.2011.01.020. PubMed PMID: 21262354.

1028 68. Osman D, Buchon N, Chakrabarti S, Huang YT, Su WC, Poidevin M, et al. Autocrine and
1029 paracrine unpaired signaling regulate intestinal stem cell maintenance and division. J Cell Sci.
1030 2012;125(Pt 24):5944-9. Epub 20121004. doi: 10.1242/jcs.113100. PubMed PMID: 23038775.

1031 69. Jiang H, Grenley MO, Bravo MJ, Blumhagen RZ, Edgar BA. EGFR/Ras/MAPK signaling
1032 mediates adult midgut epithelial homeostasis and regeneration in Drosophila. Cell Stem Cell.
1033 2011;8(1):84-95. Epub 20101216. doi: 10.1016/j.stem.2010.11.026. PubMed PMID: 21167805;
1034 PubMed Central PMCID: PMCPMC3021119.

1035 70. Bach EA, Ekas LA, Ayala-Camargo A, Flaherty MS, Lee H, Perrimon N, et al. GFP reporters
1036 detect the activation of the Drosophila JAK/STAT pathway in vivo. Gene Expr Patterns. 2007;7(3):323-
1037 31. Epub 20060822. doi: 10.1016/j.modgep.2006.08.003. PubMed PMID: 17008134.

1038 71. Rodrigues AB, Zoranovic T, Ayala-Camargo A, Grewal S, Reyes-Robles T, Krasny M, et al.
1039 Activated STAT regulates growth and induces competitive interactions independently of Myc, Yorkie,
1040 Wingless and ribosome biogenesis. Development. 2012;139(21):4051-61. Epub 20120919. doi:
1041 10.1242/dev.076760. PubMed PMID: 22992954; PubMed Central PMCID: PMCPMC3472591.

1042 72. Hatini V, Kula-Eversole E, Nusinow D, Del Signore SJ. Essential roles for stat92E in
1043 expanding and patterning the proximodistal axis of the Drosophila wing imaginal disc. Dev Biol.
1044 2013;378(1):38-50. Epub 20130307. doi: 10.1016/j.ydbio.2013.02.016. PubMed PMID: 23499656;
1045 PubMed Central PMCID: PMCPMC3776456.

1046 73. Recasens-Alvarez C, Ferreira A, Milan M. JAK/STAT controls organ size and fate specification
1047 by regulating morphogen production and signalling. Nat Commun. 2017;8:13815. Epub 20170103. doi:
1048 10.1038/ncomms13815. PubMed PMID: 28045022; PubMed Central PMCID: PMCPMC5216089.

1049 74. Colombani J, Andersen DS, Leopold P. Secreted peptide Dilp8 coordinates Drosophila tissue
1050 growth with developmental timing. Science. 2012;336(6081):582-5. doi: 10.1126/science.1216689.
1051 PubMed PMID: 22556251.

1052 75. Hay BA, Wolff T, Rubin GM. Expression of baculovirus P35 prevents cell death in Drosophila.
1053 Development. 1994;120(8):2121-9. Epub 1994/08/01. PubMed PMID: 7925015.

1054 76. Weber U, Paricio N, Mlodzik M. Jun mediates Frizzled-induced R3/R4 cell fate distinction and
1055 planar polarity determination in the Drosophila eye. Development. 2000;127(16):3619-29. Epub
1056 2000/07/21. doi: 10.1242/dev.127.16.3619. PubMed PMID: 10903185.

1057 77. Ayala-Camargo A, Anderson AM, Amoyel M, Rodrigues AB, Flaherty MS, Bach EA.
1058 JAK/STAT signaling is required for hinge growth and patterning in the Drosophila wing disc. Dev Biol.
1059 2013;382(2):413-26. Epub 20130823. doi: 10.1016/j.ydbio.2013.08.016. PubMed PMID: 23978534;
1060 PubMed Central PMCID: PMCPMC3795806.

1061 78. Stevens LJ, Page-McCaw A. A secreted MMP is required for reepithelialization during wound
1062 healing. Mol Biol Cell. 2012;23(6):1068-79. Epub 20120119. doi: 10.1091/mbc.E11-09-0745. PubMed
1063 PMID: 22262460; PubMed Central PMCID: PMCPMC3302734.

1064 79. Cheong R, Rhee A, Wang CJ, Nemenman I, Levchenko A. Information transduction capacity
1065 of noisy biochemical signaling networks. Science. 2011;334(6054):354-8. Epub 20110915. doi:
1066 10.1126/science.1204553. PubMed PMID: 21921160; PubMed Central PMCID: PMCPMC3895446.

1067 80. Balazsi G, van Oudenaarden A, Collins JJ. Cellular decision making and biological noise: from
1068 microbes to mammals. Cell. 2011;144(6):910-25. Epub 2011/03/19. doi: 10.1016/j.cell.2011.01.030.
1069 PubMed PMID: 21414483; PubMed Central PMCID: PMCPMC3068611.

1070 81. Khan I, Ponnusamy S, Rahman SU, Giubellinom A, Arany PR. Co-opting Developmental
1071 Signaling Pathways to Promote Wound Healing. Melvin A. Shiffman, Low M, editors: Springer, Cham;
1072 2018. pp 103-14 p.

1073 82. Ghilardi SJ, O'Reilly BM, Sgro AE. Intracellular signaling dynamics and their role in
1074 coordinating tissue repair. Wiley Interdiscip Rev Syst Biol Med. 2020;12(3):e1479. Epub 20200208.
1075 doi: 10.1002/wsbm.1479. PubMed PMID: 32035001; PubMed Central PMCID: PMCPMC7187325.

1076 83. Jordan JD, Landau EM, Iyengar R. Signaling networks: the origins of cellular multitasking.
1077 Cell. 2000;103(2):193-200. Epub 2000/11/01. doi: 10.1016/s0092-8674(00)00112-4. PubMed PMID:
1078 11057893; PubMed Central PMCID: PMCPMC3619409.

1079 84. Milo R, Shen-Orr S, Itzkovitz S, Kashtan N, Chklovskii D, Alon U. Network motifs: simple
1080 building blocks of complex networks. Science. 2002;298(5594):824-7. Epub 2002/10/26. doi:
1081 10.1126/science.298.5594.824. PubMed PMID: 12399590.

1082 85. Levine M, Davidson EH. Gene regulatory networks for development. Proc Natl Acad Sci U S
1083 A. 2005;102(14):4936-42. Epub 20050323. doi: 10.1073/pnas.0408031102. PubMed PMID:
1084 15788537; PubMed Central PMCID: PMCPMC555974.

1085 86. Azeloglu EU, Iyengar R. Signaling networks: information flow, computation, and decision
1086 making. Cold Spring Harb Perspect Biol. 2015;7(4):a005934. Epub 2015/04/03. doi:
1087 10.1101/cshperspect.a005934. PubMed PMID: 25833842; PubMed Central PMCID:
1088 PMCPMC4382748.

1089 87. Tyson JJ, Chen KC, Novak B. Sniffers, buzzers, toggles and blinkers: dynamics of regulatory
1090 and signaling pathways in the cell. Curr Opin Cell Biol. 2003;15(2):221-31. Epub 2003/03/22. doi:
1091 10.1016/s0955-0674(03)00017-6. PubMed PMID: 12648679.

1092 88. Eungdamrong NJ, Iyengar R. Modeling cell signaling networks. Biol Cell. 2004;96(5):355-62.
1093 Epub 2004/06/23. doi: 10.1016/j.biolcel.2004.03.004. PubMed PMID: 15207904; PubMed Central
1094 PMCID: PMCPMC3620715.

1095 89. Umulis DM, Othmer HG. The role of mathematical models in understanding pattern formation
1096 in developmental biology. Bull Math Biol. 2015;77(5):817-45. doi: 10.1007/s11538-014-0019-7.
1097 PubMed PMID: 25280665; PubMed Central PMCID: PMCPMC4819020.

1098 90. Capek D, Muller P. Positional information and tissue scaling during development and
1099 regeneration. Development. 2019;146(24). Epub 2019/12/22. doi: 10.1242/dev.177709. PubMed
1100 PMID: 31862792.

1101 91. Kondo S, Miura T. Reaction-diffusion model as a framework for understanding biological
1102 pattern formation. Science. 2010;329(5999):1616-20. Epub 2010/10/12. doi:
1103 10.1126/science.1179047. PubMed PMID: 20929839.

1104 92. Khan SJ, Abidi SNF, Skinner A, Tian Y, Smith-Bolton RK. A positive feedback loop ensures
1105 propagation of ROS production and JNK signalling throughout Drosophila tissue regeneration. 2017.
1106 doi: 10.1101/152140.

1107 93. Shlevkov E, Morata G. A dp53/JNK-dependant feedback amplification loop is essential for the
1108 apoptotic response to stress in Drosophila. Cell Death Differ. 2012;19(3):451-60. Epub 2011/09/03.
1109 doi: 10.1038/cdd.2011.113. PubMed PMID: 21886179; PubMed Central PMCID: PMCPMC3278728.

1110 94. Martin-Blanco E, Gampel A, Ring J, Virdee K, Kirov N, Tolkovsky AM, et al. puckered encodes
1111 a phosphatase that mediates a feedback loop regulating JNK activity during dorsal closure in
1112 Drosophila. Genes Dev. 1998;12(4):557-70. doi: 10.1101/gad.12.4.557. PubMed PMID: 9472024;
1113 PubMed Central PMCID: PMCPMC316530.

1114 95. Karsten P, Hader S, Zeidler MP. Cloning and expression of Drosophila SOCS36E and its
1115 potential regulation by the JAK/STAT pathway. Mech Dev. 2002;117(1-2):343-6. doi: 10.1016/s0925-
1116 4773(02)00216-2. PubMed PMID: 12204282.

1117 96. Callus BA, Mathey-Prevot B. SOCS36E, a novel Drosophila SOCS protein, suppresses
1118 JAK/STAT and EGF-R signalling in the imaginal wing disc. Oncogene. 2002;21(31):4812-21. doi:
1119 10.1038/sj.onc.1205618. PubMed PMID: 12101419.

1120 97. Madar D, Dekel E, Bren A, Alon U. Negative auto-regulation increases the input dynamic-
1121 range of the arabinose system of Escherichia coli. BMC Syst Biol. 2011;5:111. Epub 20110712. doi:
1122 10.1186/1752-0509-5-111. PubMed PMID: 21749723; PubMed Central PMCID: PMCPMC3163201.

1123 98. Li C, Zhang L, Nie Q. Landscape reveals critical network structures for sharpening gene
1124 expression boundaries. BMC Syst Biol. 2018;12(1):67. Epub 20180613. doi: 10.1186/s12918-018-
1125 0595-5. PubMed PMID: 29898720; PubMed Central PMCID: PMCPMC6001026.

1126 99. Jiang J, Struhl G. Complementary and mutually exclusive activities of decapentaplegic and
1127 wingless organize axial patterning during Drosophila leg development. Cell. 1996;86(3):401-9. Epub
1128 1996/08/09. doi: 10.1016/s0092-8674(00)80113-0. PubMed PMID: 8756722.

1129 100. Brook WJ, Cohen SM. Antagonistic interactions between wingless and decapentaplegic
1130 responsible for dorsal-ventral pattern in the Drosophila Leg. Science. 1996;273(5280):1373-7. Epub
1131 1996/09/06. doi: 10.1126/science.273.5280.1373. PubMed PMID: 8703069.

1132 101. Lee J, Lee J, Farquhar KS, Yun J, Frankenberger CA, Bevilacqua E, et al. Network of mutually
1133 repressive metastasis regulators can promote cell heterogeneity and metastatic transitions. Proc Natl
1134 Acad Sci U S A. 2014;111(3):E364-73. Epub 20140106. doi: 10.1073/pnas.1304840111. PubMed
1135 PMID: 24395801; PubMed Central PMCID: PMCPMC3903259.

1136 102. Sokolowski TR, Erdmann T, ten Wolde PR. Mutual repression enhances the steepness and
1137 precision of gene expression boundaries. PLoS Comput Biol. 2012;8(8):e1002654. Epub 20120830.
1138 doi: 10.1371/journal.pcbi.1002654. PubMed PMID: 22956897; PubMed Central PMCID:
1139 PMCPMC3431325.

1140 103. Theisen H, Haerry TE, O'Connor MB, Marsh JL. Developmental territories created by mutual
1141 antagonism between Wingless and Decapentaplegic. Development. 1996;122(12):3939-48. Epub
1142 1996/12/01. PubMed PMID: 9012514.

1143 104. Villa-Cuesta E, Modolell J. Mutual repression between msh and Iro-C is an essential
1144 component of the boundary between body wall and wing in Drosophila. Development.
1145 2005;132(18):4087-96. Epub 20050810. doi: 10.1242/dev.01977. PubMed PMID: 16093324.

1146 105. Zagorski M, Tabata Y, Brandenberg N, Lutolf MP, Tkacik G, Bollenbach T, et al. Decoding of
1147 position in the developing neural tube from antiparallel morphogen gradients. Science.

1148 2017;356(6345):1379-83. Epub 2017/07/01. doi: 10.1126/science.aam5887. PubMed PMID:
1149 28663499; PubMed Central PMCID: PMCPMC5568706.

1150 106. Ferrell JE, Jr. Self-perpetuating states in signal transduction: positive feedback, double-
1151 negative feedback and bistability. Curr Opin Cell Biol. 2002;14(2):140-8. Epub 2002/03/14. doi:
1152 10.1016/s0955-0674(02)00314-9. PubMed PMID: 11891111.

1153 107. JAK/STAT Pathway Signalling in Drosophila Melanogaster [Internet]. Landes Bioscience.

1154 108. Sarov M, Barz C, Jambor H, Hein MY, Schmied C, Suchold D, et al. A genome-wide resource
1155 for the analysis of protein localisation in Drosophila. Elife. 2016;5:e12068. Epub 2016/02/21. doi:
1156 10.7554/eLife.12068. PubMed PMID: 26896675; PubMed Central PMCID: PMCPMC4805545.

1157 109. Niu GJ, Xu JD, Yuan WJ, Sun JJ, Yang MC, He ZH, et al. Protein Inhibitor of Activated STAT
1158 (PIAS) Negatively Regulates the JAK/STAT Pathway by Inhibiting STAT Phosphorylation and
1159 Translocation. Front Immunol. 2018;9:2392. Epub 20181026. doi: 10.3389/fimmu.2018.02392.
1160 PubMed PMID: 30416501; PubMed Central PMCID: PMCPMC6212522.

1161 110. Saadin A, Starz-Gaiano M. Identification of Novel Regulators of the JAK/STAT Signaling
1162 Pathway that Control Border Cell Migration in the Drosophila Ovary. G3 (Bethesda). 2016;6(7):1991-
1163 2002. Epub 2016/05/14. doi: 10.1534/g3.116.028100. PubMed PMID: 27175018; PubMed Central
1164 PMCID: PMCPMC4938652.

1165 111. Arbouzova NI, Bach EA, Zeidler MP. Ken & barbie selectively regulates the expression of a
1166 subset of Jak/STAT pathway target genes. Curr Biol. 2006;16(1):80-8. doi: 10.1016/j.cub.2005.11.033.
1167 PubMed PMID: 16401426.

1168 112. Harris RE, Stinchfield MJ, Nystrom SL, McKay DJ, Hariharan IK. Damage-responsive,
1169 maturity-silenced enhancers regulate multiple genes that direct regeneration in Drosophila. Elife.
1170 2020;9. Epub 20200603. doi: 10.7554/eLife.58305. PubMed PMID: 32490812; PubMed Central
1171 PMCID: PMCPMC7299344.

1172 113. Muller P, Kuttenkeuler D, Gesellchen V, Zeidler MP, Boutros M. Identification of JAK/STAT
1173 signalling components by genome-wide RNA interference. Nature. 2005;436(7052):871-5. Epub
1174 2005/08/12. doi: 10.1038/nature03869. PubMed PMID: 16094372.

1175 114. Baeg GH, Zhou R, Perrimon N. Genome-wide RNAi analysis of JAK/STAT signaling
1176 components in Drosophila. Genes Dev. 2005;19(16):1861-70. Epub 20050729. doi:
1177 10.1101/gad.1320705. PubMed PMID: 16055650; PubMed Central PMCID: PMCPMC1186186.

1178 115. La Marca JE, Willoughby LF, Allan K, Portela M, Goh PK, Tiganis T, et al. PTP61F Mediates
1179 Cell Competition and Mitigates Tumorigenesis. Int J Mol Sci. 2021;22(23). Epub 20211125. doi:
1180 10.3390/ijms222312732. PubMed PMID: 34884538; PubMed Central PMCID: PMCPMC8657627.

1181 116. Willoughby LF, Manent J, Allan K, Lee H, Portela M, Wiede F, et al. Differential regulation of
1182 protein tyrosine kinase signalling by Dock and the PTP61F variants. FEBS J. 2017;284(14):2231-50.
1183 Epub 20170630. doi: 10.1111/febs.14118. PubMed PMID: 28544778.

1184 117. Schertel C, Huang D, Bjorklund M, Bischof J, Yin D, Li R, et al. Systematic screening of a
1185 Drosophila ORF library in vivo uncovers Wnt/Wg pathway components. Dev Cell. 2013;25(2):207-19.
1186 Epub 2013/04/16. doi: 10.1016/j.devcel.2013.02.019. PubMed PMID: 23583758.

1187 118. Meinhardt H. Cell determination boundaries as organizing regions for secondary embryonic
1188 fields. Dev Biol. 1983;96(2):375-85. doi: 10.1016/0012-1606(83)90175-6. PubMed PMID: 6832478.

1189 119. Martinez Arias A, Steventon B. On the nature and function of organizers. Development.
1190 2018;145(5). Epub 20180309. doi: 10.1242/dev.159525. PubMed PMID: 29523654; PubMed Central
1191 PMCID: PMCPMC5868996.

1192 120. Bilder D, Li M, Perrimon N. Cooperative regulation of cell polarity and growth by Drosophila
1193 tumor suppressors. Science. 2000;289(5476):113-6. Epub 2000/07/07. doi:
1194 10.1126/science.289.5476.113. PubMed PMID: 10884224.

1195 121. Pagliarini RA, Xu T. A genetic screen in Drosophila for metastatic behavior. Science.
1196 2003;302(5648):1227-31. Epub 2003/10/11. doi: 10.1126/science.1088474. PubMed PMID:
1197 14551319.

1198 122. Dillard C, Reis JGT, Rusten TE. Ras(V12); scrib(-/-) Tumors: A Cooperative Oncogenesis
1199 Model Fueled by Tumor/Host Interactions. Int J Mol Sci. 2021;22(16). Epub 20210818. doi:
1200 10.3390/ijms22168873. PubMed PMID: 34445578; PubMed Central PMCID: PMCPMC8396170.

1201 123. Igaki T, Pastor-Pareja JC, Aonuma H, Miura M, Xu T. Intrinsic tumor suppression and
1202 epithelial maintenance by endocytic activation of Eiger/TNF signaling in Drosophila. Dev Cell.
1203 2009;16(3):458-65. Epub 2009/03/18. doi: 10.1016/j.devcel.2009.01.002. PubMed PMID: 19289090;
1204 PubMed Central PMCID: PMCPMC2729686.

1205 124. Ohsawa S, Sugimura K, Takino K, Xu T, Miyawaki A, Igaki T. Elimination of oncogenic
1206 neighbors by JNK-mediated engulfment in Drosophila. Dev Cell. 2011;20(3):315-28. Epub 2011/03/15.
1207 doi: 10.1016/j.devcel.2011.02.007. PubMed PMID: 21397843.

1208 125. Uhlirova M, Jasper H, Bohmann D. Non-cell-autonomous induction of tissue overgrowth by
1209 JNK/Ras cooperation in a Drosophila tumor model. Proc Natl Acad Sci U S A. 2005;102(37):13123-8.
1210 Epub 2005/09/10. doi: 10.1073/pnas.0504170102. PubMed PMID: 16150723; PubMed Central
1211 PMCID: PMCPMC1201591.

1212 126. Amoyel M, Anderson AM, Bach EA. JAK/STAT pathway dysregulation in tumors: a Drosophila
1213 perspective. Semin Cell Dev Biol. 2014;28:96-103. Epub 20140328. doi:
1214 10.1016/j.semcdb.2014.03.023. PubMed PMID: 24685611; PubMed Central PMCID:
1215 PMCPMC4037387.

1216 127. Dhanasekaran DN, Reddy EP. JNK-signaling: A multiplexing hub in programmed cell death.
1217 Genes Cancer. 2017;8(9-10):682-94. Epub 2017/12/14. doi: 10.18632/genesandcancer.155. PubMed
1218 PMID: 29234486; PubMed Central PMCID: PMCPMC5724802.

1219 128. Trivedi S, Starz-Gaiano M. Drosophila Jak/STAT Signaling: Regulation and Relevance in
1220 Human Cancer and Metastasis. Int J Mol Sci. 2018;19(12). Epub 20181214. doi:
1221 10.3390/ijms19124056. PubMed PMID: 30558204; PubMed Central PMCID: PMCPMC6320922.

1222 129. Herrera SC, Bach EA. JAK/STAT signaling in stem cells and regeneration: from Drosophila to
1223 vertebrates. Development. 2019;146(2). Epub 20190129. doi: 10.1242/dev.167643. PubMed PMID:
1224 30696713; PubMed Central PMCID: PMCPMC6361132.

1225 130. Tsai YC, Sun YH. Long-range effect of upd, a ligand for Jak/STAT pathway, on cell cycle in
1226 Drosophila eye development. Genesis. 2004;39(2):141-53. Epub 2004/06/02. doi:
1227 10.1002/gene.20035. PubMed PMID: 15170700.

1228 131. Du L, Wang J. JAK/STAT pathway promotes *Drosophila* neuroblast proliferation via the direct
1229 *CycE* regulation. bioRxiv. 2020:2020.07.10.195875. doi: 10.1101/2020.07.10.195875.

1230 132. Beira JV, Torres J, Paro R. Signalling crosstalk during early tumorigenesis in the absence of
1231 Polycomb silencing. PLoS Genet. 2018;14(1):e1007187. Epub 2018/01/23. doi:
1232 10.1371/journal.pgen.1007187. PubMed PMID: 29357360; PubMed Central PMCID:
1233 PMCPMC5794193.

1234 133. Wang Z, Shi C. Cellular senescence is a promising target for chronic wounds: a
1235 comprehensive review. Burns Trauma. 2020;8:tkaa021. Epub 20200623. doi: 10.1093/burnst/tkaa021.
1236 PubMed PMID: 32607375; PubMed Central PMCID: PMCPMC7309580.

1237 134. Schindelin J, Arganda-Carreras I, Frise E, Kaynig V, Longair M, Pietzsch T, et al. Fiji: an open-
1238 source platform for biological-image analysis. Nat Methods. 2012;9(7):676-82. doi:
1239 10.1038/nmeth.2019. PubMed PMID: 22743772; PubMed Central PMCID: PMC3855844.

1240 135. Rausenberger J, Tscheuschler A, Nordmeier W, Wust F, Timmer J, Schafer E, et al.
1241 Photoconversion and nuclear trafficking cycles determine phytochrome A's response profile to far-red
1242 light. Cell. 2011;146(5):813-25. Epub 2011/09/03. doi: 10.1016/j.cell.2011.07.023. PubMed PMID:
1243 21884939.

**Figure 1**

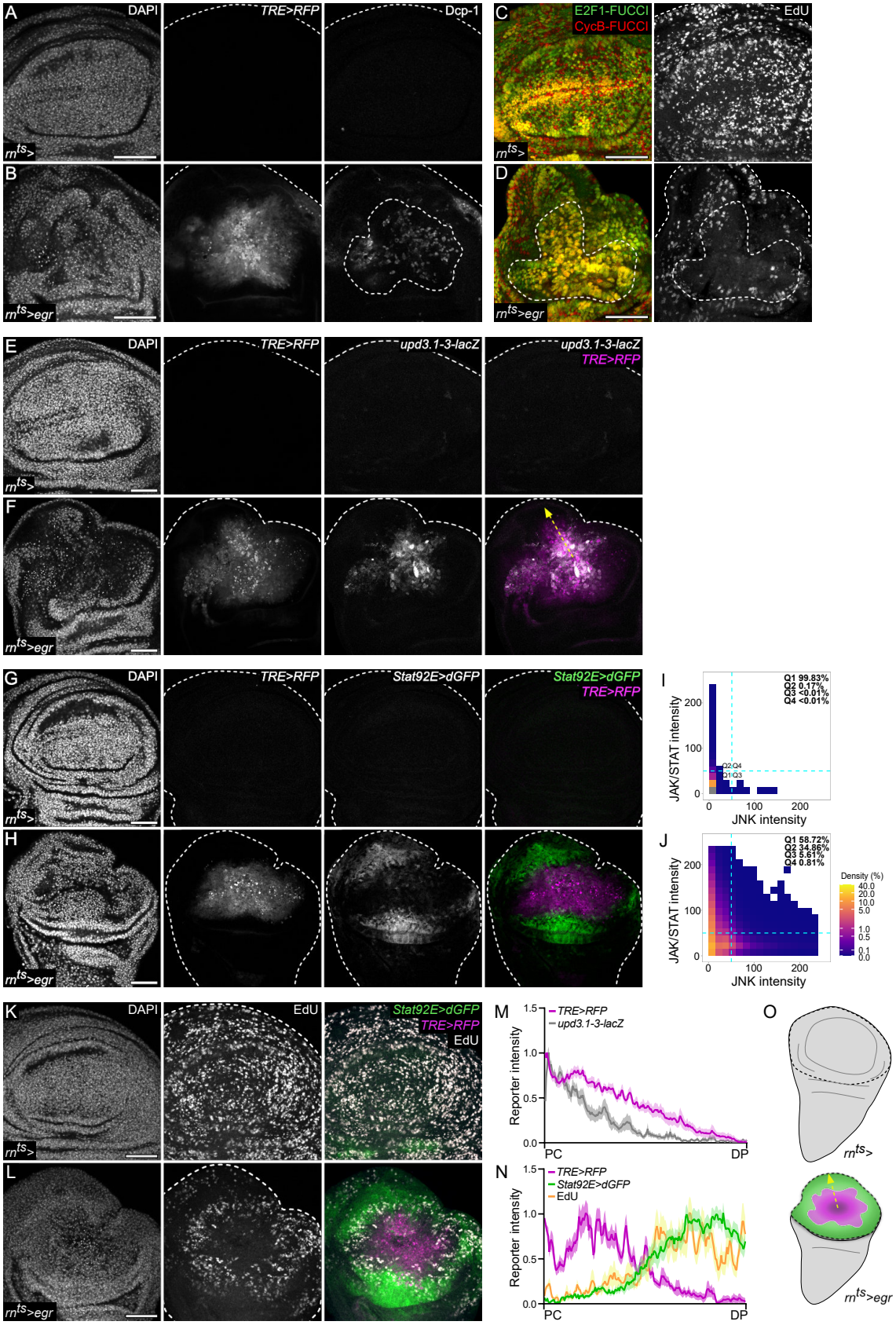
A
DAPI
TRE>RFP
Dcp-1
rn^ts>
B
rn^ts>egr
C
E2F1-FUCCI
CycB-FUCCI
EdU
rn^ts>
D
rn^ts>egr
E
DAPI
TRE>RFP
upd3.1-3-lacZ
upd3.1-3-lacZ
TRE>RFP
rn^ts>
F
rn^ts>egr
G
DAPI
TRE>RFP
Stat92E>dGFP
Stat92E>dGFP
TRE>RFP
rn^ts>
H
rn^ts>egr
I
Q1 99.83%
Q2 0.17%
Q3 <0.01%
Q4 <0.01%
JAK/STAT intensity
JNK intensity
J
Q1 58.72%
Q2 34.66%
Q3 5.61%
Q4 0.81%
Density (%)
JAK/STAT intensity
JNK intensity
K
DAPI
EdU
Stat92E>dGFP
TRE>RFP
EdU
rn^ts>
L
rn^ts>egr
M
TRE>RFP
upd3.1-3-lacZ
Reporter intensity
PC
DP
N
TRE>RFP
Stat92E>dGFP
EdU
Reporter intensity
PC
DP
O
rn^ts>
rn^ts>egr

**Figure 1**

**JNK/AP-1 and JAK/STAT are activated in distinct spatial domains upon tissue damage**

---

**(A-B)** A control wing disc **(A)** and wing disc after 24h of *egr*-expression **(B)** in the pouch (R0) (see also **S1.1, B**) under the control of the inducible *rn-GAL4* (*rotund-GAL4*) driver ($rn^{ts}$>) in the pouch domain. Discs express the JNK/AP-1 reporter *TRE>RFP* and were stained for cleaved Dcp-1 to visualize apoptosis.

**(C-D)** A control wing disc **(C)** and wing disc after 24h of *egr*-expression **(D)** in the pouch (R0), under the control of the inducible *rn-GAL4* (*rotund-GAL4*) driver ($rn^{ts}$>). Discs also express the FUCCI cell cycle reporters *mRFP-NLS-CycB*$^{1-266}$ (red) and *GFP-E2f1*$^{1-230}$ (green) (see also **S1.1A**) and were assessed for DNA replication by EdU incorporation assay.

**(E-F)** A control **(E)** and *egr*-expressing disc **(F)** at R0, expressing the *upd3.1-3-LacZ* (gray) and the JNK/AP-1 reporter *TRE>RFP* (magenta). Discs were stained for β-Galactosidase.

**(G-H)** A control **(G)** and *egr*-expressing disc **(F)** at R0, expressing the JNK/AP-1 reporter *TRE>RFP* (magenta) and the dynamic JAK/STAT reporter *Stat92E>dGFP* (green).

**(I-J)** 2D density plots mapping pixel fluorescence intensity values for the *TRE>RFP* (JNK intensity, X-axis) and *Stat92E>dGFP* (JAK/STAT intensity, Y-axis) reporters, measured in the combined wing pouch and hinge domains (black dashed lines in **O**) in control, *rn-GAL4*-expressing discs **(I)** or *egr*-expressing discs **(J)** . Dashed lines (cyan) represent visually defined thresholds distinguishing low or high reporter activity in the quadrants Q1,Q2,Q3 and Q4. Note that less than 1% of pixels show both high JNK and high JAK/STAT signaling activity in the combined JNK and JAK/STAT signaling domains (i.e. pouch and hinge). Graphs represent pooled values from *n=4*, control and *n=3, egr*-expressing discs.

**(K-L)** A control **(K)** and *egr*-expressing disc **(L)** assessed for S-phase activity using EdU incorporation assays. Discs also express the *TRE>RFP* (magenta) and *Stat92E>dGFP* (green) reporters.

**(M-N)** Fluorescence intensity profiles for *upd3.1-3LacZ* (gray) and *TRE>RFP* (magenta) reporters **(M)**, or *TRE>RFP* (magenta), *Stat92E>dGFP* (green) reporters and EdU (yellow) reporter intensities **(N)** traced from the pouch center (PC) to the disc periphery (DP) (yellow arrows in **F** and **O**). Graph represents mean ± SEM of reporter fluorescence intensity values from *n=15* tracks across a representative disc, scaled to the maximum measured value.

**(O)** Schematic representation of undamaged control discs and spatially segregated patterns of JNK/AP-1 (magenta) and JAK/STAT (green) reporter activity in 24h *egr*-expressing discs (R0).

Maximum projections of multiple confocal sections are shown in **K-L**.
Discs were stained with DAPI to visualize nuclei. Scale bars: 50 µm

**Figure S1.1**

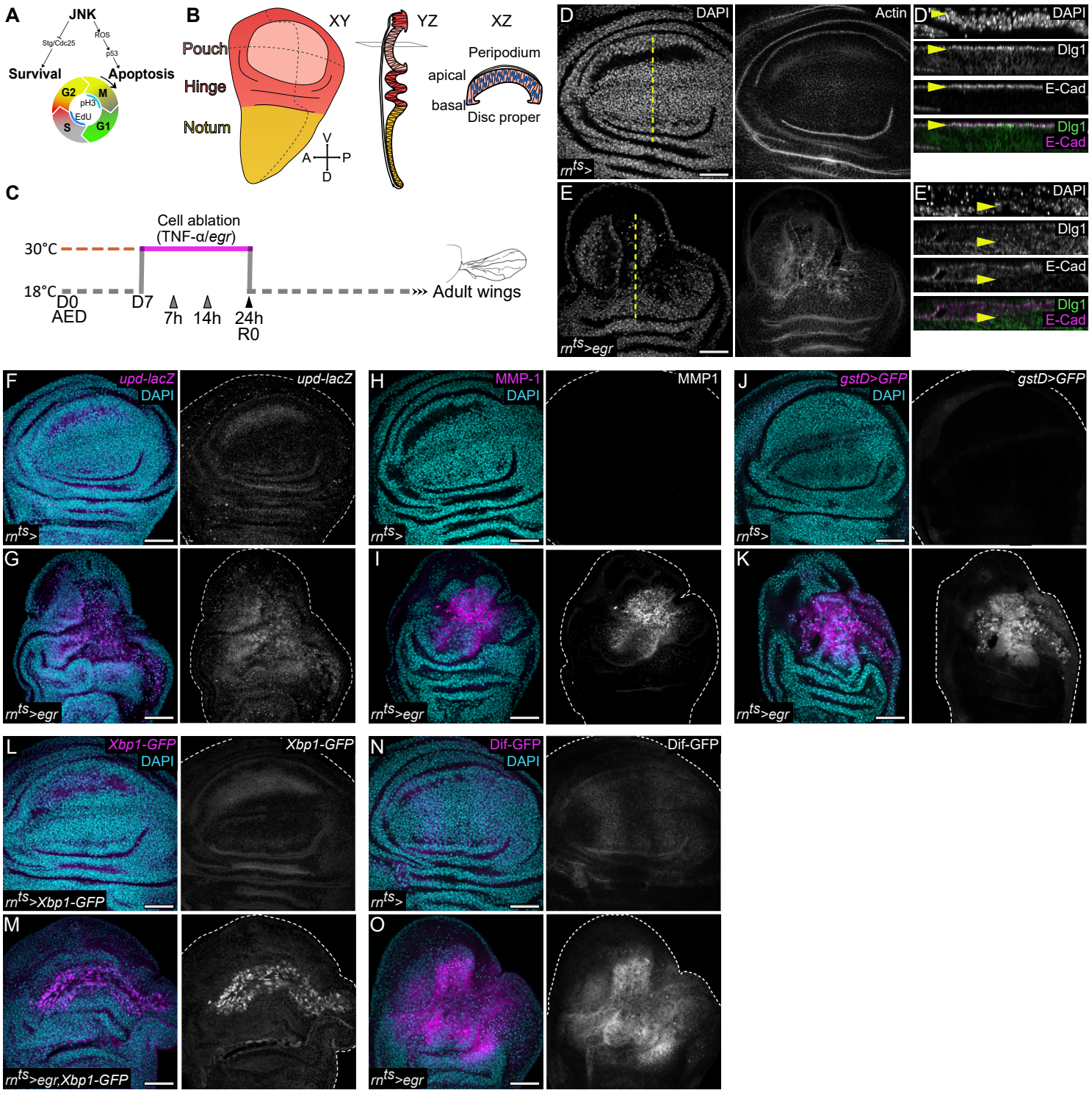
A
JNK
Stg/Cdc25
ROS
p53
Survival
Apoptosis
G2
M
pH3
EdU
S
G1
B
Pouch
Hinge
Notum
XY
YZ
XZ
Peripodium
apical
basal
Disc proper
V
A
P
D
C
Cell ablation
(TNF-α/egr)
30°C
18°C
D0
AED
D7
7h
14h
24h
R0
Adult wings
D
DAPI
Actin
D'
DAPI
Dlg1
E-Cad
Dlg1
E-Cad
rn^ts>
E
E'
DAPI
Dlg1
E-Cad
Dlg1
E-Cad
rn^ts>egr
F
upd-lacZ
DAPI
upd-lacZ
rn^ts>
H
MMP-1
DAPI
MMP1
rn^ts>
J
gstD>GFP
DAPI
gstD>GFP
rn^ts>
G
rn^ts>egr
I
rn^ts>egr
K
rn^ts>egr
L
Xbp1-GFP
DAPI
Xbp1-GFP
rn^ts>Xbp1-GFP
N
Dif-GFP
DAPI
Dif-GFP
rn^ts>
M
rn^ts>egr,Xbp1-GFP
O
rn^ts>egr

**Figure S1.1**

***egr*-expressing wing discs display hallmarks of tissue inflammation**

---

**(A)** Schematic of the FUCCI toolkit, utilizing the degradable *mRFP-NLS-CycB*$^{1-266}$ (red) *and GFP-E2F1*$^{1-230}$ (green) reporters as readouts for G1 and late S/early G2 phases of the cell-cycle respectively. Cells with elevated levels of both FUCCI reporters (yellow) are in the late G2 phase of the cell-cycle (Zielke et al. 2014). Cell in the S-phase and M-phase are detected using EdU and PH3 respectively. Damage-induced JNK/AP-1 signaling mediates survival or apoptosis through control of control of cell cycle progression (Cosolo et al. 2019).

**(B)** Schematic of a central XY, YZ and XZ section through a third instar wing imaginal disc. Different shades in the XY section represent the pouch, hinge and notum domains. Dashed lines represent the anterior-posterior (A/P) and dorsal-ventral (D/V) compartment boundaries. The YZ section visualizes the pseudostratified monolayer organization of the disc proper, and the overlying peripodial epithelium layer. XZ section visualizes the apical to basal orientation of epithelial cells in the wing pouch.

**(C)** Experimental timeline denoting the protocol used for induction of cell-ablation in this study. Larvae were raised at 18°C, and on D7 After Egg Deposition (AED), vials were transferred to 30°C to induce expression of pro-apoptotic transgenes for 24 h in the wing imaginal discs (also referred to as Recovery timepoint 0 or R0), using the pouch-specific *rotund-GAL4* (*rn-GAL4*) driver. Gray arrowheads represent additional recovery points used for time-course experiments. Shifting the larvae back to 18°C terminates expression of pro-apoptotic transgenes and thus ablation. The prospective adult wing blade arising from the damaged wing pouch allows for assessment of regenerative capacity.

**(D-E')** XY view of control **(D)** and *egr*-expressing **(E)** discs at R0 stained for actin. XZ-sections through the tissue **(D',E')** were visualized along dotted yellow lines. Immunostaining for E-cadherin (E-Cad, magenta) and Discs large (Dlg, green) reveals loss of barrier integrity (yellow arrowheads) in an *egr*-expressing disc **(E')** when compared to a control disc **(D')**.

**(F-O)** Control **(F,H,J,L,N)** and *egr*-expressing **(G,I,K,M,O)** discs at R0. *egr*-induced JNK/AP-1 signaling results in strong upregulation of various markers associated with inflammation and senescent properties – cytokines – *upd*-LacZ **(F,G)**, metalloproteases – MMP-1 **(H,I)**, ROS response – *gstD*>GFP **(J,K)**, UPR – spliced Xbp1-GFP **(L,M)** and NF-kB signaling – Dif-GFP **(N,O)**.

Maximum projections of multiple confocal sections are shown in **F-O**.
Discs were stained with DAPI to visualize nuclei. Scale bars: 50 µm

**Figure S1.2**

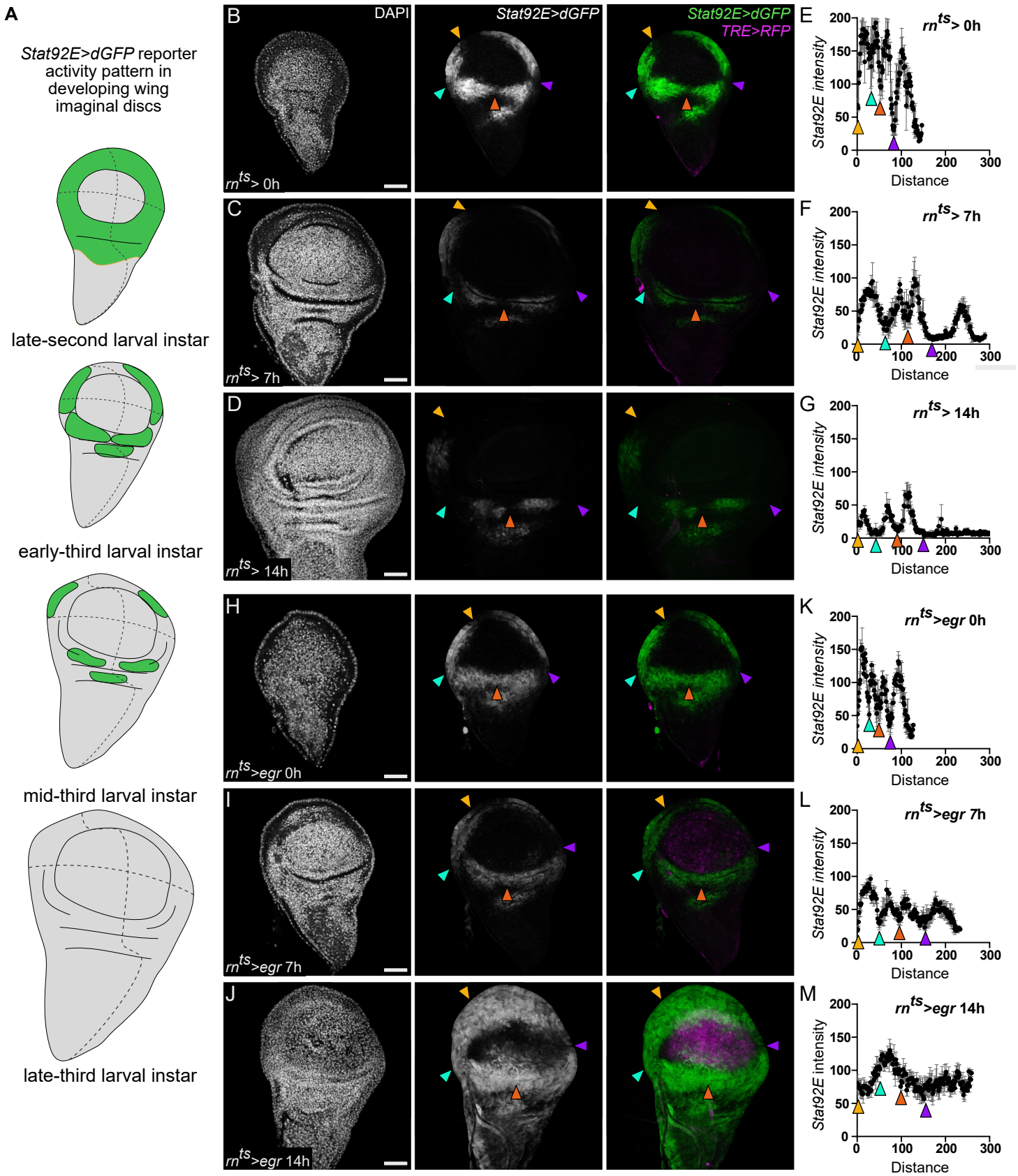
A
Stat92E>dGFP reporter activity pattern in developing wing imaginal discs
late-second larval instar
early-third larval instar
mid-third larval instar
late-third larval instar
B
DAPI
Stat92E>dGFP
Stat92E>dGFP
TRE>RFP
rnts> 0h
C
rnts> 7h
D
rnts> 14h
H
rnts>egr 0h
I
rnts>egr 7h
J
rnts>egr 14h
E
rnts> 0h
F
rnts> 7h
G
rnts> 14h
K
rnts>egr 0h
L
rnts>egr 7h
M
rnts>egr 14h
Stat92E intensity
Distance
0
50
100
150
200
300

**Figure S1.2**

**JAK/STAT is activated *de novo* downstream of JNK/AP-1 signaling upon tissue damage.**

---

**(A)** Schematic showing dynamic patterning of the JAK/STAT signaling reporter (*Stat92E>dGFP,* green) activity in developing, undamaged wing imaginal discs. Note the gradual loss of hinge-specific patterns from mid to late third larval instar stages.

**(B-D)** Undamaged control discs at 0h **(B)**, 7h **(C)** and 14h **(D)** visualized for JNK/AP-1 and JAK/STAT reporter activity patterns using the *TRE>RFP* (magenta) and *Stat92E>dGFP* (green) reporters.

**(H-J)** Wing discs after 0h **(H)**, 7h **(I)** and 14h **(J)** of *egr*-expression in the pouch domain. Increasing JNK/AP-1 reporter activity is seen in the pouch from 7h to 14h of *egr*-expression.

**(E-G, K-M)** *Stat92E>dGFP* reporter fluorescence intensity, traced along the hinge of control and *egr*-expressing discs at 0h **(E,K)**, 7h **(F,L)** and 14h **(G,M)**. Colored arrowheads indicate similar positions along hinge regions where JAK/STAT reporter activity is progressively lost. Note the *de novo* increase in the mean JAK/STAT reporter intensity in the hinge domain of *egr*-expressing discs **(M)** compared to control, undamaged discs **(G)** at 14h. Graphs display mean ± SEM for control 0h, *n=2*; 7h, *n=2* and 14h, *n=2* discs and *egr* 0h, *n=2*; 7h, *n=4* and 14h, *n=5* discs.

Maximum projections of multiple confocal sections are shown in **B-D**, **H-J.**
Discs were stained with DAPI to visualize nuclei. Scale bars: 50 µm

**Figure 2**

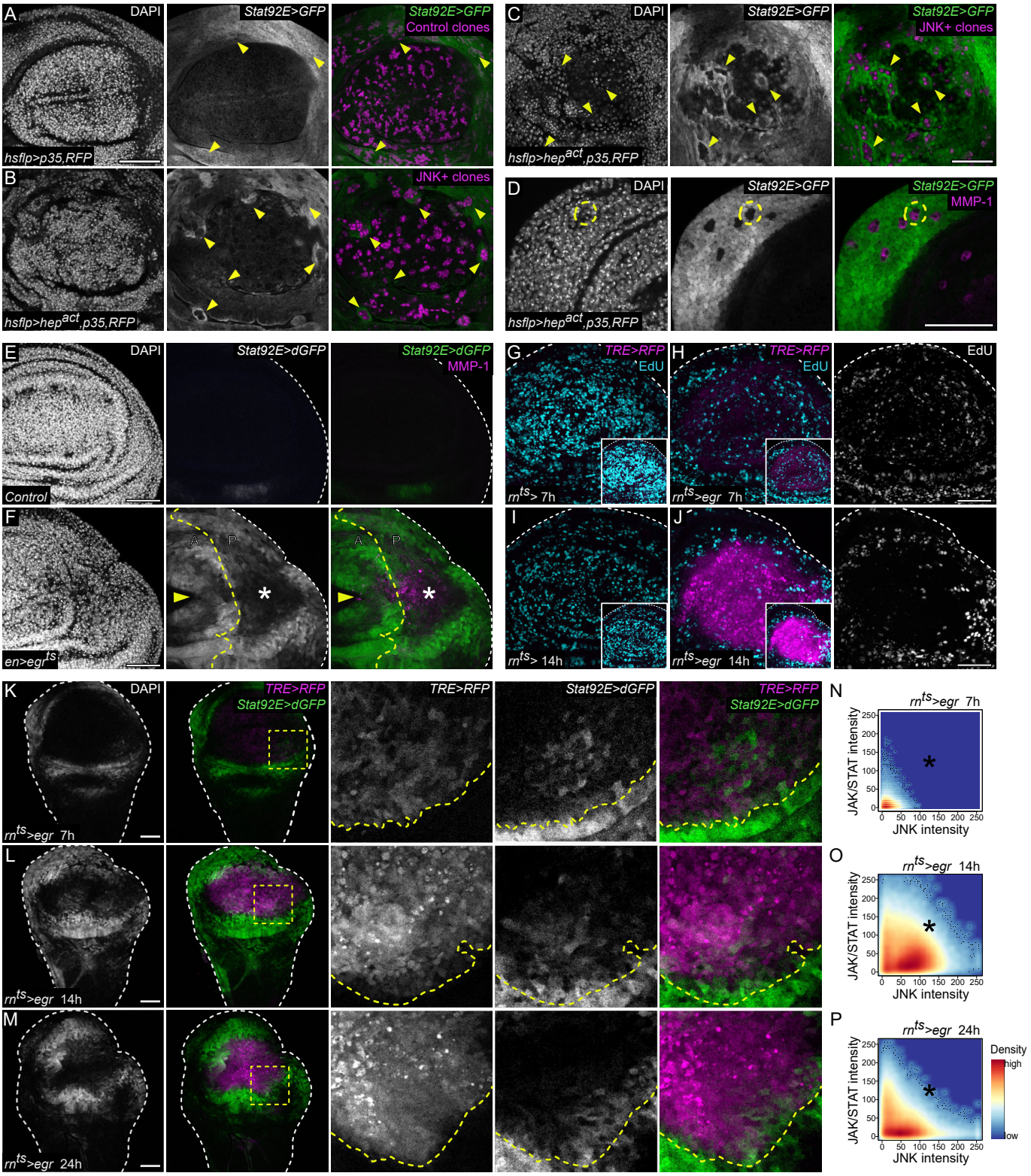
A
DAPI
Stat92E>GFP
Stat92E>GFP
Control clones
hsflp>p35,RFP
B
JNK+ clones
hsflp>hep^act,p35,RFP
C
DAPI
Stat92E>GFP
Stat92E>GFP
JNK+ clones
hsflp>hep^act,p35,RFP
D
DAPI
Stat92E>GFP
Stat92E>GFP
MMP-1
hsflp>hep^act,p35,RFP
E
DAPI
Stat92E>dGFP
Stat92E>dGFP
MMP-1
Control
F
A
P
en>egr^ts
G
TRE>RFP
EdU
rn^ts> 7h
H
TRE>RFP
EdU
rn^ts>egr 7h
EdU
I
rn^ts> 14h
J
rn^ts>egr 14h
K
DAPI
TRE>RFP
Stat92E>dGFP
TRE>RFP
Stat92E>dGFP
TRE>RFP
Stat92E>dGFP
rn^ts>egr 7h
L
rn^ts>egr 14h
M
rn^ts>egr 24h
N
rn^ts>egr 7h
JAK/STAT intensity
JNK intensity
O
rn^ts>egr 14h
JAK/STAT intensity
JNK intensity
P
rn^ts>egr 24h
JAK/STAT intensity
JNK intensity
Density
high
low

**Figure 2**

**JNK/AP-1 signaling represses JAK/STAT activity cell-autonomously**

---

**(A-C)** RFP expression marks *p35*-expressing control clones in the pouch (magenta, **A**) or *p35,hep$^{act}$*-expressing JNK+ clones in the pouch (magenta, **B**) and peripodium (magenta, **C**) 28h after clone induction in discs expressing the stable *Stat92E>GFP* reporter (green). Yellow arrowheads indicate clones of interest. Note the cell-autonomous repression of *Stat92E>GFP* reporter activity in JNK+ clones in the pouch periphery and hinge **(B)**, as well as in the peripodium **(C)**, when compared to control clones in the pouch **(A)** and peripodium **(**see **S2A)**

**(D)** *p35,hep$^{act}$*-expressing JNK+ clones in a disc expressing the *Stat92E>GFP* reporter (green), stained with anti-MMP-1 (magenta) - a downstream target of the JNK/AP-1 signaling pathway. The yellow circle highlights a JNK+ clone of interest, which shows a strong cell-autonomous repression of the JAK/STAT reporter activity in the JAK/STAT-signaling competent hinge, 48h after clone induction.

**(E-F)** Control disc **(E)** and a disc expressing *egr* **(F)** in the posterior compartment using the *enGAL4* driver at R0. Dashed yellow line marks the A/P boundary. Both discs express the *Stat92E>dGFP* reporter (green) and are stained for the JNK/AP-1 target MMP-1 (magenta). White asterisk indicates JNK/AP-1 reporter activity in the posterior pouch region. Note the non-cell autonomous JAK/STAT reporter activity in the anterior pouch, indicated by yellow arrowheads in **F**.

**(G-J)** Control **(G,I)** and *egr*-expressing **(H,J)** discs at 7h or 14h after ablation expressing the *TRE>RFP* reporter (magenta) and assessed for S-phase activity using EdU incorporation assay (cyan). While the number of S-phase cells are uniformly distributed in the pouch domain of undamaged control discs **(G,I)**, note the successive decrease in the S-phase cells (cyan) from 7h **(H)** to 14h **(J)** of *egr*-expression, coinciding with increasing *TRE>RFP* reporter activity in the pouch. Insets show the same images, with settings adjusted to visualize the JNK/AP-1 activity in the pouch of 7h *egr*-expressing discs.

**(K-M)** A time-course analysis of *TRE>RFP* (magenta) and *Stat92E>dGFP* (green) reporter activity in *egr*-expressing discs after 7h **(K)**, 14h **(L)** and 24h **(M)** of ablation. Yellow squares show magnified regions. Yellow lines mark the interface between JNK/AP-1 and JAK/STAT signaling cells. Note the increasing dominance of JNK/AP-1 signaling and decreasing JAK/STAT activation inside the boundary of JNK/AP-1 signaling cells at the JNK/AP-1-JAK/STAT interface.

**(N-P)** Representative 2D density plots of pixel fluorescence intensity for the *TRE>RFP* (JNK intensity, X-axis) and *Stat92E>dGFP* (JAK/STAT intensity, Y-axis) reporters, measured exclusively within the JNK/AP-1 signaling pouch domain (magenta in Fig. **1O**) from 7h **(L)**, 14h **(M)** and 24h **(N)** *egr*-expressing discs. Black asterisks highlight the region of increase and subsequent decline in the density of co-localizing pixels with medium and high reporter activities from 7h to 14h **(N,O)**, and 14h to 24h **(O,P)** respectively.

Maximum projections of multiple confocal sections are shown in **E-J**.
Discs were stained with DAPI to visualize nuclei. Scale bars: 50 µm

**Figure S2**

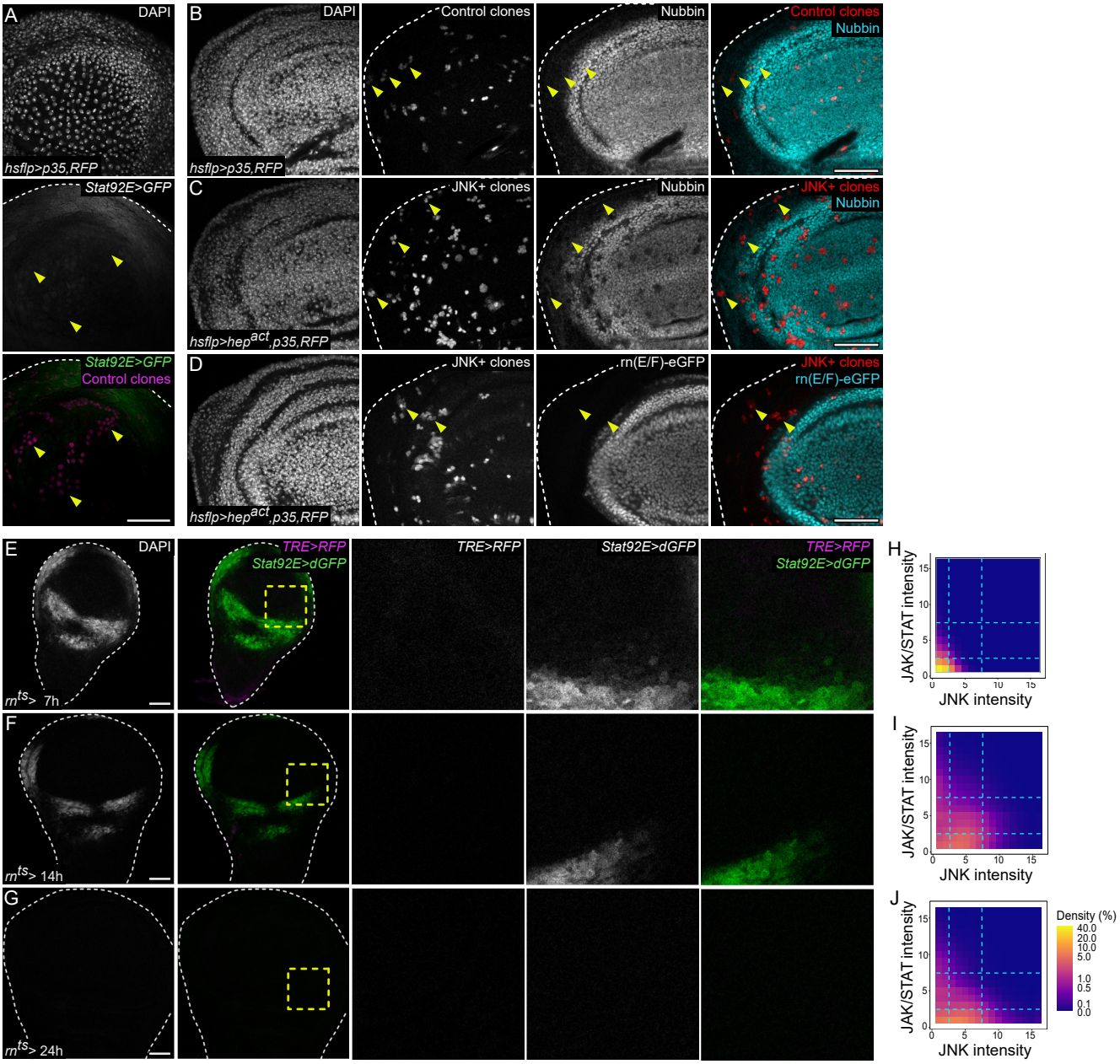
A
DAPI
hsflp>p35,RFP
Stat92E>GFP
Stat92E>GFP
Control clones
B
DAPI
hsflp>p35,RFP
Control clones
Nubbin
Control clones
Nubbin
C
hsflp>hep^act,p35,RFP
JNK+ clones
Nubbin
JNK+ clones
Nubbin
D
hsflp>hep^act,p35,RFP
JNK+ clones
rn(E/F)-eGFP
JNK+ clones
rn(E/F)-eGFP
E
DAPI
rn^ts> 7h
TRE>RFP
Stat92E>dGFP
TRE>RFP
Stat92E>dGFP
TRE>RFP
Stat92E>dGFP
F
rn^ts> 14h
G
rn^ts> 24h
H
JAK/STAT intensity
JNK intensity
I
JAK/STAT intensity
JNK intensity
J
JAK/STAT intensity
JNK intensity
Density (%)
40.0
20.0
10.0
5.0
1.0
0.5
0.1
0.0

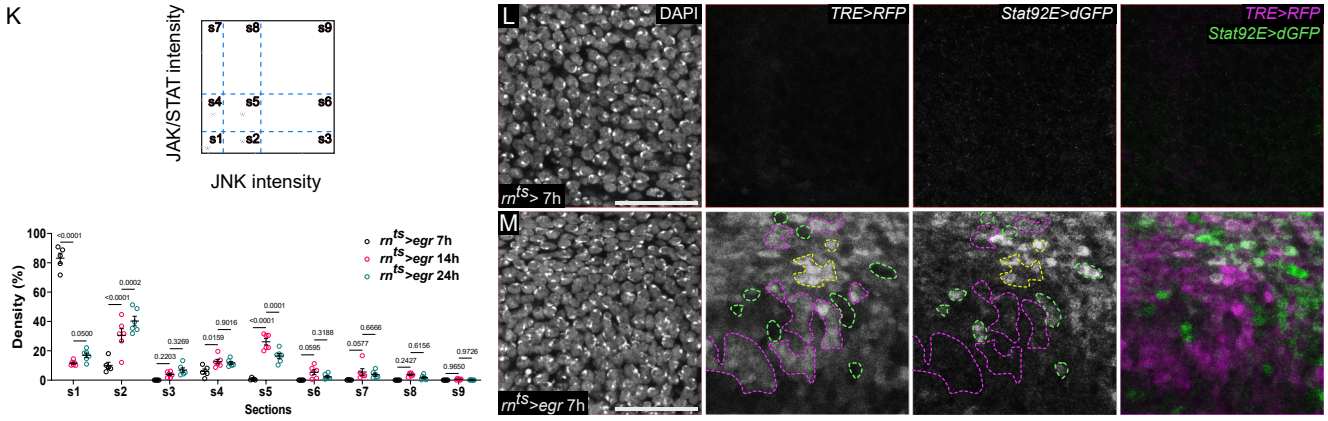
K
JAK/STAT intensity
JNK intensity
s1
s2
s3
s4
s5
s6
s7
s8
s9
Density (%)
Sections
rn^ts>egr 7h
rn^ts>egr 14h
rn^ts>egr 24h
L
DAPI
rn^ts> 7h
TRE>RFP
Stat92E>dGFP
TRE>RFP
Stat92E>dGFP
M
rn^ts>egr 7h

**Figure S2**

**JNK/AP-1 represses JAK/STAT activity independent of pouch-specific transcription factors**

---

**(A)** RFP expression marks *p35*-expressing control clones in the peripodium (magenta) 28h after clone induction in discs expressing the *Stat92E>GFP* reporter (green). Yellow arrowheads indicate clones of interest. Note the absence of ectopic/non-cell-autonomous *Stat92E>GFP* reporter activity around the control clones **(A)** when compared *p35,hep*$^{act}$-expressing JNK+ clones in Figure 2C.

**(B-C)** *p35*-expressing control clones (red, **B**) and *p35,hep*$^{act}$-expressing JNK+ clones (red, **C**) 28h after clone induction, stained for the pouch-specific TF Nubbin (cyan). JNK/AP-1 signaling clones show no ectopic expression of Nubbin in hinge, however, Nubbin is completely repressed intra-clonally within the pouch.

**(D)** *p35,hep*$^{act}$-expressing clones (red) in a disc expressing the Rn(E/F)-eGFP reporter (cyan) as a readout for the expression of the pouch-specific TF Rotund (Rn) 28h after clone induction. JNK/AP-1 signaling clones show no ectopic intra-clonal expression of Rn in the hinge domain. Yellow arrowheads indicate clones in the hinge.

**(E-G)** A time-course analysis of *TRE>RFP* (magenta) and *Stat92E>dGFP* (green) reporter activity in *rn*-expressing control discs after 7h **(E)**, 14h **(F)** and 24h **(G)** of inductive temperature shift to 30°C. Yellow squares show magnified regions.

**(H-J)** 2D density plots of averaged pixel fluorescence intensity for the *TRE>RFP* (JNK intensity,) and *Stat92E>dGFP* (JAK/STAT intensity) measured exclusively within the JNK/AP-1 signaling domain (magenta region in Figure 1M) of 7h **(H)**, 14h **(I)** and 24h **(J)** *egr*-expressing discs. Data was binned with a bin size of 16 and X and Y-axis denote the number of bins. Dashed lines (cyan) represent visually defined thresholds for distinguishing low, intermediate and high reporter activity regions. Plots represent averaged density values per bin across 7h, *n=5*; 14h, *n=6* and 24h, *n=6* discs. The same density color scale applies to all genotypes.

**(K)** Schematic showing different sections (s1-s9) from which mean pixel density values were obtained for 7h, 14h and 24h discs for statistical analysis. Black asterisks mark sections of interest. Graph comparing mean density of pixels in each section (s1-s9) for different durations of cell ablation Ordinary 2-way ANOVA with Dunnett's multiple comparisons test was used to test for statistical significance. Graphs represent mean ± SEM for 7h, *n=5*; 14h, *n=6* and 24h, *n=6* discs. Note the reduction in medium JAK/STAT activity within JNK/AP-1 signaling cells in S5 from 14h (15.37%) to 24h (5.25%) in *egr*-expressing discs.

**(L-M)** Selected regions from a control wing disc pouch **(L)** and a pouch after 7h of *egr*-expression **(M)** expressing the *TRE>RFP* (magenta) and *Stat92E>dGFP* (green) reporter. Dashed outlines (magenta) of cells activating JNK/AP-1 show an absence of JAK/STAT activity. Dashed outlines (green) cells activating JAK/STAT show an absence of the JNK/AP-1 activity. Dashed outlines (yellow) show a small proportion of cells that can strongly activate both the JNK/AP-1 and JAK/STAT reporters cell-autonomously.

Maximum projections of multiple confocal sections are shown in **B-D, L-M**
Discs were stained with DAPI to visualize nuclei. Scale bars: 50 µm

**Figure 3**

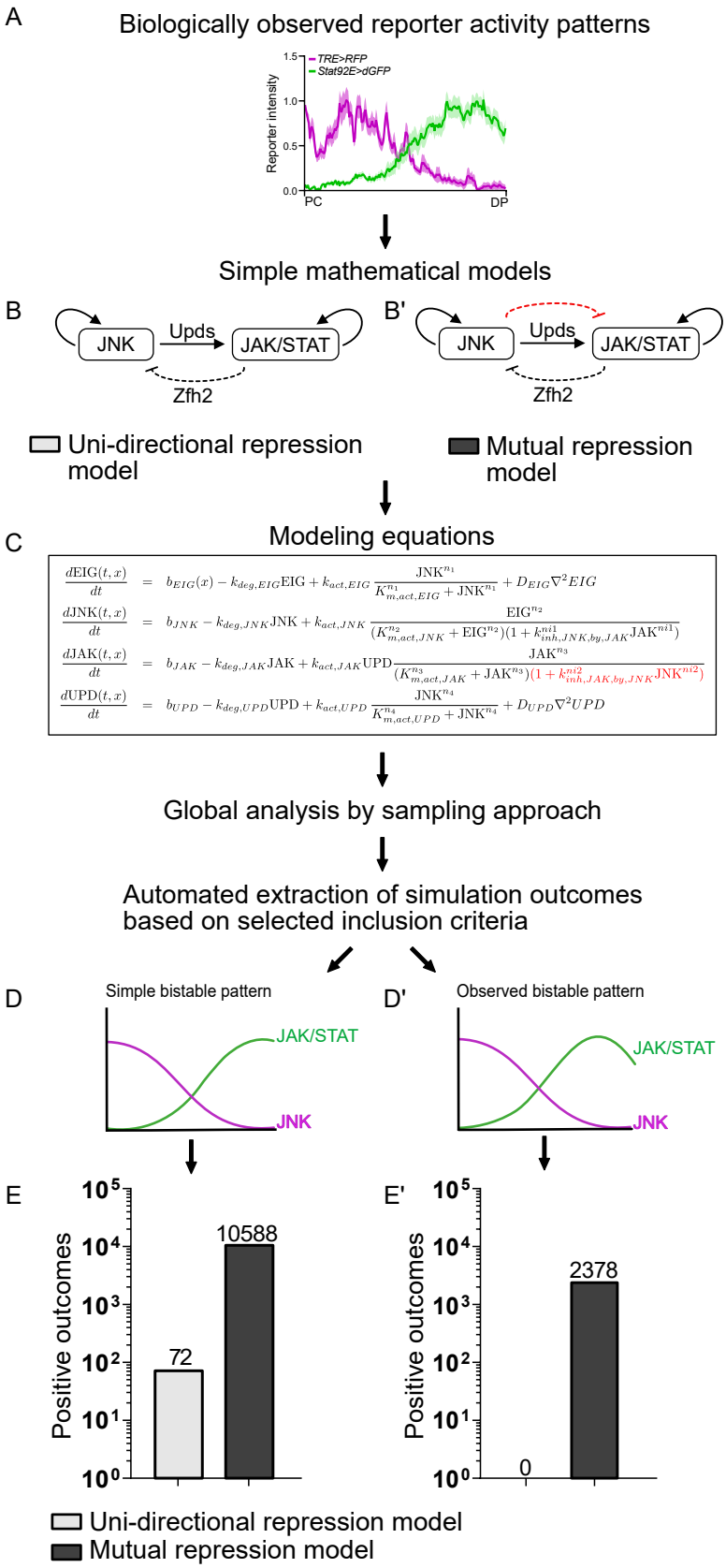
A
Biologically observed reporter activity patterns
TRE>RFP
Stat92E>dGFP
Reporter intensity
1.5
1.0
0.5
0.0
PC
DP
Simple mathematical models
B
JNK
Upds
JAK/STAT
Zfh2
B'
JNK
Upds
JAK/STAT
Zfh2
Uni-directional repression model
Mutual repression model
C
Modeling equations
$\frac{d\mathrm{EIG}(t,x)}{dt} = b_{EIG}(x) - k_{deg,EIG}\mathrm{EIG} + k_{act,EIG}\frac{\mathrm{JNK}^{n_1}}{K^{n_1}_{m,act,EIG} + \mathrm{JNK}^{n_1}} + D_{EIG}\nabla^2 EIG$
$\frac{d\mathrm{JNK}(t,x)}{dt} = b_{JNK} - k_{deg,JNK}\mathrm{JNK} + k_{act,JNK}\frac{\mathrm{EIG}^{n_2}}{(K^{n_2}_{m,act,JNK} + \mathrm{EIG}^{n_2})(1 + k^{ni1}_{inh,JNK,by,JAK}\mathrm{JAK}^{ni1})}$
$\frac{d\mathrm{JAK}(t,x)}{dt} = b_{JAK} - k_{deg,JAK}\mathrm{JAK} + k_{act,JAK}\mathrm{UPD}\frac{\mathrm{JAK}^{n_3}}{(K^{n_3}_{m,act,JAK} + \mathrm{JAK}^{n_3})(1 + k^{ni2}_{inh,JAK,by,JNK}\mathrm{JNK}^{ni2})}$
$\frac{d\mathrm{UPD}(t,x)}{dt} = b_{UPD} - k_{deg,UPD}\mathrm{UPD} + k_{act,UPD}\frac{\mathrm{JNK}^{n_4}}{K^{n_4}_{m,act,UPD} + \mathrm{JNK}^{n_4}} + D_{UPD}\nabla^2 UPD$
Global analysis by sampling approach
Automated extraction of simulation outcomes based on selected inclusion criteria
D
Simple bistable pattern
JAK/STAT
JNK
D'
Observed bistable pattern
JAK/STAT
JNK
E
Positive outcomes
$10^5$
$10^4$
$10^3$
$10^2$
$10^1$
$10^0$
72
10588
E'
Positive outcomes
$10^5$
$10^4$
$10^3$
$10^2$
$10^1$
$10^0$
0
2378
Uni-directional repression model
Mutual repression model

**Figure 3**

**A mutual-repression loop promotes bistable segregation of JNK/AP-1 and JAK/STAT activation patterns**

---

**(A-E')** Workflow to investigate the presence of a regulatory motif between the JNK/AP-1 and JAK/STAT signaling pathways driving pattern formation in *egr*-expressing discs. Fluorescence intensity profiles for the *TRE>RFP* (magenta) and *Stat92E>dGFP* (green) reporter patterns show bistable segregation in 24h egr-expressing discs. Intensity profiles are traced from the pouch center (PC) to the disc periphery (DP) **(A)**. Schematic showing the models tested – a uni-directional repression model acting only on JNK/AP-1 signaling **(B)** and a mutual repression model acting on both JNK/AP-1 and JAK/STAT signaling **(B')**. Modeling equations were generated, and a global analysis by sampling approach was used to analyze 21 selected parameters **(C)** (see also Fig.**S3**) and test for outcomes that produce bistable, switch-like patterns **(D-D')**. Number of simple bistable outcomes **(D)** from the mutual repression model (dark grey) are substantially greater than those from the uni-directional repression model (light grey) **(E)**. Applying stringent selection criteria based on the biologically observed reporter activity pattern **(D')**, positive outcomes reduce to 0 in the model without the mutual repression **(E')**.

**Figure S3**

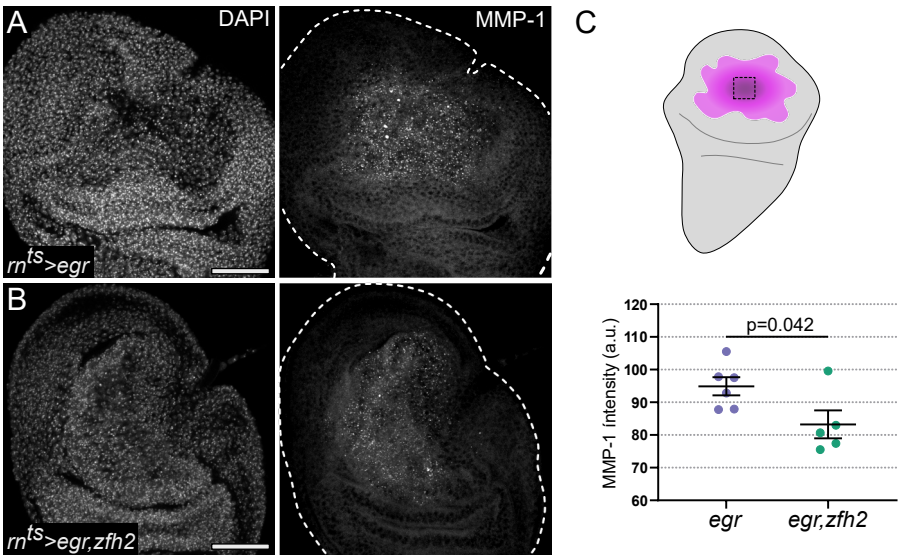


D

Mathematical modeling parameters

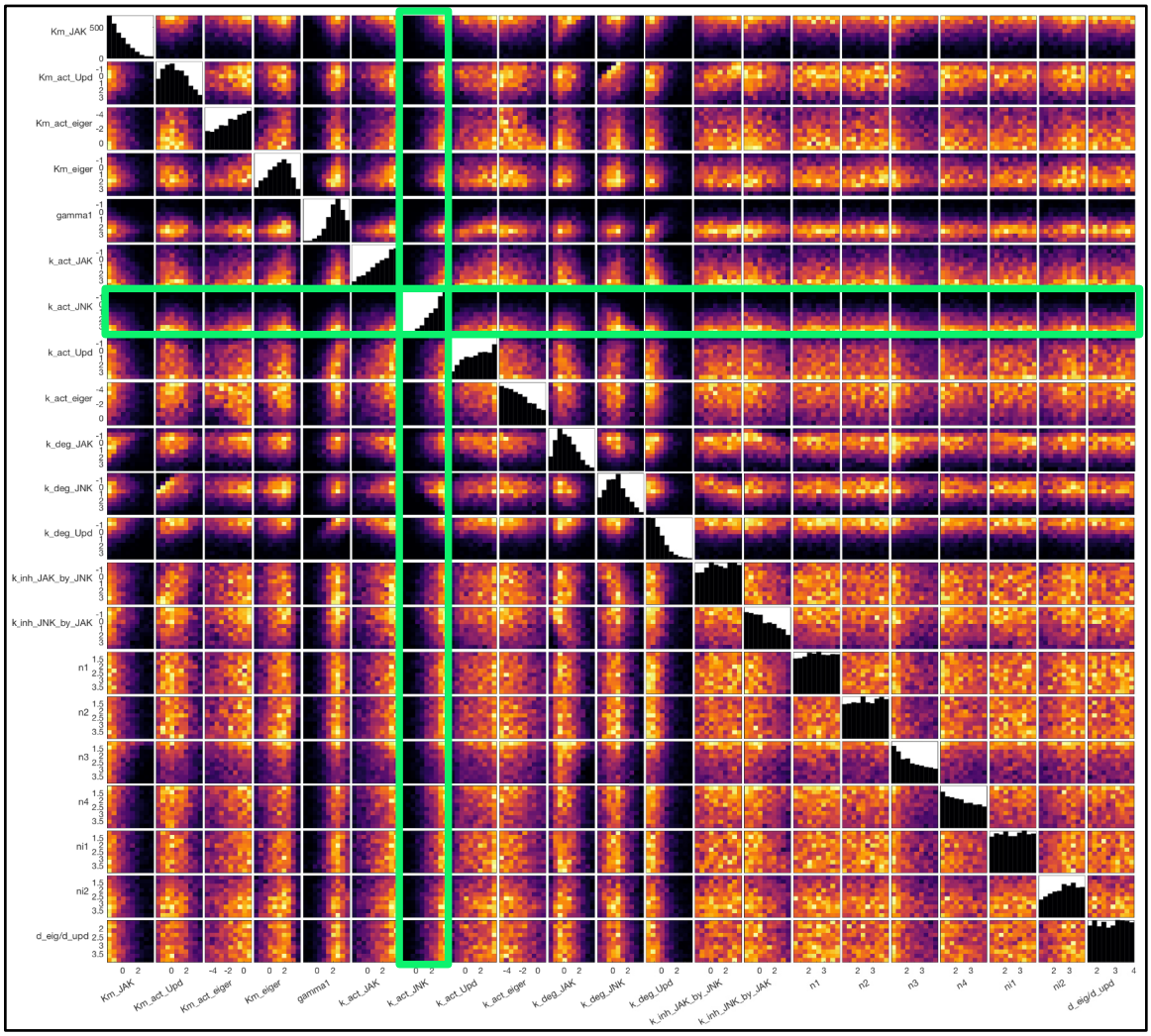

**Figure S3**

**A mutual-repression loop promotes bistable segregation of JNK/AP-1 and JAK/STAT activation patterns**

---

**(A-C)** An *egr*-expressing **(A)** and *egr,zfh2*-co-expressing disc **(B)** at R0, stained for MMP-1. Overexpression of Zfh2 leads to decreased JNK/AP-1 signaling in the central pouch region, as assayed by MMP-1 staining.

**(C)** Quantification of MMP-1 fluorescence intensity measured within the JNK/AP-1 signaling pouch domain. Black square in schematic shows measured region. Graphs display mean ± SEM for *n=6*, *egr*-expressing and *n=5*, *egr,zfh2*-co-expressing discs. T-tests were performed to test for statistical significance.

**(D)** 21 parameters, their numerical distributions and influence on positive bistable solutions obtained from the mutual repression model (Figure **3B'**) where JNK/AP-1 represses JAK/STAT. Parameters represent reaction rates - for activation, degradation and inhibition of simulated components, as well as hill coefficients and diffusion coefficients for different variables of the model. Bar graphs show the frequency of positive solutions within the tested range of values for each parameter. Our model supports that higher activation rates of JNK/AP-1 ($k_{act}$ JNK) have a strong influence on the total number of positive bistable solutions, highlighted in green rectangles.

Maximum projections of multiple confocal sections are shown in **A-B**
Discs were stained with DAPI to visualize nuclei. Scale bars: 50 µm

**Figure 4**

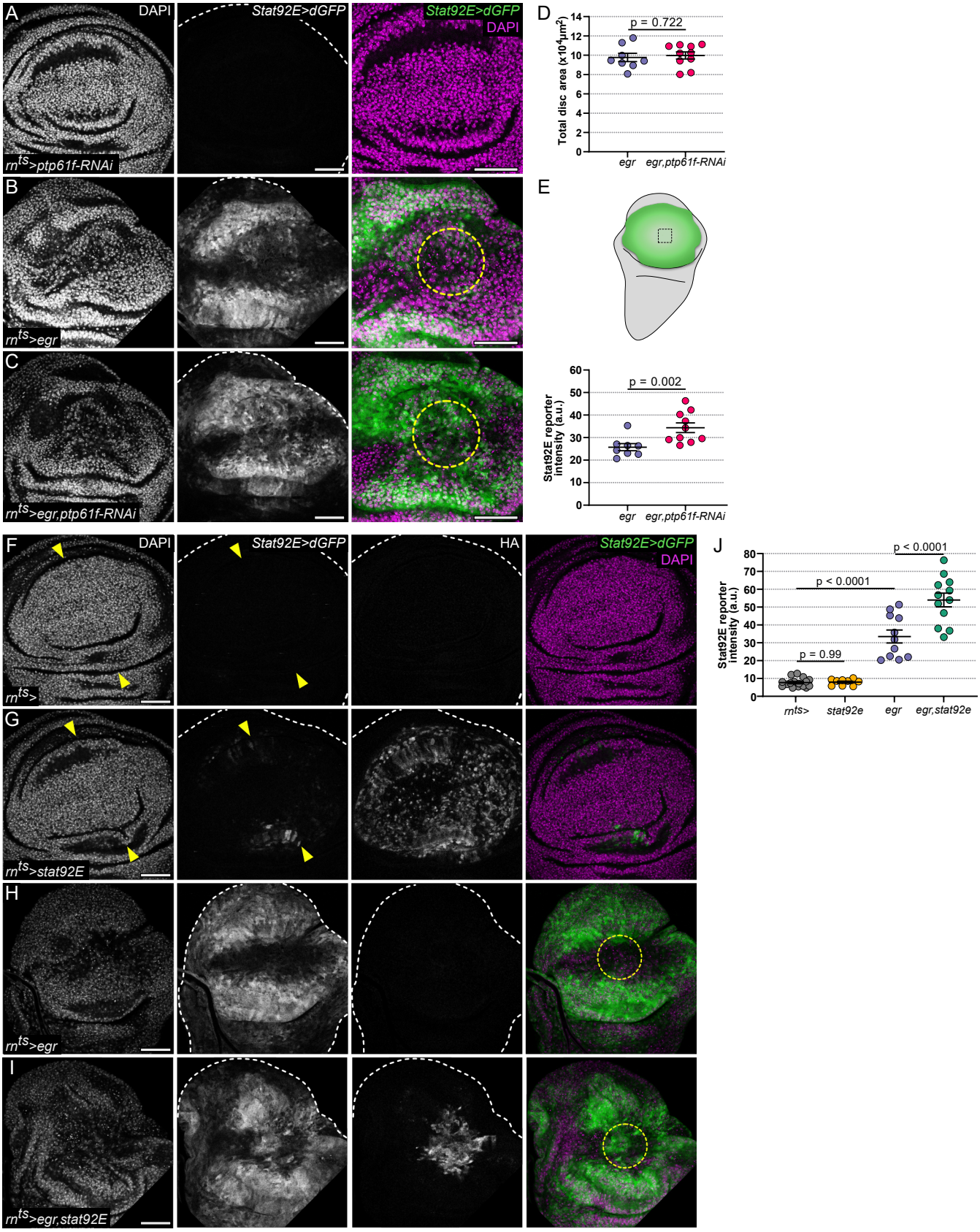
A
DAPI
Stat92E>dGFP
Stat92E>dGFP
DAPI
rnts>ptp61f-RNAi
B
rnts>egr
C
rnts>egr,ptp61f-RNAi
D
Total disc area (x10^4 µm^2)
p = 0.722
egr
egr,ptp61f-RNAi
E
Stat92E reporter intensity (a.u.)
p = 0.002
egr
egr,ptp61f-RNAi
F
DAPI
Stat92E>dGFP
HA
Stat92E>dGFP
DAPI
rnts>
G
rnts>stat92E
H
rnts>egr
I
rnts>egr,stat92E
J
Stat92E reporter intensity (a.u.)
p < 0.0001
p < 0.0001
p = 0.99
rnts>
stat92e
egr
egr,stat92e

**Figure 4**

**Ptp61F represses JAK/STAT activity in JNK/AP-1 signaling cells**

---

**(A-C)** A *ptp61F-RNAi*-expressing **(A)**, *egr*-expressing **(B)** and *egr,ptp61F-RNAi*-co-expressing disc **(C)** at R0. All discs also express the *Stat92E>dGFP* reporter (green). Yellow circles highlight the central domain of remaining *rn-GAL4* expressing cells. Note the derepression and ectopic JAK/STAT activity in the *egr,ptp61F-RNAi*-co-expressing disc.

**(D)** Quantification of total area of wing discs. Graphs display mean ± SEM for *n=8*, *egr*-expressing and *n=10*, *egr,ptp61F-RNAi*-co-expressing discs. T-tests were performed to test for statistical significance.

**(E)** Quantification of the *Stat92E>dGFP* reporter fluorescence intensity measured within the JNK/AP-1 signaling pouch domain. Black square in schematic shows measured region. Graphs display mean ± SEM for *n=8*, *egr*-expressing and *n=10*, *egr,ptp61F-RNAi*-co-expressing discs. U-tests were performed to test for statistical significance.

**(F-I)** A control **(F)**, *stat92E*-expressing **(G)**, *egr*-expressing **(H)** and *egr,stat92E*-co-expressing disc **(I)**. All discs also express the dynamic *Stat92E>dGFP* reporter (green). Staining for HA confirms expression and nuclear/cytoplasmic localization of the *UAS-stat92E-3xHA* construct. Yellow arrowheads point to the restricted, non-autonomously induced JAK/STAT activity in the peripheral pouch in control discs **(F,G)**. Yellow circles highlight the central domain of remaining *rn-GAL4* expressing cells **(H,I)**.

**(J)** Quantification of the *Stat92E>dGFP* reporter fluorescence intensity measured within the JNK/AP-1 signaling pouch domain. Black square in schematic **(E)** shows measured region. Graphs display mean ± SEM for *n=16*, control discs ($rn^{ts}$>), *n=9*, *stat92E*-expressing discs, *n=11*, *egr*-expressing and *n=12*, *egr,stat92E*-co-expressing discs. One-way ANOVA with multiple comparisons was performed to test for statistical significance.

Discs were stained with DAPI (magenta) to visualize nuclei. Scale bars: 50 µm

**Figure S4.1**

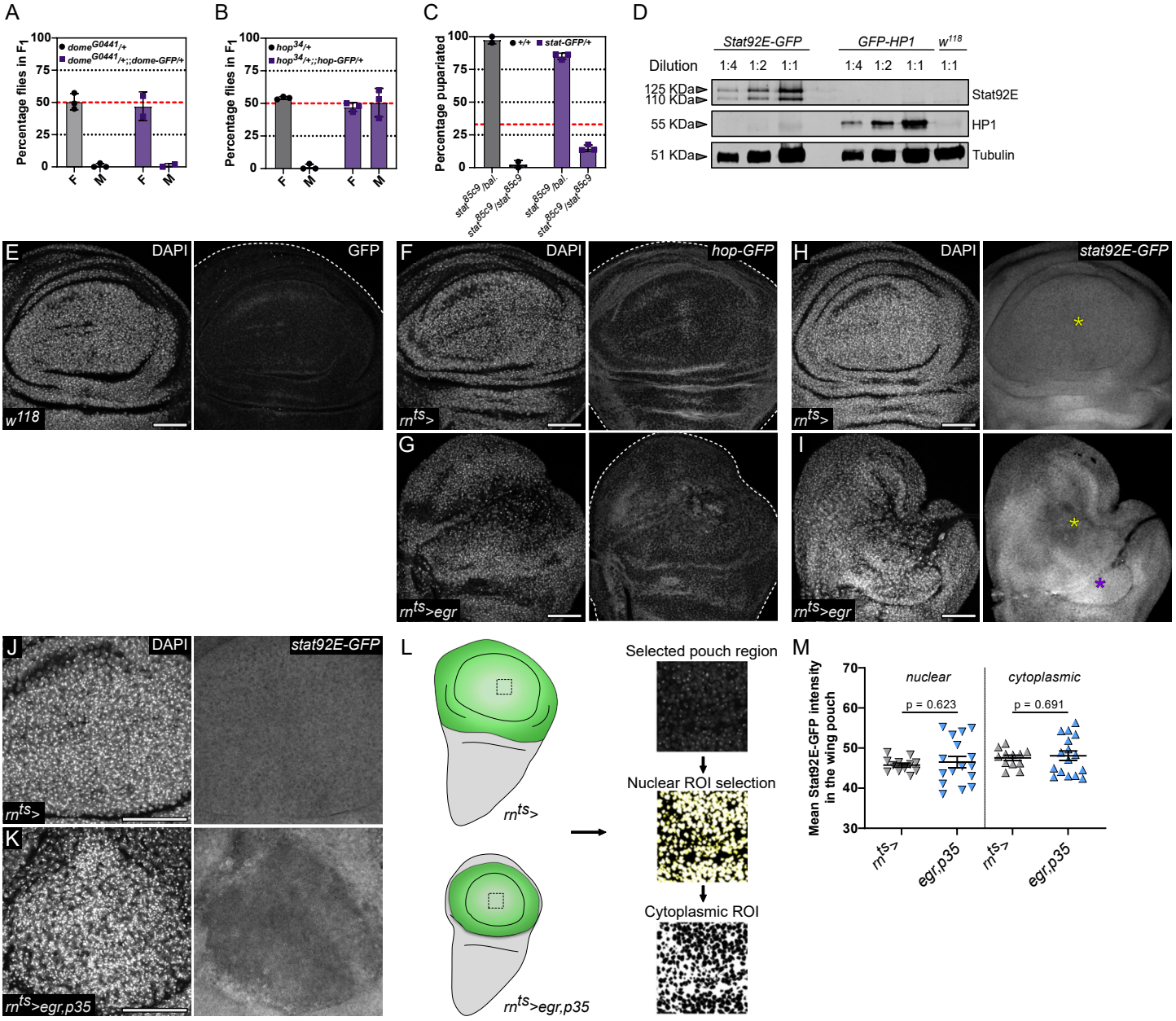
A
Percentage flies in F1
dome G0441/+
dome G0441/+;;dome-GFP/+
F M F M
B
Percentage flies in F1
hop 34/+
hop 34/+;;hop-GFP/+
F M F M
C
Percentage pupariated
+/+
stat-GFP/+
stat 85c9 /pal.
stat 85c9 /stat 85c9
D
Stat92E-GFP
GFP-HP1
w118
Dilution
1:4 1:2 1:1
1:4 1:2 1:1 1:1
125 KDa
110 KDa
55 KDa
51 KDa
Stat92E
HP1
Tubulin
E
DAPI
GFP
w118
F
DAPI
hop-GFP
rnts>
G
rnts>egr
H
DAPI
stat92E-GFP
rnts>
I
rnts>egr
J
DAPI
stat92E-GFP
rnts>
K
rnts>egr,p35
L
rnts>
rnts>egr,p35
Selected pouch region
Nuclear ROI selection
Cytoplasmic ROI
M
Mean Stat92E-GFP intensity in the wing pouch
nuclear
cytoplasmic
p = 0.623
p = 0.691
rnts>
egr,p35
rnts>
egr,p35

**Figure S4.1**

**Core components of the JAK/STAT pathway are not altered in JNK/AP-1 signaling cells**

---

**(A-C)** Test for genetic complementation of the LOF mutants *dome*$^{G0441}$, *hop*$^{9p5}$ and *stat*$^{85C9}$ (grey bars) by GFP-tagged Dome, Hop and Stat92E fosmid lines (purple bars) (see Experimental procedures). Dome-GFP is unable to rescue male lethality in *dome*$^{G0441}$ LOF background to the expected rate of rescue, i.e. 50% of adults in F1 (red dashed line), *n=2* independent replicates **(A)**. Hop-GFP successfully rescues male lethality in *hop*$^{9p5}$ LOF background from 0% to 47% of viable adults, at the expected rate of rescue in F1 (red dashed line), *n=3* independent replicates **(B)**. Stat92E-GFP partially rescues larval lethality in *stat*$^{85c9}$ null mutants from 0% to 15% pupariation, at approximately half the expected rate of a full rescue (red dashed line), *n=3* independent replicates **(C)**. Thus, the Hop-GFP and Stat92E-GFP fosmid lines were used as proxies for further analysis of protein localization in *egr*-expressing discs.

**(D)** Western blots analyzed for Stat92E-GFP expression in imaginal discs. HP-1-GFP genotypes were included as positive control, along with a non-tagged negative control from wild type imaginal disc extracts. Increasing concentrations were loaded, and probed with anti-GFP and anti-Tubulin antibody. The GFP-tagged Stat92E protein is detected at the expected MW (125Kda and 110Kda), and likely representing overlapping isoforms running in two separate weight ranges (71.2-76.8 kD and 85.6-92.8 kD plus GFP-tag).

**(E)** A control *w*$^{118}$ disc used as a negative control to determine anti-GFP antibody background.

**(F-G)** A control **(F)** and *egr*-expressing disc **(G)** expressing the GFP-tagged Hop protein.

**(H-I)** A Control **(H)** and *egr*-expressing disc **(I)** expressing the GFP-tagged Stat92E protein. While Stat92E expression is low in the medial hinge folds of control discs, the hinge shows elevated expression in *egr* discs (purple asterisk). This is consistent with JAK/STAT activity inducing expression of Stat92E to promote self-activation. In contrast, Stat92E-GFP protein levels remains low in the pouch (yellow asterisk).

**(J-K)** A control pouch **(J)** and a larger domain of *p35,egr*-expressing cells in the pouch **(K)** was used to test for changes in nuclear versus cytoplasmic localization of Stat92E-GFP within high JNK/AP-1-signaling cells.

**(L)** Schematic showing the centrally selected region (black square) in control and *egr,p35*-expressing discs, used to measure Stat92E-GFP fusion protein intensity in the JNK/AP-1 signaling pouch domain. Automated workflows were used to generate nuclear and cytoplasmic ROIs from selected regions, to quantify Stat92E-GFP protein levels within these area fractions.

**(M)** Stat92E-GFP reporter fluorescence intensity within nuclear and cytoplasmic area fractions of the JNK/AP-1 signaling pouch, calculated for *n=12* independent regions from control and *n=16* independent regions from *egr,p35*-expressing discs. The pouch signaling domain in *egr,p35*-expressing discs fails to exhibit an increase in nuclear translocation of the Stat92E-GFP protein, indicative of basal levels of JAK/STAT signaling in these cells similar to controls. The surrounding hinge domain recapitulated elevated JAK/STAT signaling by elevated Stat92E-GFP protein expression and nuclear translocation (data not shown).

Maximum projections of multiple confocal sections are shown in **H-K**
Discs were stained with DAPI to visualize nuclei. Scale bars: 50 µm

**Figure S4.2**

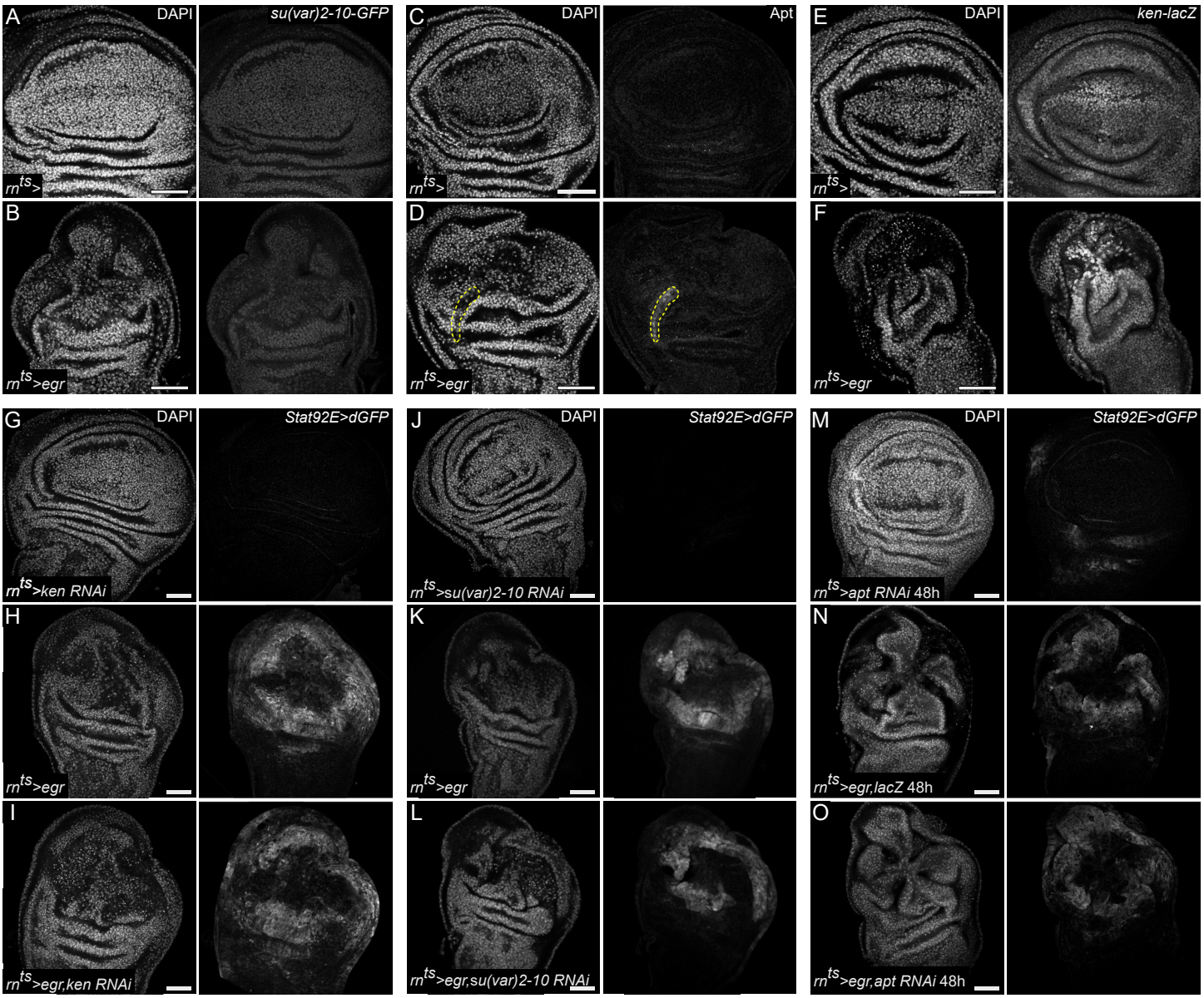
A
DAPI
su(var)2-10-GFP
rn^ts>
B
rn^ts>egr
C
DAPI
Apt
rn^ts>
D
rn^ts>egr
E
DAPI
ken-lacZ
rn^ts>
F
rn^ts>egr
G
DAPI
Stat92E>dGFP
rn^ts>ken RNAi
H
rn^ts>egr
I
rn^ts>egr,ken RNAi
J
DAPI
Stat92E>dGFP
rn^ts>su(var)2-10 RNAi
K
rn^ts>egr
L
rn^ts>egr,su(var)2-10 RNAi
M
DAPI
Stat92E>dGFP
rn^ts>apt RNAi 48h
N
rn^ts>egr,lacZ 48h
O
rn^ts>egr,apt RNAi 48h

**Figure S4.2**

**Known negative regulators of JAK/STAT signaling are not required for JNK/AP-1-mediated repression of JAK/STAT**

---

**(A-B)** A control **(A)** and *egr*-expressing disc **(B)**, also expressing GFP-tagged Su(var)2-10/dPIAS and stained for GFP.

**(C-D)** A control **(C)** and *egr*-expressing disc **(D)** stained for Apontic (Apt). Yellow outlines mark non-specific tracheal staining in **D**.

**(E-F)** A control **(E)** and *egr*-expressing disc **(F),** also expressing *ken-Lac*Z and stained for anti-β-Galactosidase.

**(G-O)** *RNAi*-expressing control discs **(G,J,M)**, *egr*-expressing **(H,K,N)** and *egr,RNAi*-co-expressing discs **(I,L,O)** visualized for *Stat92E>dGFP* reporter activity. *egr, ken RNAi* **(I)** and *egr, su(var)2-10 RNAi* **(L)** co-expressing discs were dissected after 24 h of expression. *egr, apt RNAi* co-expressing discs **(O)** were even dissected after 48 h of *egr* expression. Note how knockdown of these negative regulators does not lead to increase in the JAK/STAT reporter activity in the JNK/AP-1 signaling domain.

Discs were stained with DAPI to visualize nuclei. Scale bars: 50 µm

**Figure S4.3**

Validation of lines based on derepression of developmentally regulated JAK/STAT activity

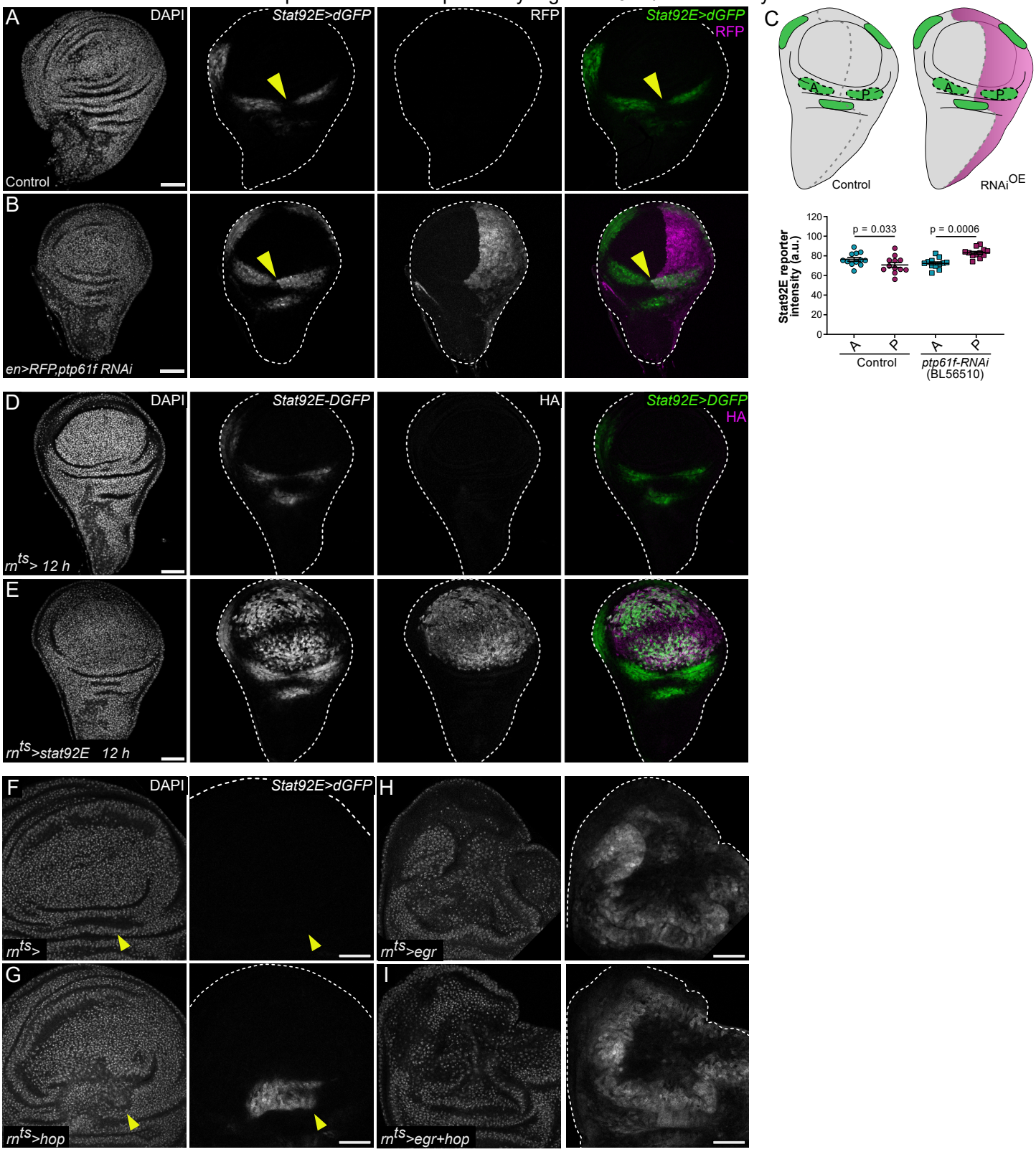

**Figure S4.3**

**Testing the ability of *ptp61F-RNAi* and *UAS-Stat92E-HA* to elevate developmentally regulated JAK/STAT activity in the hinge or pouch**

---

**(A-B)** Expression of *UAS-ptp61F-RNAi* (BL56510) and *UAS-RFP* (magenta) using the *en-GAL4* driver **(B)** leads to a distinct increase in developmentally patterned *Stat92E>dGFP* reporter (green) activity in the posterior wing hinge (yellow arrowheads) compared to stage-matched controls **(A)** dissected on D7 AED.

**(C)** Quantification of changes to the development pattern of JAK/STAT activation, using fluorescence intensity measurements for the *Stat92E>dGFP* reporter. Black dashed lines in schematic show measured regions in the anterior (A) and posterior (P) wing hinge in control and *RNAi*-expressing (*en>RNAi*) discs. Graphs display mean ± SEM for *n=10,* controls and *n=12* RNAi-expressing discs. Paired t-tests were performed to test for statistical significance.

**(D-E)** A Control **(D)** and a *UAS-STAT92E-3xHA* expressing disc, under the control of the *rn-GAL4* driver **(E)**, stained for HA (magenta). 12h of expression on D7 AED leads to strong upregulation of the *Stat92E>dGFP* reporter (green) in the wing pouch.

**(F-I)** Compared to control discs **(E)**, overexpression of hop (UAS-hop.H) **(F)** leads to restricted, ectopic activation of the *Stat92E>dGF* reporter in the medial hinge fold (yellow arrowheads). However, compared to *egr*-expressing discs **(G)**, *egr,hop*-co-expressing discs **(H)** at R0 do not induce ectopic JAK/STAT activity in the central JNK/AP-1 signaling pouch domain.

Discs were stained with DAPI to visualize nuclei. Scale bars: 50 µm

**Figure 5**

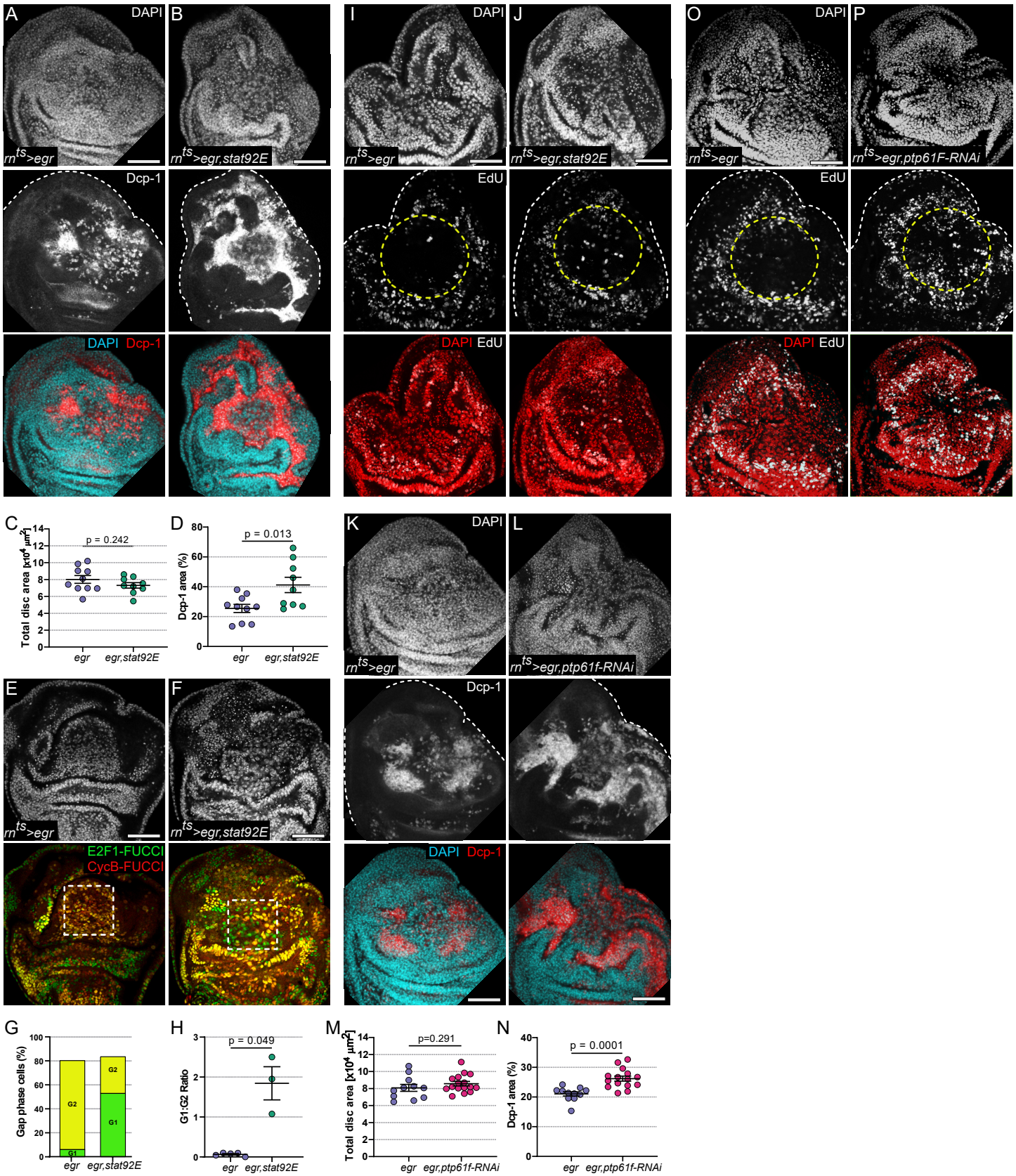
A
DAPI
rn^ts>egr
B
rn^ts>egr,stat92E
Dcp-1
DAPI Dcp-1
I
DAPI
rn^ts>egr
J
rn^ts>egr,stat92E
EdU
DAPI EdU
O
DAPI
rn^ts>egr
P
rn^ts>egr,ptp61F-RNAi
EdU
DAPI EdU
C
Total disc area [x10^4 µm^2]
p = 0.242
egr
egr,stat92E
D
Dcp-1 area (%)
p = 0.013
egr
egr,stat92E
K
DAPI
rn^ts>egr
L
rn^ts>egr,ptp61f-RNAi
Dcp-1
DAPI Dcp-1
E
rn^ts>egr
F
rn^ts>egr,stat92E
E2F1-FUCCI
CycB-FUCCI
G
Gap phase cells (%)
G2
G1
egr
egr,stat92E
H
G1:G2 Ratio
p = 0.049
egr
egr,stat92E
M
Total disc area [x10^4 µm^2]
p=0.291
egr
egr,ptp61f-RNAi
N
Dcp-1 area (%)
p = 0.0001
egr
egr,ptp61f-RNAi

**Figure 5**

**JAK/STAT repression by JNK/AP-1 is required for the G2 arrest and protects central wound cells from apoptosis.**

---

**(A-B)** An *egr*-expressing **(A)** and *egr,stat92E*-coexpressing disc **(B)** at R0, stained for DAPI (cyan), and cleaved Dcp-1 (red) to visualize apoptosis.

**(C-D)** Quantification of total wing disc area **(C)** and normalized area occupied by cleaved Dcp-1 **(D)**. Graphs display mean ± SEM for *n=10, egr*-expressing and *n=9, egr,stat92E*-co-expressing discs. T-tests were performed to test for statistical significance.

**(E-F)** An *egr*-expressing **(E)** and *egr,stat92E*-coexpressing disc **(F)** at R0, also expressing the FUCCI reporter. Dashed white squares highlight the distinct shift from G2 (yellow cells) to G1 (green cells) in the pouch domain.

**(G-H)** Bar graph **(G)** representing the cumulative proportion of gap phase cells in G1 (green) and G2 (yellow) for each genotype. Graph **(H)** displays G1-phase:G2-phase ratios obtained from *n=5, egr*-expressing and *n=3, egr,stat92E*-co-expressing discs. Dashed white squares in **E-F** show measured regions. T-test with Welch's correction was performed to test for statistical significance.

**(I-J)** EdU incorporation assay to detect S-phase cells (gray) in *egr*-expressing **(I)**, or *egr,stat92E*-co-expressing **(J)** disc. Discs were stained with DAPI (red) to visualize nuclei.

**(K-L)** An *egr*-expressing **(K)** and *egr,ptp61F-RNAi*-coexpressing **(L)** disc at R0, stained for DAPI (cyan), and cleaved Dcp-1 (red) to visualize apoptosis.

**(M-N)** Quantification of total wing disc area **(M)** and normalized area occupied by cleaved Dcp-1 **(N)**. Graphs display mean ± SEM for *n=11, egr*-expressing and *n=15, egr,ptp61F-RNAi*-coexpressing discs. T-tests were performed to test for statistical significance.

**(O-P)** EdU incorporation assay to detect S-phase cells (gray) in an *egr*-expressing **(O)**, and *egr,ptp61F-RNAi*-coexpressing **(P)** disc. Discs were also stained with DAPI (red) to visualize nuclei.

Maximum projections of multiple confocal sections are shown in **A-B, I-L, O-P**. Scale bars: 50 μm

**Figure S5**

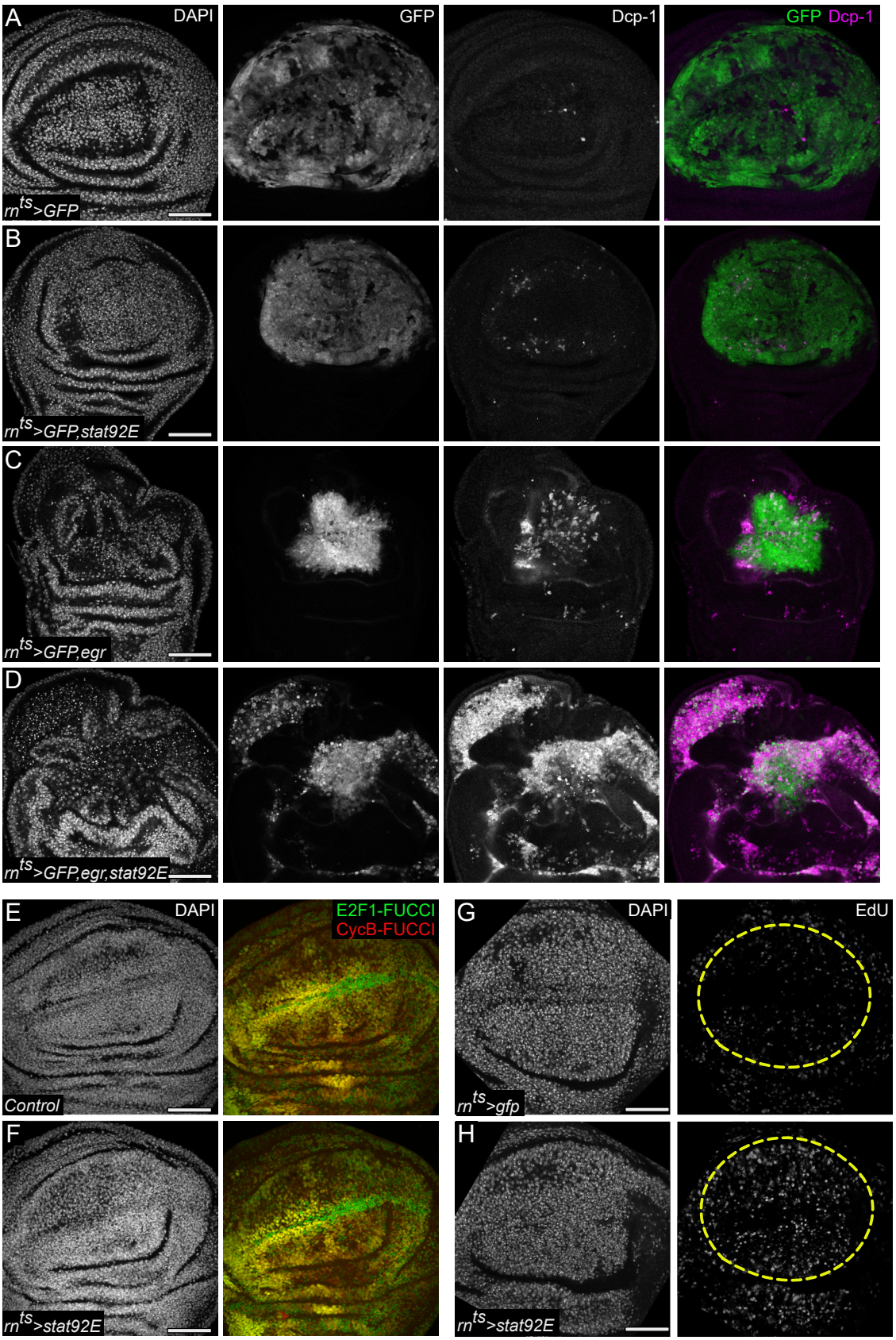
A
DAPI
GFP
Dcp-1
GFP Dcp-1
rn^ts>GFP
B
rn^ts>GFP,stat92E
C
rn^ts>GFP,egr
D
rn^ts>GFP,egr,stat92E
E
DAPI
E2F1-FUCCI
CycB-FUCCI
Control
F
rn^ts>stat92E
G
DAPI
EdU
rn^ts>gfp
H
rn^ts>stat92E

**Figure S5**

**Cell-autonomous co-activation of JNK/AP-1 and JAK/STAT signaling gives rise to apoptosis**

---

**(A-D)** A control wing disc **(A)**, *stat92E*-expressing **(B)**, *egr*-expressing **(C)** and *egr,stat92E*-co-expressing disc **(D)**, which also express UAS-GFP (green), all under the control of *rn-GAL4.* Discs were stained for cleaved Dcp-1 (magenta) to visualize apoptosis. Note how almost all apoptotic debris is labelled by GFP **(D)**, demonstrating that apoptotic cells truly originate from *egr,stat92E*-coexpressing cells.

**(E-F)** A control **(E)** and *stat92E*-expressing wing disc **(F)** at R0, also expressing the FUCCI reporter.

**(G-H)** A *gfp*-expressing control **(G)** and *stat92E*-expressing disc **(H)** at R0, assayed for S-phase activity by EdU incorporation. Elevated EdU is detected in the pouch domain ectopically expressing Stat92E. However, no changes were observed in the FUCCI cell-cycle profile.

Maximum projections of multiple confocal sections are shown in **E-F**
Discs were stained with DAPI to visualize nuclei. Scale bars: 50 µm

**Figure 6**

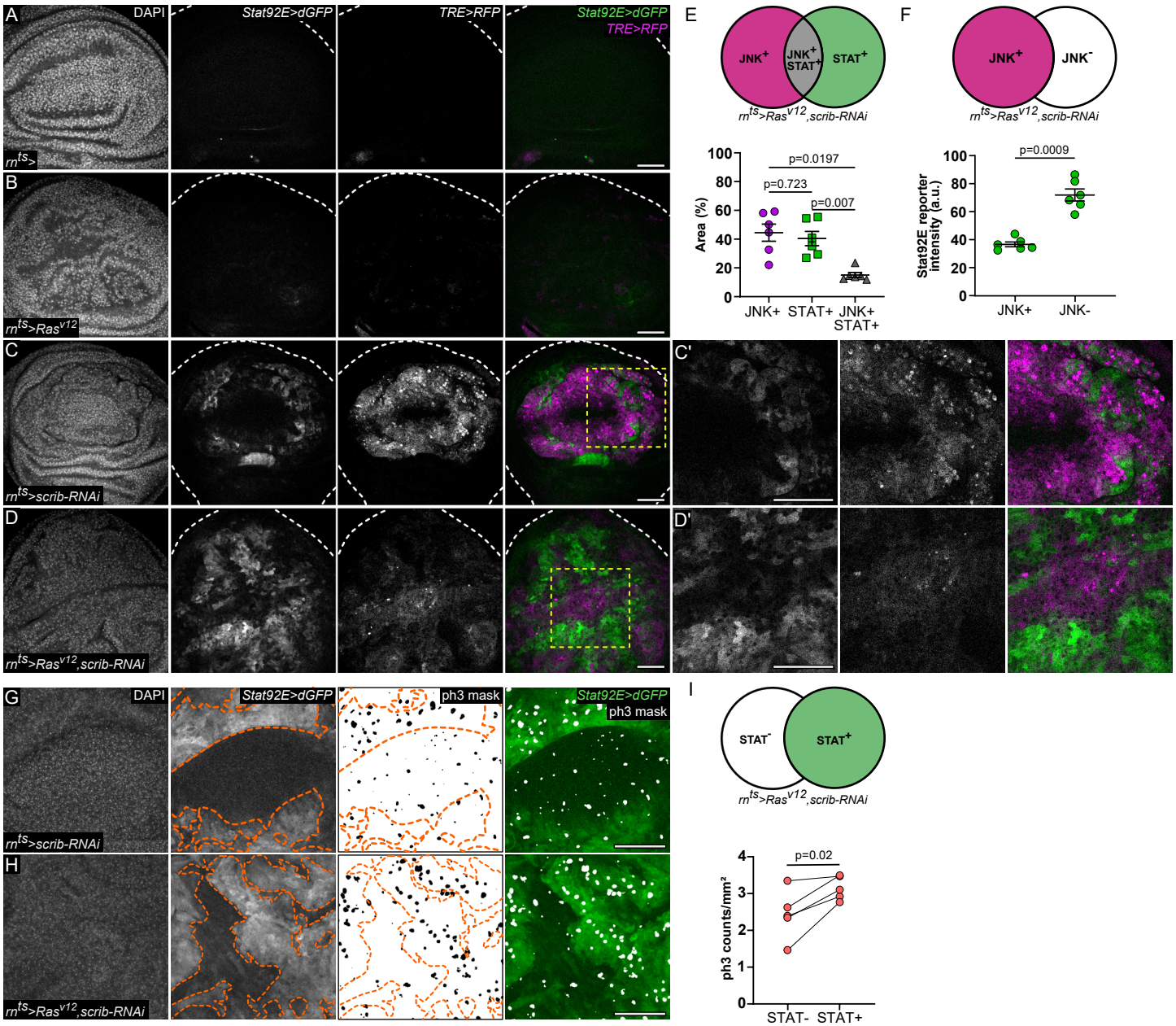
A
DAPI
Stat92E>dGFP
TRE>RFP
Stat92E>dGFP
TRE>RFP
rn^ts>
B
rn^ts>Ras^v12
C
rn^ts>scrib-RNAi
C'
D
rn^ts>Ras^v12,scrib-RNAi
D'
E
JNK+
JNK+ STAT+
STAT+
rn^ts>Ras^v12,scrib-RNAi
Area (%)
p=0.0197
p=0.723
p=0.007
JNK+
STAT+
JNK+ STAT+
F
JNK+
JNK-
rn^ts>Ras^v12,scrib-RNAi
Stat92E reporter intensity (a.u.)
p=0.0009
JNK+
JNK-
G
DAPI
Stat92E>dGFP
ph3 mask
Stat92E>dGFP
ph3 mask
rn^ts>scrib-RNAi
H
rn^ts>Ras^v12,scrib-RNAi
I
STAT-
STAT+
rn^ts>Ras^v12,scrib-RNAi
ph3 counts/mm²
p=0.02
STAT-
STAT+

**Figure 6**

**The wound organizer network segregates JNK/AP-1 and JAK/STAT signaling to drive oncogenic growth**

---

**(A-D)** A control wing disc **(A)** and wing discs expressing *Ras$^{v12}$* **(B)**, *scrib-RNAi* **(C, C')**, or *Ras$^{v12}$,scrib-RNAi* **(D,D')** for 44 h D6 AED. Discs also express the JNK/AP-1 reporter *TRE>RFP* (magenta) and the JAK/STAT reporter *Stat92E>dGFP* (green). Yellow squares in mark area of magnification shown in **(C',D')**.

**(E)** Schematic shows the *TRE>RFP*-positive (JNK$^+$, magenta), *Stat92E>dGFP*-positive (STAT$^+$, green) and JNK/AP-1 and JAK/STAT double positive regions (JNK$^+$STAT$^+$, gray) selected for measurements. Graph represents normalized area of measured regions based on the total signaling area. Note that only 15% of regions within the tumor express both the JNK/AP-1 and JAK/STAT signaling reporters. Graph represents mean ± SEM for *n=6, Ras$^{v12}$,scrib-RNAi*-expressing discs. One-way paired ANOVA with Holm-Šídák's multiple comparison test was performed to test for statistical significance.

**(F)** Schematic shows *TRE>RFP*-positive (JNK$^+$, magenta) and *TRE>RFP*-negative (JNK$^-$, white) regions selected for measurements. Graph represents *Stat92E>dGFP* fluorescence intensity measured within selected JNK$^+$ and JNK$^-$ regions. Note the reduction in the reporter intensity from 71.91±4.32 to 36.66±1.74 within the JNK$^-$ vs. JNK$^+$ region. Graph represents mean ± SEM for *n=6,* ras$^{v12}$,scrib-RNAi-expressing discs. Paired t-tests was performed to test for statistical significance.

**(G-H)** A wing disc expressing *scrib-RNAi* **(G)** and *Ras$^{v12}$,scrib-RNAi* **(H)** at 44 h. Discs also express the *Stat92E>dGFP* reporter and were stained for phospho-Histone3 (ph3) to visualize cells in mitosis. Segmented masks of ph3 were generated for quantifications and an overlay of the *Stat92E>dGFP* reporter (green) and ph3 (white) is represented. Orange dashed lines mark the STAT$^+$ regions within the discs.

**(I)** Schematic shows *Stat92E>dGFP*-positive (STAT$^+$, green) and *Stat92E>dGFP*-negative (STAT$^-$, white) regions selected for measurements. Graph represents ph3 counts normalized to area in the STAT$^+$ and STAT$^-$ regions for *n=5, Ras$^{v12}$,scrib-RNAi*-expressing discs.

Maximum projections of multiple confocal sections are shown in **G-H**
Discs were stained with DAPI to visualize nuclei. Scale bars: 50 µm

**Figure S6**

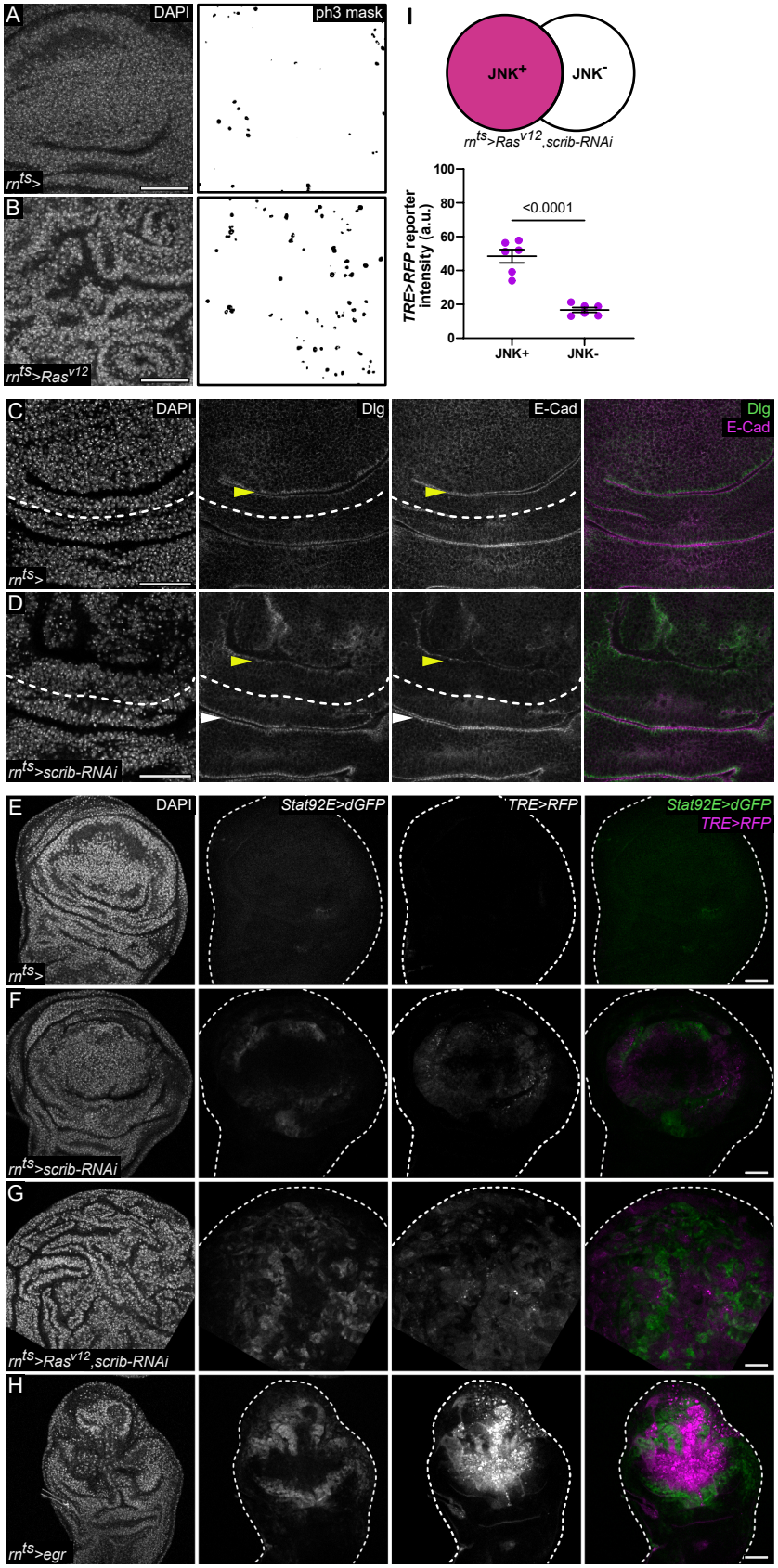
A
DAPI
ph3 mask
rn^ts>
B
rn^ts>Ras^v12
I
JNK+
JNK-
rn^ts>Ras^v12,scrib-RNAi
TRE>RFP reporter intensity (a.u.)
<0.0001
JNK+
JNK-
C
DAPI
Dlg
E-Cad
Dlg
E-Cad
rn^ts>
D
rn^ts>scrib-RNAi
E
DAPI
Stat92E>dGFP
TRE>RFP
Stat92E>dGFP
TRE>RFP
rn^ts>
F
rn^ts>scrib-RNAi
G
rn^ts>Ras^v12,scrib-RNAi
H
rn^ts>egr

**Figure S6**

**Tumors utilize lower but persistent levels of JNK/AP-1 activation to drive overgrowth**

---

**(A-B)** A control wing disc **(A)** and wing disc expressing *Ras$^{v12}$* **(B)** for 44 h. Discs were stained for phospho-Histone3 (ph3) to visualize cells in mitosis. Segmented masks of ph3 are shown.

**(C-D)** A control wing disc **(C)** and wing discs expressing *scrib-RNAi* **(D)** for 44 h stained for E-cad (magenta) and Dlg (green) reveals loss of barrier integrity (yellow arrowheads in **D**) in the *scrib-RNAi*-expressing pouch domain when compared to its respective hinge domain (white arrowheads in **D**), as well as to the undamaged control pouch (yellow arrowhead in **C**). The pouch-hinge interface is marked with white dashed lines.

**(E-H)** A control wing disc **(E)** and wing discs expressing *scrib-RNAi* **(F)**, *Ras$^{v12}$,scrib-RNAi* **(G)** and *egr* **(H)** for 44h. Discs also express the JNK/AP-1 reporter *TRE>RFP* (magenta) and JAK/STAT reporter *Stat92E>dGFP* (green). *TRE>RFP* and *Stat92E>dGFP* reporter fluorescence intensities were adjusted to subsaturation in *egr*-expressing discs and all genotypes were imaged at comparable settings.

**(I)** Schematic shows *TRE>RFP*-positive (JNK+, magenta) and *TRE>RFP*-negative (JNK-, white) regions selected for measurements. Graph represents *TRE>RFP* reporter fluorescence intensity measured within selected JNK+ and JNK- regions. Graphs represent mean ± SEM for *n=6, Ras$^{v12}$,scrib-RNAi*-expressing discs. Paired t-tests was performed to test for statistical significance.

Maximum projections of multiple confocal sections are shown in **A-B**
Discs were stained with DAPI to visualize nuclei. Scale bars: 50 µm

**Figure 7**

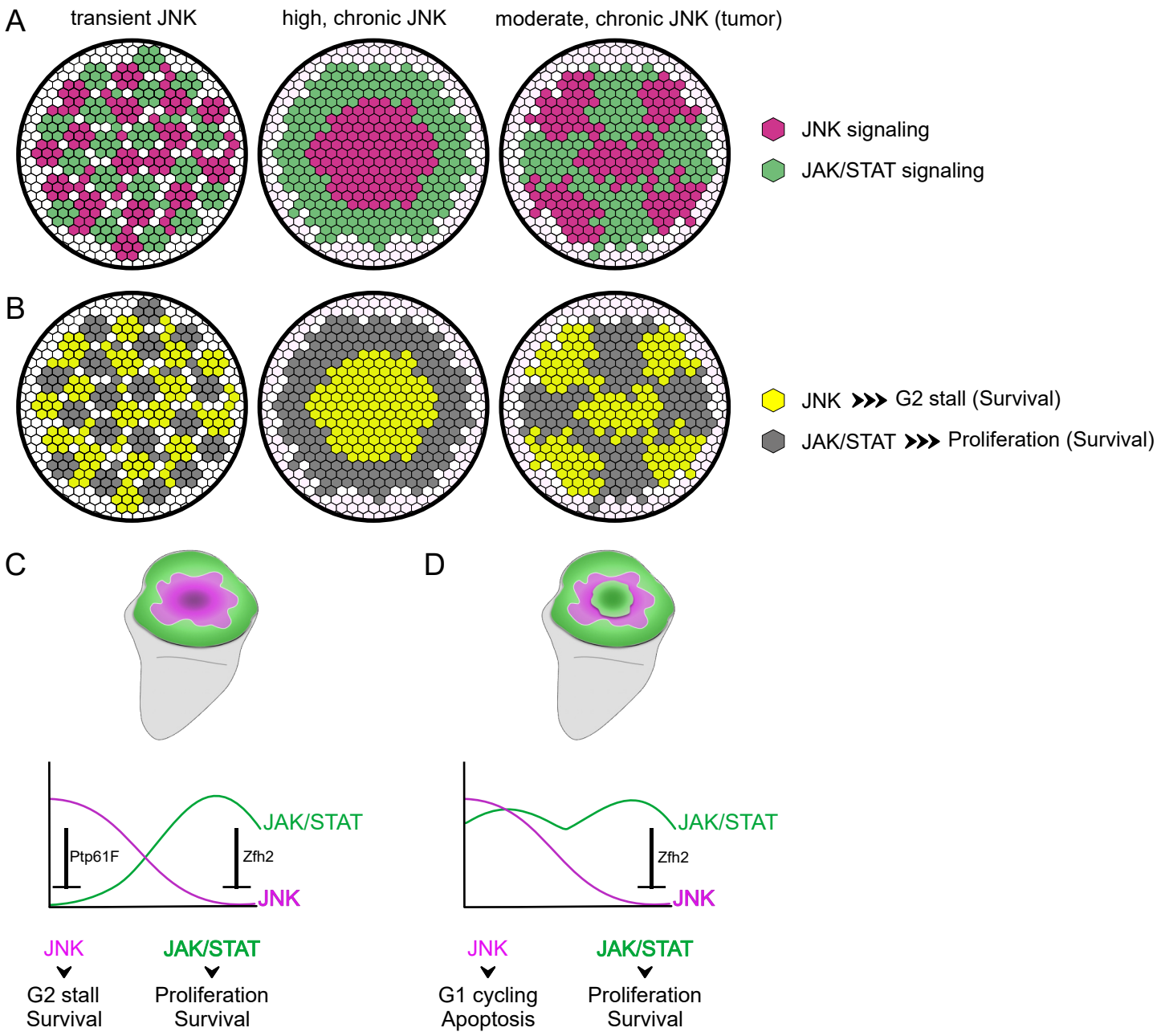
A
transient JNK
high, chronic JNK
moderate, chronic JNK (tumor)
JNK signaling
JAK/STAT signaling
B
JNK ➤➤➤ G2 stall (Survival)
JAK/STAT ➤➤➤ Proliferation (Survival)
C
Ptp61F
Zfh2
JAK/STAT
JNK
JNK
G2 stall
Survival
JAK/STAT
Proliferation
Survival
D
Zfh2
JAK/STAT
JNK
JNK
G1 cycling
Apoptosis
JAK/STAT
Proliferation
Survival

**Figure 7**

**Mutual repression between JNK/AP-1 and JAK/STAT sets up wound organizer activity**

---

**(A-B)** Transient (7h *egr*-expression), and chronic (24h *egr*-expression or 44h *Ras$^{v12}$,scrib-RNAi*-expression) activation of JNK/AP-1 signaling stratifies JNK-activating tissue into distinct JNK/AP-1 and JAK/STAT signaling domains **(A)** and cell behaviors **(B)**.

**(C)** *egr*-expressing discs spatially stratify tissue repair behaviors via a mutual repression motif. JNK/AP-1 represses JAK/STAT signaling activitiy via Ptp61F, while JAK/STAT represses JNK/AP-1 activation via Zfh2. JNK signaling ensures G2 arrest and cell survival, while JAK/STAT signaling ensures proliferation and supports survival in the absence of JNK.

**(D)** Disruption of the mutual repression motif by cell-autonomous activation of JNK/AP-1 and JAK/STAT signaling overrides the protective G2 stall and drives cells into mitotic cycling and G1, where p53 activation can lead to apoptotic outcomes.